

---

JUSTUS-LIEBIG-



UNIVERSITÄT  
GIESSEN

Justus-Liebig-Universität Gießen

Fachbereich für Biologie und Chemie

Institut für Anorganische und Analytische Chemie

---

# Investigation of the Reactivity of Dioxygen with Copper Complexes in Homogeneous and Heterogeneous Phases

Kumulativ-Dissertation zur Erlangung  
des Doktorgrades der Naturwissenschaften

Dr. rer. nat.

vorgelegt von

Tim Brückmann

aus Wetzlar

August 2021



## Selbstständigkeitserklärung

Ich erkläre: Ich habe die vorgelegte Dissertation selbstständig und ohne unerlaubte fremde Hilfe und nur mit den Hilfen angefertigt, die ich in der Dissertation angegeben habe. Alle Textstellen, die wörtlich oder sinngemäß aus veröffentlichten Schriften entnommen sind, und alle Angaben, die auf mündlichen Auskünften beruhen, sind als solche kenntlich gemacht. Ich stimme einer evtl. Überprüfung meiner Dissertation durch eine Antiplagiat-Software zu. Bei den von mir durchgeführten und in der Dissertation erwähnten Untersuchungen habe ich die Grundsätze guter wissenschaftlicher Praxis, wie sie in der „Satzung der Justus-Liebig-Universität Gießen zur Sicherung guter wissenschaftlicher Praxis“ niedergelegt sind, eingehalten.

---

Ort, Datum

---

Tim Brückmann

Erstgutachter:

Prof. Dr. Siegfried Schindler

Zweitgutachter:

Prof. Dr. Richard Göttlich



## **Danksagung**

Ich möchte mich bei Prof. Dr. Siegfried Schindler bedanken, dass er mir die Möglichkeit gegeben hat, in seiner Arbeitsgruppe zu promovieren und ich mir seiner Unterstützung stets sicher sein konnte. Darüber hinaus bedanke ich mich auch bei Prof. Dr. Richard Göttlich für das Zweitgutachten dieser Arbeit.

Weiter bedanke ich mich bei Prof. Dr. Bernd Smarsly für die Kooperation im Rahmen der Komplex-Immobilisierung und seiner Arbeitsgruppe, im Besonderen Dr. Rafael Meinsch für die Bereitstellung der Silica-Monolithe und die Einweisung in das Raman-Mikroskop sowie Dr. Kevin Turke für die BET-Bestimmungen und die Einführung in die DRIFTS-Apparatur. Ebenso bedanke ich mich bei Prof. Dr. Klaus Müller-Buschbaum und seinen Mitarbeitern Dominik Heuler und Marcel Seuffert für die Vorbereitung, Durchführung und Auswertung meiner Proben mittels PXRD. Gleicher Dank geht auch an Prof. Dr. Roland Marschall und Dr. Morten Weiß zur Durchführung der Festkörper-UV-Vis-Messungen sowie Dr. Jonathan Becker zur Messung und Auswertung meiner zahlreichen Einkristall-Proben.

Danken möchte ich auch Raoul Brand, Giovanni Parolin und Marvin Domanski, welche ich im Rahmen ihrer Bachelorarbeit, ihres Erasmus-Aufenthalts und ihrer Vertiefungsarbeiten betreuen durfte, für ihre Unterstützung meiner Projekte sowie die anregenden Diskussionen und Ideen.

Ganz herzlichen Dank geht an meine Kolleginnen und Kollegen sowie Ehemalige der gesamten Arbeitsgruppe Schindler, Dr. Christopher Gawlig, Markus Lerch, Frank Mehlich, Dr. Andreas Miska, Alexander Petrillo, Florian Ritz, Thomas Rotärmel, Stefan Schaub, Lars Schneider, Dr. Pascal Specht und Dr. Miriam Wern für das kollegiale Miteinander, die gute Arbeitsatmosphäre und die schönen Zeiten außerhalb der Laborarbeit. Besonderer Dank geht dabei an Annabelle Matter, Dr. Pascal Specht und Dr. Miriam Wern für das Korrekturlesen dieser Arbeit.

Abschließend möchte ich mich besonders bei meiner Familie und meiner Freundin bedanken, da sie mich während meines gesamten Studiums und der anschließenden Promotion unterstützt haben.



*„Der Sinn des Lebens besteht nicht darin ein erfolgreicher  
Mensch zu sein, sondern ein wertvoller.“*

Albert Einstein



## Table of Contents

Abstract .....	1
1. Introduction .....	3
1.1 Catalytic Reactions and Oxygen Activation .....	3
1.2 Oxygen Activation in Biological Processes .....	4
1.3 Copper in Biological Systems .....	6
1.4 Dioxygen Activation in Copper Enzymes .....	8
1.4.1 Non-Coupled Binuclear Copper Active Sites .....	9
1.4.2 Coupled Binuclear Copper Active Sites .....	11
1.5 Cu/O <sub>2</sub> Model Complexes .....	13
1.5.1 Mononuclear Model Complexes .....	13
1.5.2 Binuclear Model Complexes .....	16
1.6 Benzaldehyde - Application and Production .....	19
1.7 Immobilization of Active Species .....	21
2. Research Goals .....	25
3. Immobilization of a copper complex based on the tripodal ligand (2-aminoethyl)bis(2-pyridylmethyl)amine (uns-penp) .....	27
4. Characterization of copper complexes with derivatives of the ligand (2-aminoethyl)bis(2-pyridylmethyl)amine (uns-penp) and their reactivity towards oxygen .....	41
5. References .....	55

### Abstract

Benzaldehyde is an important basic compound in the chemical industry. However, established synthetic processes still have some disadvantages such as high resource consumption and non-selective material conversion. In the context of advancing *green chemistry*, there is a necessity of a more resource-conserving method for selective syntheses. Biological systems for activating atmospheric oxygen, such as copper-containing enzymes, are promising models to be industrially used a selective oxygenation by means of model complexes. However, so far only a low material conversions and high catalyst consumption have been achieved, so that further research in this area is essential.

For this reason **Chapter 3** extends the concept of dioxygen activation by copper complexes with tripodal ligands. The ligand (2-aminoethyl)bis(2-pyridylmethyl)amine (uns-penp) was bound covalently to silica gel for this purpose. The immobilization should counteract the self-decomposition and promote the formation of a stable *end-on* superoxido species. Here, the resulting copper complexes showed reversible oxygen binding through the formation of a dark green solid at -80 °C. Oxygenation of toluene to benzaldehyde could be carried out by suspending the oxygen species in toluene. Mobile complexes with uns-penp derivatives as comparison resulted in higher conversions, but offered a lower purity of the product mixture.

**Chapter 4** deals with the derivatization of the uns-penp ligand at the terminal nitrogen atom and its influence on the oxygen activation. Identical aliphatic groups and the attachment of ferrocene as well caused a passivation of the solid complex. However, different aliphatic substituents usually led to a reversible oxygen attachment, though the resulting species could not be finally characterized. Substitution of an ethyl- and an isopropyl residue allowed the rapid formation of an *end-on* peroxido complex in the solid state. In contrast to similar compounds the crystal structure remained almost unchanged during the reaction, which allowed a characterization by X-ray crystallographic analysis.

## Zusammenfassung

Benzaldehyd ist eine wichtige Grundchemikalie der chemischen Industrie. Etablierte Syntheseverfahren bergen jedoch nach wie vor einige Nachteile wie hoher Ressourcenverbrauch und nichtselektiver Stoffumsatz. Im Rahmen der fortschreitenden *Grünen Chemie* besteht somit Bedarf an einer rohstoffschonenderen Methode zur selektiven Synthese. Biologische Systeme zur Aktivierung von atmosphärischem Sauerstoff, wie kupferhaltige Enzyme, erweisen sich als aussichtsreiche Vorbilder, selektive Oxygenierung durch Modellkomplexe industriell nutzbar zu machen. Bisherige Anstrengungen offenbarten bislang geringe Stoffumsätze und einen hohen Katalysatorenverbrauch, was weitere Forschungen auf diesem Gebiet notwendig machte.

Hierfür erweitert **Kapitel 3** das Konzept der Sauerstoffaktivierung durch Kupferkomplexe mit tripodalen Liganden. Der Ligand (2-aminoethyl)bis(2-pyridylmethyl)amin (uns-penp) wurde hierzu kovalent auf Kieselgel gebunden. Die Immobilisierung sollte der Selbstersetzung entgegenwirken und die Bildung einer stabilen *end-on* Superoxidospezies begünstigen. Dabei zeigten die resultierenden Kupferkomplexe eine reversible Sauerstoffanbindung unter Bildung eines dunkelgrünen Feststoffs bei  $-80\text{ °C}$ . Durch Suspension der Sauerstoffspezies in Toluol konnte eine Oxygenierung von Toluol zu Benzaldehyd durchgeführt werden. Mobile Komplexe mit uns-penp Derivaten ergaben im Vergleich höhere Umsätze, wiesen jedoch eine niedrigere Reinheit des Produktgemischs auf.

**Kapitel 4** behandelt die Derivatisierung des uns-penp Liganden am terminalen Stickstoffatom und deren Einfluss auf die Sauerstoffaktivierung. Identische aliphatische Gruppen führten zu einer Passivierung im Festkörper, ebenso die Anbringung von Ferrocen. Unterschiedliche aliphatische Substituenten führten jedoch meist zu einer reversiblen Sauerstoffanbindung, wobei die entstehende Spezies nicht abschließend charakterisiert werden konnte. Substitution eines Ethyl- und eines Isopropylrestes erlaubte die schnelle Bildung eines *end-on* Peroxidokomplexes im Festkörper. Im Gegensatz zu vergleichbaren Substanzen, blieb die Kristallstruktur während der Reaktion nahezu unverändert, was eine röntgenkristallografische Analyse erlaubte.

### 1. Introduction

#### 1.1 Catalytic Reactions and Oxygen Activation

Catalytic processes play an important role in biology and chemical industry. Chemical catalysis has been ubiquitous since the dawn of human civilization e.g. fermentation to produce alcoholic beverages like beer and wine.<sup>[1]</sup> Some historians even see the development of beer brewing as a driving force in social development.<sup>[2]</sup> The term *catalysis* was coined 1835 by Jöns Jakob Berzelius, the father of modern chemistry, and originates from the Greek words “*kata*” and “*lyein*” meaning “*loose down*”.<sup>[3]</sup> Today, the implementation of catalytic processes still is a wide field of interest: 60% of today’s chemical products and 90% of current chemical processes are performed by catalysis-based chemical syntheses.<sup>[1]</sup> Thus, catalytic processes play an essential role in the chemical industry, which in turn plays an essential role in every national economy in the western states (e.g. USA: 10% of national manufacturing).<sup>[4]</sup>

Since the beginnings of industrial catalysis in the middle of the 18<sup>th</sup> century (*lead-chamber process*)<sup>[1]</sup>, the activation of small molecules like O<sub>2</sub>, NO, CO<sub>2</sub> and H<sub>2</sub> has become a crucial field of interest. Especially the activation of dioxygen attracted attention due to its clear benefits: it is an ideal oxidant as it produces only benign by-products (e.g. water); in addition, it is available in large quantities as a major constituent of the atmosphere (21%).<sup>[5,6]</sup> Thus, the activation of atmospheric oxygen in chemical processes is an important contribution to *green chemistry*.<sup>[7]</sup>

A major task is the activation of the commonly kinetic non-active dioxygen molecule to synthesize oxygen containing products.<sup>[8]</sup> In the ground state, dioxygen has two unpaired electrons in the  $\pi^*$  molecular orbital and possesses therefore a triplet spin state (Figure 1A). A direct reaction of dioxygen with e.g. carbon is kinetically hindered as the most carbon-oxygen products show a closed shell electronic configuration and therefore a singlet spin state. These reactions are *spin forbidden*.<sup>[9]</sup> To perform oxygen inserting reactions dioxygen has to be converted into an activated state. Figure 1 shows three possible electronic states of the dioxygen molecule.

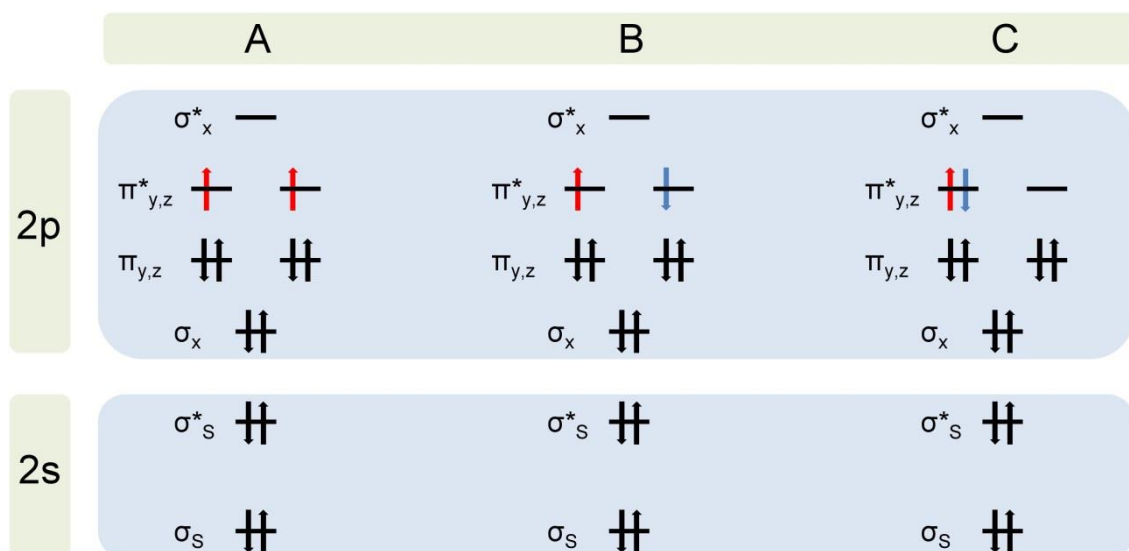
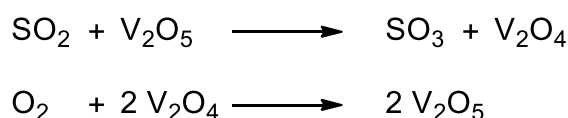


**Figure 1.** Electron configuration of the dioxygen molecule: **A** triplet (ground) spin state of dioxygen ( ${}^3\Sigma_g^-$ ), **B** singlet (excited) spin state with two electrons with different spin in each of the two  $\pi^*$  orbitals ( ${}^1\Sigma_g^+$ ), **C** singlet (excited) spin state with two coupled electrons in one  $\pi^*$  orbital ( ${}^1\Delta_g$ ). Redrawn according to reference.<sup>[9]</sup>

In industrial chemistry, oxygen inserting reactions are often supported by metal oxides. They are indispensable in various processes, e.g. refining, petrochemical processes and production of specialty chemicals.<sup>[10]</sup> An example of a large-scale use of metal oxides is the sulfuric acid ( $\text{H}_2\text{SO}_4$ ) production: the desired sulfur trioxide is obtained by oxygen insertion *via* a vanadium pentoxide catalyst  $\text{V}_2\text{O}_5$ . The generated  $\text{V}_2\text{O}_4$  will be reactivated by contact with dioxygen (Scheme 1).<sup>[11]</sup>



**Scheme 1.** Oxidation of sulfur dioxide *via* vanadium pentoxide  $\text{V}_2\text{O}_5$ . The catalyst can be re-obtained by oxidation with dioxygen.<sup>[11]</sup>

## 1.2 Oxygen Activation in Biological Processes

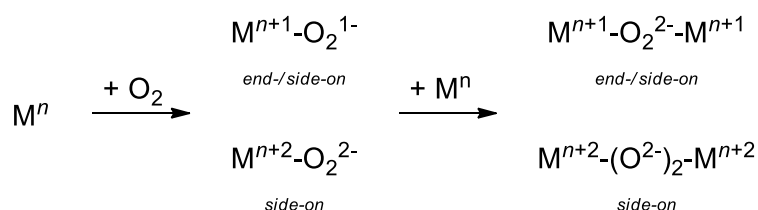
Particularly in nature the activation of the omnipresent dioxygen plays an important role in several processes, like respiration chain and the biosynthesis of proteins. In enzymes the oxygen activation takes place by means of transition metals. However, in these biological systems the metal ions are not present in form of oxides. But they are complexed within an organic framework instead.<sup>[12]</sup> The abundance and

## 1. Introduction

---

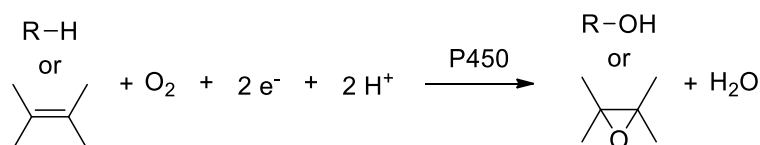
bioavailability of metal ions in the earth's crust is a crucial factor of the application into biological systems. Therefore, transition metals that can be found in living organisms are mainly iron, nickel, manganese, zinc and copper. Elements such as aluminium in fact own a great abundance but due to its natural appearance it is not available for biosynthesis.<sup>[13]</sup>

The actual activation of dioxygen takes place *via* the coordination at a complexed metal center (active site). The type of activation depends on the central ion, the ligand and its denticity. Scheme 2 shows the reaction of the metal ion of the active site with dioxygen (inside a protein or any complex). First, predominantly a mononuclear species occurs as an intermediate, which may further react with another metal centre to a binuclear species.<sup>[9,14,15]</sup>



**Scheme 2.** Reaction of a complexed metal ion with dioxygen. The formed mononuclear species may react further with another complex to form a binuclear species. The coordination of the dioxygen molecule can occur in an *end-on* (only one oxygen atom is connected to the metal ion) or in a *side-on* fashion (both oxygen atoms are connected to the metal ion)<sup>[9,14,15]</sup>

Because of its relative abundance in the earth's crust (4.7%), iron is an important element for the biological oxygen activation.<sup>[16]</sup> The most prominent representative is haemoglobin, which is found in red blood cells and acts as an oxygen carrier.<sup>[17]</sup> Iron-containing proteins can also act as catalysts in various biosyntheses, such as in the enzymes of the P450 family, which perform epoxidations, hydroxylations and heteroatom oxidations (Scheme 3).<sup>[18]</sup>



**Scheme 3.** Schematic equation of P450 catalyst reaction of alkanes and carbon double bonds.<sup>[19]</sup>

In addition to iron, other transition metals in the active centres of proteins and enzymes are capable to activate dioxygen. For example some organisms use manganese containing oxidases in the oxalate metabolism.<sup>[20]</sup> Moreover, manganese plays an important role in the oxidation of the oxygen in the water molecule during photosynthesis.<sup>[21]</sup> Nickel-containing enzymes can also activate dioxygen and serve as dioxygenases in some soil bacteria.<sup>[22]</sup>

The ability to activate atmospheric oxygen makes these metal complexes constant subjects of research.<sup>[17,23]</sup> In contrast to the “inorganic way”, the mild conditions for oxygen activation make corresponding model complexes promising candidates for industrial use. However, a few decades ago, another transition metal moved into the focus of research, which was supposed to combine all these properties: copper.

### 1.3 Copper in Biological Systems

Copper is a much less abundant transition metal compared to iron (0.0047% in earth’s crust).<sup>[16]</sup> Nevertheless, it is an essential trace element of organic life. The daily intake of a human body is about 0.6 to 1.6 mg, of which 55 to 75% is absorbed by the digestive tract.<sup>[24]</sup> Copper can be described as a modern bio-element because it first became bioavailable with the occurrence of photosynthesis and the resulting oxidation of copper(I) to copper(II). As a result dioxygen activating enzymes like monooxygenases, dioxygenases and oxidases contain copper ions in their active sites.<sup>[25]</sup> Further copper proteins are involved in electron transferring reactions (ET), NO<sub>2</sub><sup>-</sup> and N<sub>2</sub>O reduction, and substrate activation.<sup>[26]</sup>

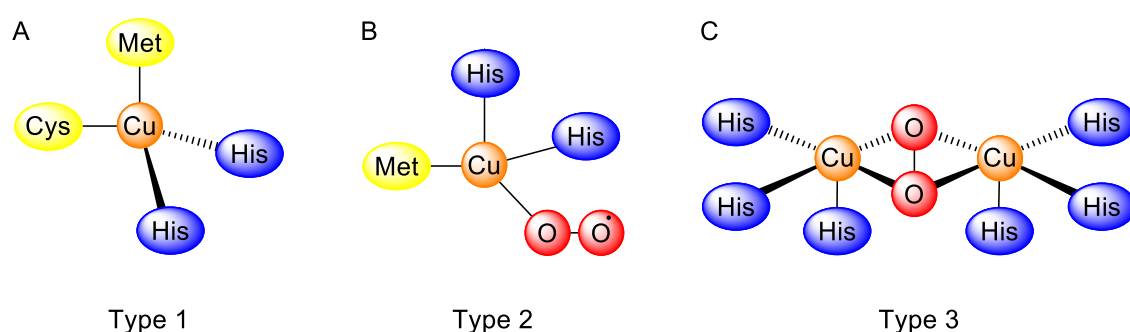


**Figure 2.** Examples for the three different copper protein types: **A** type 1: plastocyanin;<sup>[27]</sup> **B** type 2: *end-on* superoxido-bound in peptidylglycine  $\alpha$ -hydroxylating monooxygenase (PHM);<sup>[28]</sup> **C** type 3: *side-on* peroxido-bound in binuclear tyrosinase.<sup>[29]</sup>

## 1. Introduction

---

Historically, copper proteins were classified into three classes depending on their spectroscopic properties and functions. Figure 2 gives an overview of their general structures.

Type 1 copper proteins have been referred to as *blue proteins* due to their strong LMCT (ligand metal charge transfer) between the copper centre and the attached cysteinate ligand. They are involved in electron transferring reactions and mostly appear in small proteins, such as plastocyanin (Figure 2A).<sup>[27,28]</sup> The ligand coordination leads to a distorted tetrahedral structure. However, Cu(II) species often prefer a square-planar geometry whereas Cu(I) prefers a tetrahedral one. Therefore, this structure has to be seen as a compromise between both geometries.

Type 2 copper proteins are coordinated mainly in a square-planar manner (Figure 2B).<sup>[28]</sup> Since there is no thiolate group in the coordinating ligands, those copper proteins are referred to as *non-blue proteins* due to the absence of a strong LMCT. Here, the colour is caused by symmetry forbidden d-d transitions of the copper ion. They can function as oxidases by reducing oxygen to water or peroxide (e.g. amine oxidase) or oxygenases which insert oxygen into a substrate (e.g. peptidylglycine  $\alpha$ -hydroxylating monooxygenase (PHM)).<sup>[28]</sup> Additionally type 2 proteins can promote the dismutation of superoxides (e.g. superoxide dismutase (SOD)).<sup>[27]</sup>

Type 3 proteins possess two antiferromagnetic coupled copper centres, bridged by dioxygen or hydroxyl (Figure 2C).<sup>[28]</sup> The oxygen carrier hemocyanin in invertebrates is an example of a type 3 protein. One copper centre is coordinated by three histidine residues, oxygen will be inserted in a *side-on* way.<sup>[25,27]</sup> Type 3 proteins can also act as oxygenase and oxidase. One example of an oxygenase and oxidase as well is the enzyme tyrosinase which catalyses the hydroxylation of monophenols (e.g. tyrosine) as well as the oxidation of catechols to quinones. Investigations on this protein led to the first proof of dioxygen activation *via* a copper containing enzyme in 1955.<sup>[30]</sup>

Further development of crystallographic and spectroscopic methods, extended the number of protein types. Type 4: a combination of type 2 and 3 leads to a trinuclear cluster (e.g. laccase, ceruplasmin); Cu<sub>A</sub>: two copper ions, bridged *via* two cysteine residues, form a mixed-valence species with a formal copper oxidation state of +1.5.

Its function is a long-range electron transfer (e.g. the cytochrome c oxidase); Cu<sub>B</sub>: the copper centre is coordinated by three histidine residues; the fourth position is directly connected to the iron centre of cytochrome c oxidase. It is responsible for the dioxygen reduction; Cu<sub>Z</sub>: copper cluster consisting of four ions. It functions the reduction of N<sub>2</sub>O to N<sub>2</sub> in nitrous oxide reductase.<sup>[31]</sup>

### 1.4 Dioxygen Activation in Copper Enzymes

As the reaction with dioxygen and most organic substrates is kinetically hindered, the major task of enzymes is the conversion of the common triplet state of dioxygen into a more reactive state. Copper proteins are capable to activate dioxygen in different ways. The most common species appear in mono- and binuclear fashion. Figure 3 shows the most common copper oxygen species. However, only two of the six displayed complexes have proven their biological relevance: copper *end-on*  $\eta^1$ -superoxido and *side-on*  $\mu$ - $\eta^2$ : $\eta^2$ -peroxido.<sup>[32]</sup>

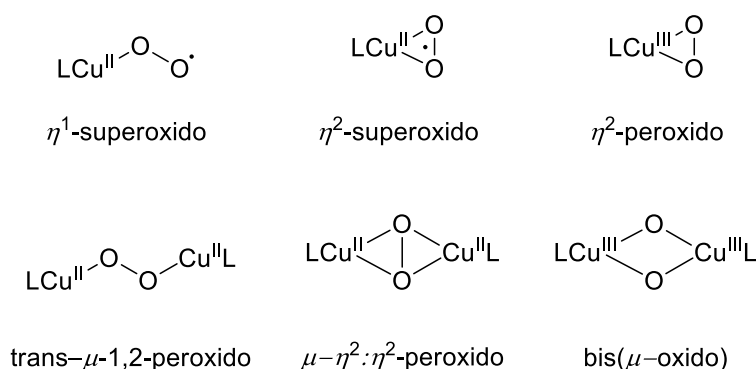


**Figure 3.** Copper oxygen species formed by the reaction with the active site of a copper containing complex with molecular dioxygen.<sup>[33]</sup>

The dioxygen activation mainly occurs by *coupled* and *non-coupled binuclear* copper active sites. Figure 4 gives some examples of oxygen activations, which are catalysed by copper-containing enzymes and proteins.

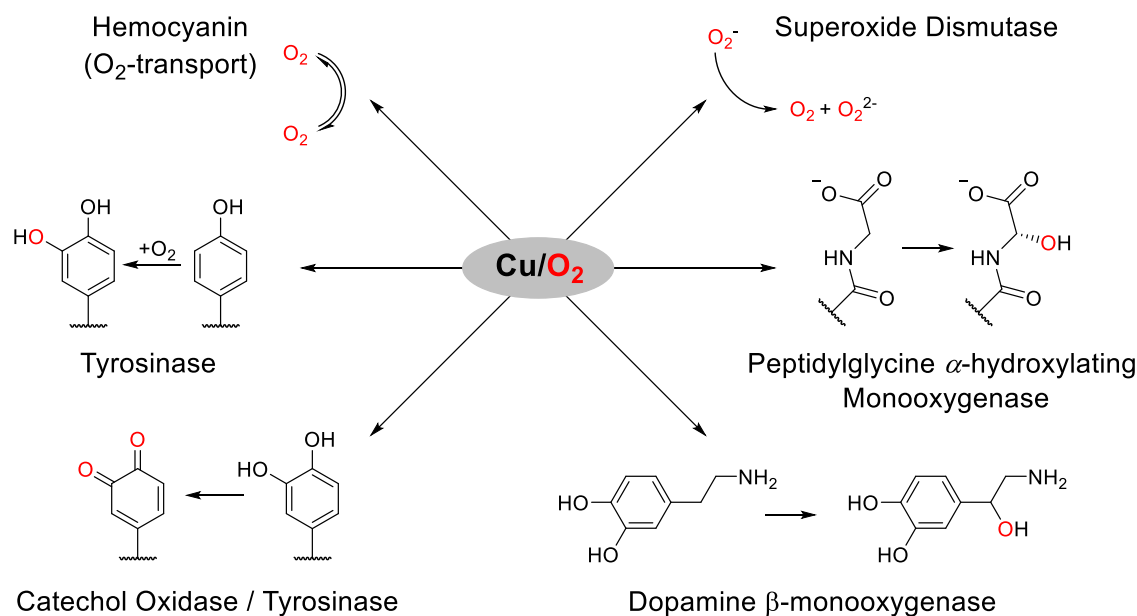


**Figure 4.** Copper catalysed dioxygen activation. Left side of the picture displays reactions with proteins containing two coupled copper ions in their active sites. Right side of the picture displays the species with two uncoupled copper ions.<sup>[33]</sup>

### 1.4.1 Non-Coupled Binuclear Copper Active Sites

Proteins with one copper ion in their active site capable to coordinate dioxygen predominantly occur in oxygen transferring processes. Examples of these systems are the enzymes PHM, dopamine  $\beta$ -monooxygenase (D $\beta$ M), tyramine  $\beta$ -monooxygenase (T $\beta$ M, in insects) and lytic polysaccharide monooxygenases (LPMOs) (Figure 4).<sup>[34,35]</sup> These enzymes are capable of hydrogen abstraction of a CH-bond and the subsequent insertion of a hydroxide group. To cleave the strong CH bond ( $\sim 95 - 103$  kcal/mol) dioxygen is transferred into a  $\eta^1$ -superoxido species.<sup>[36]</sup> One  $\pi^*$  orbital of the dioxygen molecule overlaps with the  $d_{z^2}/d_{x^2-y^2}$  orbital of the copper ion.<sup>[33]</sup> This results in a weak  $\sigma$  bonding and in an energetically increased d orbital, while the other  $\pi^*$  orbital remains as non-bonding orbital. As the orbital splitting is not high enough to overcome the spin repulsion, the oxygen molecule appears in an activated triplet state. (see Figure 5, left).<sup>[37]</sup> This leads to a low lying half-occupied  $\pi^*_v$  orbital with high oxygen character that is primed for hydrogen abstraction.<sup>[38,39]</sup>

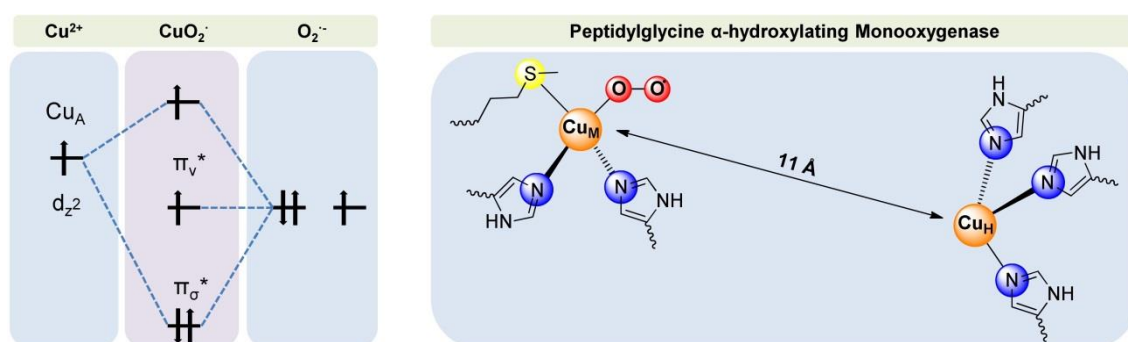


**Figure 5.** Left: orbital scheme of an *end-on* copper superoxido species. Since the energy gap between non- and antibonding orbitals is not high enough, the complex occurs in triplet state.<sup>[40]</sup> Right: active site of the copper containing enzyme PHM, dioxygen coordinates the copper ion  $\text{Cu}_M$ .<sup>[41]</sup>

Next to the dioxygen activating copper ion of PHM ( $\text{Cu}_M$ ), there exists another one in the active site ( $\text{Cu}_H$ ). The copper centre is located in a distance about 11 Å (hence the term *non-coupled binuclear*, Figure 5 right).<sup>[39]</sup>  $\text{Cu}_H$  is serving as an electron reservoir if a reaction requires a further reduction or as “structural” cofactor (in PHM).<sup>[42]</sup>

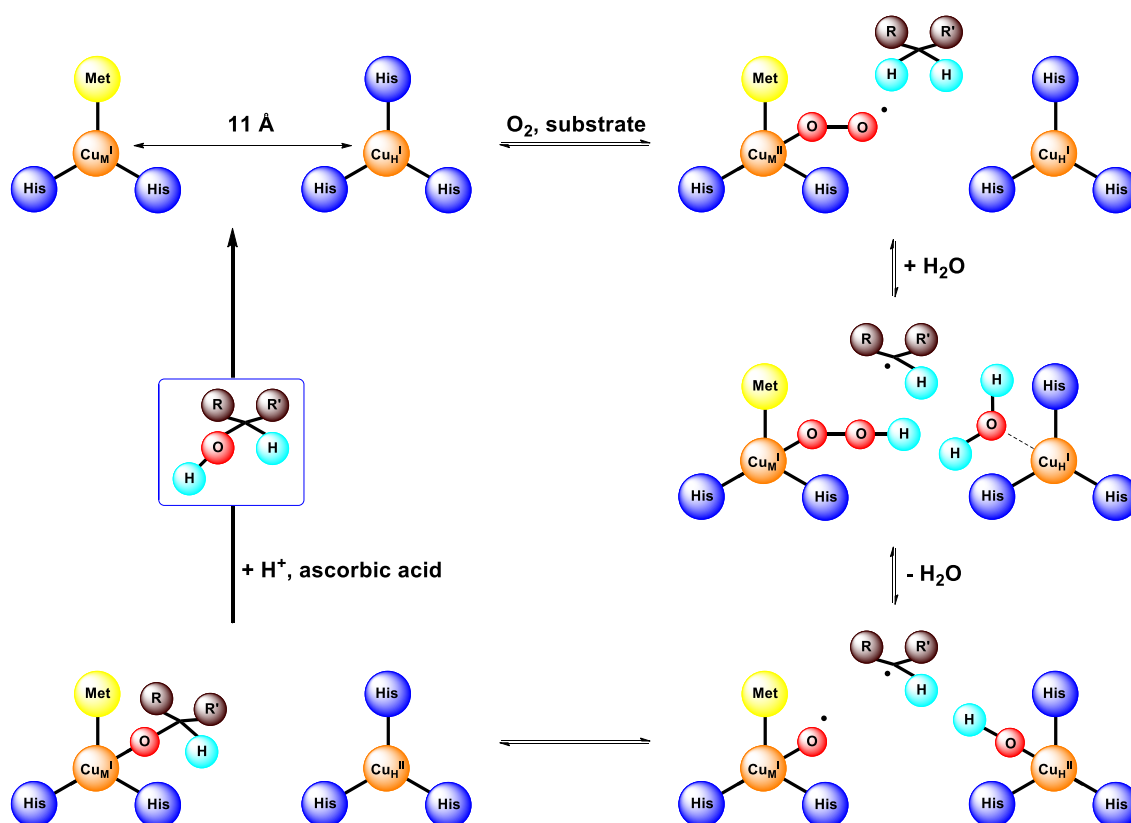


**Figure 6.** Mechanism of substrate hydroxylation *via* an *end-on* copper superoxido species in the *non-coupled binuclear* system of PHM and  $\text{D}\beta\text{M}$  proposed by Klingman. Redrawn according to reference.<sup>[43]</sup>

## 1. Introduction

The structure of the precatalytic complex was first structurally characterized in 2004 by Prigge *et al.*<sup>[44]</sup> In 2006 Klinman proposed a mechanism about the H atom abstraction with subsequent hydroxylation catalysed by PHM and D $\beta$ M (Figure 6).<sup>[43]</sup> However, there are different approaches and researches to elucidate the actual mechanism of substrate hydroxylation *via* PHM and D $\beta$ M are still in progress.<sup>[42]</sup>

### 1.4.2 Coupled Binuclear Copper Active Sites

Besides the activation of dioxygen by two *non-coupled* copper centres, dioxygen can also be activated by two paired copper ions, resulting in a  $\mu$ - $\eta^2$ : $\eta^2$ -peroxido (*side-on*) complex.<sup>[45]</sup> These systems are referred to as *coupled binuclear* copper active sites. In contrast to a mononuclear species, these perform a change in the spin state of the dioxygen molecule (Figure 7).

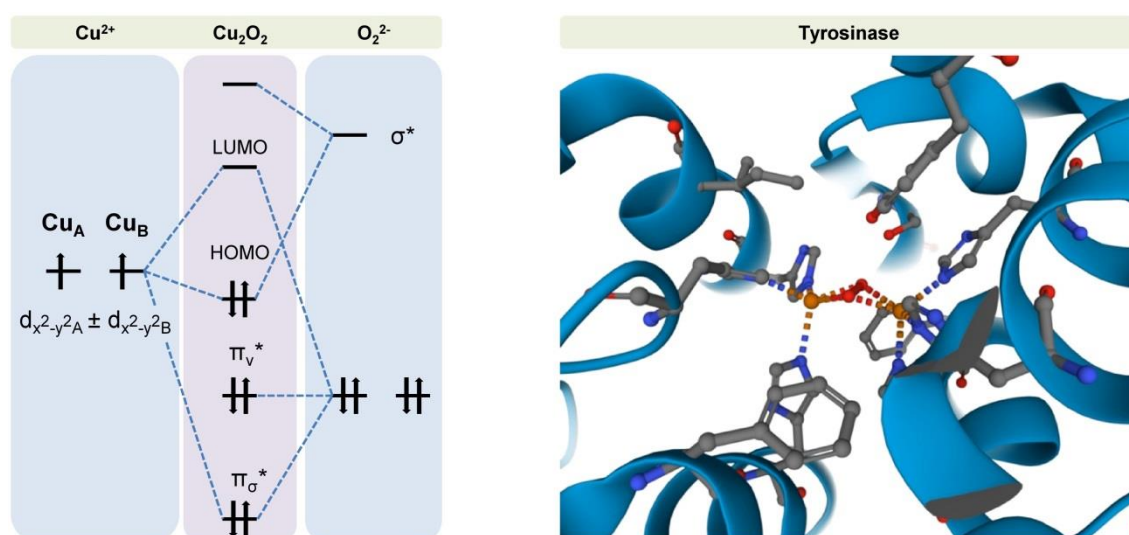


**Figure 7. Left:** orbital scheme of a *side-on* copper peroxido species. HOMO/ $\sigma^*$  interaction leads to weaker O-O bond.<sup>[26]</sup> **Right:** active site of the copper containing enzyme tyrosinase, dioxygen coordinates the copper in “type 3” way, PDB ID: 1WX4. Image from the RCSB PDB (rcsb.org, accessed on: 19 July 2021) of PDB ID 1WX4<sup>[46]</sup> created with Mol\*<sup>[47]</sup>.

One  $\pi^*$  orbital of the peroxide anion overlaps with the  $d_{x^2-y^2}$  orbitals of the two copper ions resulting in a strong  $\sigma$  bonding. The other  $\pi^*$  orbital remains in energy as non-bonding orbital. Although the electron density at the  $\pi^*$  orbital is lowered, the oxygen bond is weakened. This can be explained by a bonding/antibonding interaction of the  $\sigma^*$  orbital of the peroxide with the HOMO of the copper ion. This transfers electron density from the copper ions to the peroxide  $\sigma^*$  bonding and in turn

causes the weaker O-O interaction.<sup>[39]</sup> The conversion into the singlet spin state is initialized by a large HOMO/LUMO splitting which leads to an antiferromagnetic exchange of the copper centres and thus overcomes the spin repulsion (Figure 7, left).

Two representatives of *coupled binuclear* copper active sites are the molecules hemocyanin which acts as an oxygen carrier in invertebrates and tyrosinase (Figure 7, right) which is involved in the tanning process of skin and fruits.<sup>[46]</sup> Although both proteins activate dioxygen in the same way, they show significant differences in reactivity towards substrates: hemocyanin only serves to transport dioxygen, without any reactivity towards substrates, whereas tyrosinase is capable to oxygenate and oxidize substrates.<sup>[39]</sup> The reaction mechanisms of phenol oxygenation and oxidization by tyrosinase is shown in Figure 8.<sup>[48]</sup>

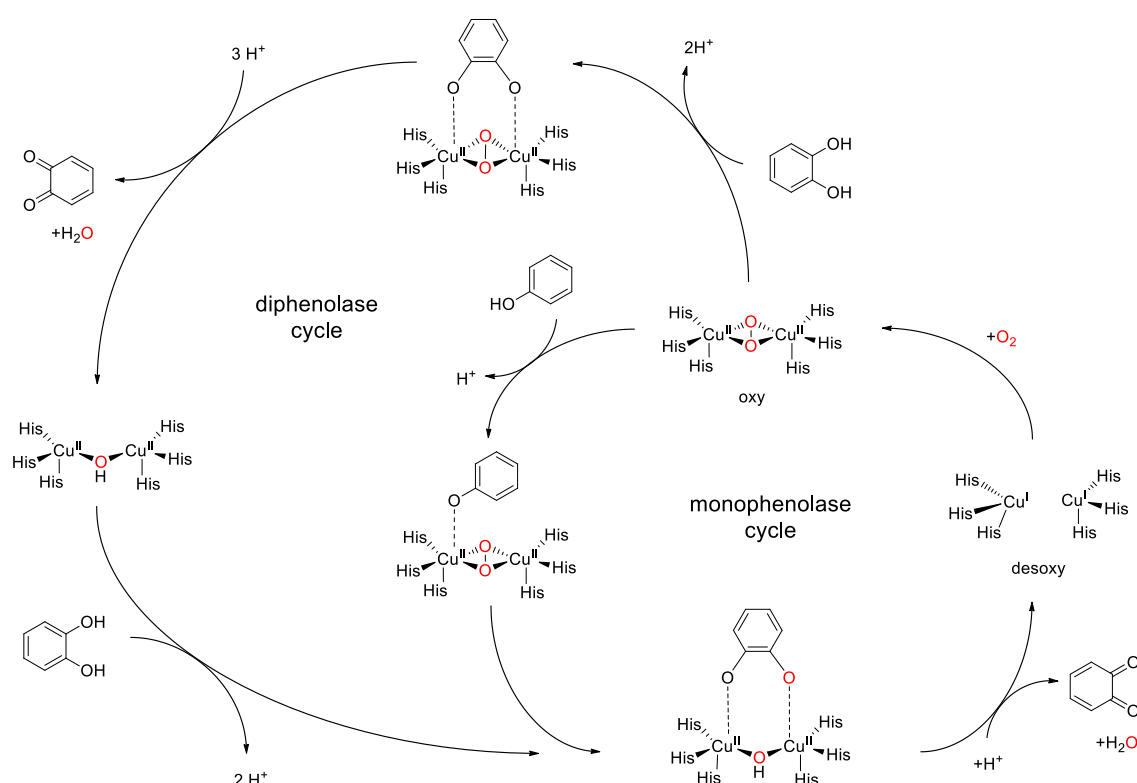


**Figure 8.** Bio catalytic activities of tyrosinase depicted as two interpenetrating cycles. Redrawn according to reference.<sup>[48]</sup>

Reasonable for the different reactivity is the surrounding protein structure: the active site of tyrosinase is accessible for external substrates, whereas the active center of hemocyanin is deeply buried in the protein matrix and thus inaccessible to external

substrates.<sup>[48]</sup> However, Decker *et al.* revealed an oxidizing performance of “activated” hemocyanin in some chelicerates.<sup>[49]</sup>

### 1.5 Cu/O<sub>2</sub> Model Complexes

Due to the capability of selective oxygenation and oxidation under benign conditions model complexes based on their biological role models have been a broad field of research over the last decades.<sup>[50]</sup> Particular interest is placed on the productions of commercially crucial chemicals, such as phenol or adipic acid.<sup>[51–53]</sup> The dioxygen activation *via* model complexes is a well characterized procedure. In general, it takes place *via* the formation of a superoxido complex, which then reacts with a second Cu(I) unit to form a *binuclear* species, often a peroxido complex (Scheme 2 and Figure 3).<sup>[33]</sup>

#### 1.5.1 Mononuclear Model Complexes

Mononuclear systems mimic the features of *non-coupled binuclear* copper active sites in PHM and DβM. The activation of dioxygen occurs in three forms (Figure 9) with different electronic properties: *end-on* coordination leads to a superoxido species with triplet spin state (Figure 9A), whereas the *side-on* coordination commonly causes a singlet spin state due to a greater overlap of the  $\pi^*$  with the  $d_{x^2-y^2}$  orbital leading to a larger orbital splitting which overcomes the spin repulsion (Figure 9B).<sup>[26]</sup> However, if the energy difference is not large enough, the triplet spin state remains.<sup>[54]</sup> The first *side-on*  $\eta^2$ -superoxido was isolated and characterised by Kitajima and co-workers in 1994.<sup>[55]</sup> Utilization of sterically demanding ligands is necessary which prevent the dimerization, the formation of *binuclear* species (Scheme 2). Although no biological model of a *side-on* superoxido has been detected yet, some of these oxygen species are capable to H-abtract as well.<sup>[54,56]</sup> Further raising of the  $d_{x^2-y^2}$  orbital with stronger donor ligands leads to a copper(III) species and a peroxide anion (Figure 9C).<sup>[26,57]</sup> The copper-oxygen species depends on a variety of factors, e.g. the shape of the ligand, the type of donor atoms and denticity (two or three donating atoms generally lead to a *side-on* species, four donating atoms lead to an *end-on* activation).<sup>[33]</sup>

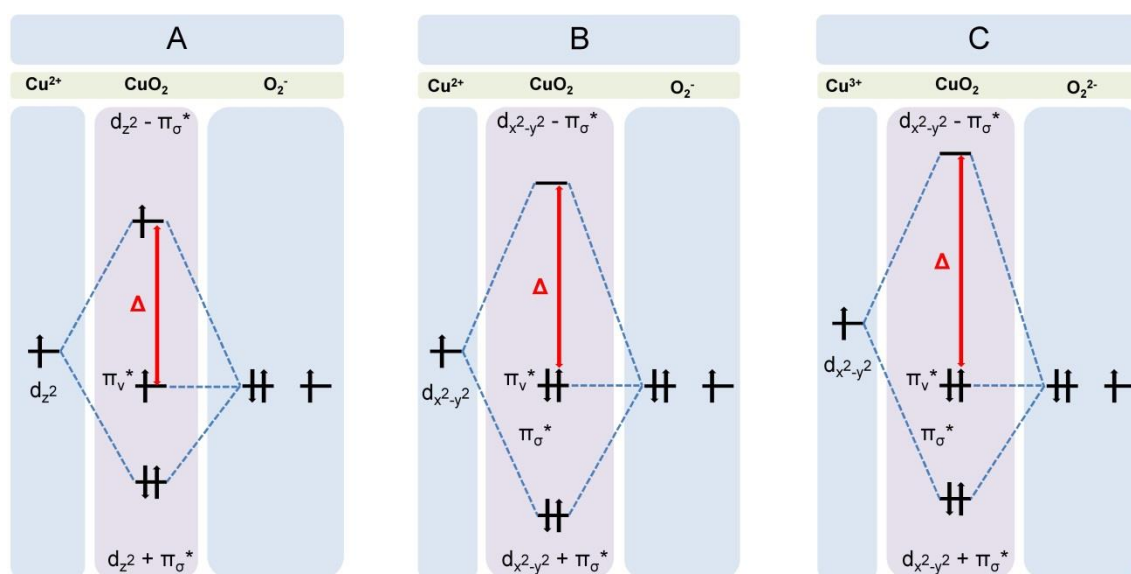


**Figure 9.** Molecule orbital scheme of mononuclear copper oxygen centres, **A**  $\eta^1$ -superoxido (*end-on*), **B**  $\eta^2$ -superoxido (*side-on*), **C**  $\eta^2$ -peroxido (*side-on*). The *end-on* species possesses a triplet spin state, *side-on* complexes generally a singlet spin state. Redrawn according to reference [26]

However, copper  $\eta^1$ -superoxido complexes best model compounds for the active site of *non-coupled binuclear* enzymes such as PHM and D $\beta$ M. Especially the research group of Karlin was quiet successful in the field of mimicking these oxygen adducts by stabilizing the superoxido intermediate (Scheme 2).<sup>[32,50,58]</sup> For this purpose the ligand tmpa (tris(2-pyridylmethyl)amine, Figure 10, left) was modified:<sup>[59,60]</sup> The  $\alpha$  position of the pyridine ring was substituted with several residues to establish a secondary coordination sphere which either contains sterically bulky residues or hydrogen bonding moieties. Especially strong and multiple H-bonding residues were stabilizing the superoxido intermediate and enhanced the H-abstraction ability of strong OH- and weak CH-bonds. A more accurate model of PHM and D $\beta$ M could be synthesized by replacing a nitrogen donor with a thioether. Dioxygen will be activated in a superoxido fashion which features H-abstraction capability.<sup>[41,61]</sup>

Since activated PHM and D $\beta$ M shows a four-coordinate tetrahedral geometry, Itoh *et al.* synthesized a tridentate ligand (without sterically bulky or electron-donating substituents) which stabilizes the superoxido species by forming a distorted tetrahedron (1-(2-*p*-X-phenethyl)-5-(2-pyridin-2-ylethyl)-1,5-diazacyclooctane ( $L^{\text{Phe(X)}}$ , Figure 10, middle). The activated complex also possesses H-abstraction abilities.<sup>[62-64]</sup>

## 1. Introduction

---

The first structural characterization of an *end-on* superoxido copper complex was performed by the research group of Schindler. Stabilization was achieved using the TMG<sub>3</sub>tren ligand (tris(tetramethylguanidino)tren, Figure 10, right) which contains sterically bulky superbasic guanidino residues.<sup>[65,66]</sup> In solution the complex exhibits a reversible oxygen binding ability. The activated oxygen complex also performs H-abstraction.<sup>[58,67]</sup>

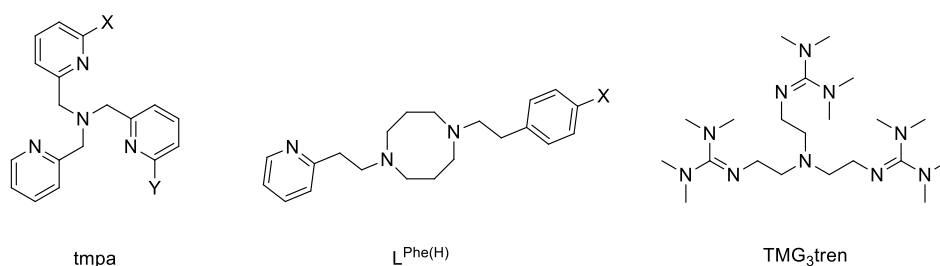


**Figure 10.** Basic forms of ligands, which stabilize, copper superoxido complexes that perform hydrogen abstraction of CH-bondings. **Left:** tmpa, X and Y implicates the addition of sterically bulky, electron donating or H-bonding residues.<sup>[61]</sup> **Middle:** tridentate nitrogen ligand reported by Itoh and co-workers, which mimics structural backbone of PHM without strong steric and electronic effects. X implicates electron withdrawing or donating groups.<sup>[64]</sup> **Right:** TMG<sub>3</sub>tren, reported by the research group of Schindler which supports the structural characterization of copper superoxido complexes with tripodal ligands.<sup>[66]</sup>

As mentioned above the substituents of the ligands play an important role in stabilizing the resulting oxygen adducts. Next to electron interacting and H-bonding groups, sterically demanding residues influence the stability. For example, the stepwise substitution of the pyridine rings by quinoline residues at the tmpa ligand influences the reactivity towards dioxygen:<sup>[68]</sup> the exchange of one or two pyridine rings still allows a reaction, whereas three attached quinoline residues make the complex resistant. Another factor which impacts the reactivity and stability is the geometry around the copper center. Recent studies revealed that trigonal bipyramidal geometries better support the formation of a reactive Cu-OOH species than square-pyramidal structures.<sup>[69]</sup>

However, all demonstrated examples only show reactivity towards substrates at low temperatures. Therefore, the creation of a superoxido complex which is robust and producible at ambient conditions will be focused on in future research.

### 1.5.2 Binuclear Model Complexes

To mimic the reaction behaviour of *coupled binuclear* enzymes like tyrosinase and hemocyanin, two centred copper model complexes have been synthesized.<sup>[33]</sup> The activation of oxygen mainly occurs in three different ways:  $\mu\text{-}\eta^2\text{:}\eta^2$ -peroxido (*side-on*), trans- $\mu$ -1,2-peroxido (*end-on*) and bis( $\mu$ -oxido), as depicted in Figure 3. As mentioned above, to date only the *side-on* peroxido species has proven its biological relevance in binuclear systems. Therefore, this seems to be the most promising way to activate dioxygen with corresponding model complexes to imitate catalytic features. In 1989 Kitajima *et al.* published the first crystal structure of a synthetic copper *side-on* peroxido species (Figure 11, left).<sup>[70]</sup> Pioneering work in the catalytic application of these peroxido adducts were performed by Casella. He reported one of the earliest model systems which can hydroxylate substrates in the ortho position by using hexadentate polybenzimidazole ligands (Figure 11, right).<sup>[71]</sup>

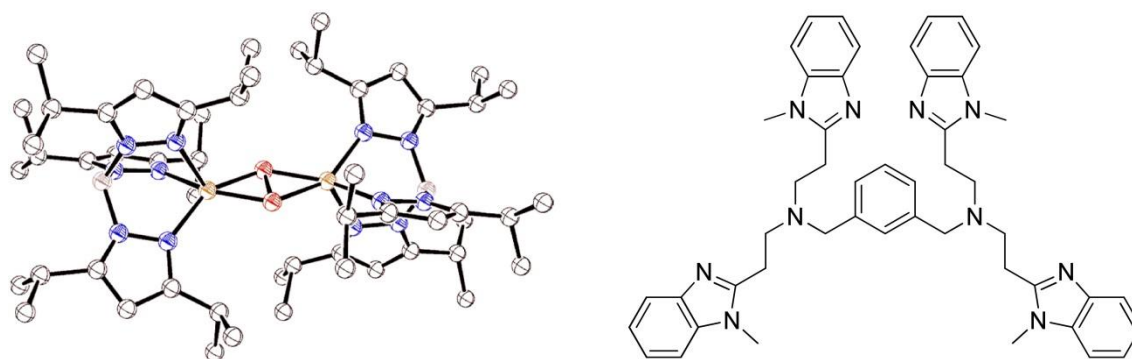


**Figure 11.** **Left:** ligand system of Kitajima *et al.* which demonstrates the first crystal structure of a *side-on* peroxido model complex.<sup>[70]</sup> **Right:** polybenzimidazole ligand of Casella. Resulting copper complexes forms *side-on* peroxido species which were capable for hydroxylation reactions.<sup>[71]</sup>

A  $\mu\text{-}\eta^2\text{:}\eta^2$ -peroxido species can be converted into a bis( $\mu$ -oxido) form by changing the solvent, the ligand (geometry, steric influence, electronic effects) and the anion. A lowered energy of the peroxido  $\sigma^*$  orbital leads to a cleavage of the dioxygen bonding. Simultaneously the copper centre will be oxidized (Cu(II) to Cu(III)).<sup>[33,72]</sup> Tolman and co-workers demonstrated that an equilibrium can exist between both species.<sup>[73]</sup> Current studies on particulate methane monooxygenase (pMMO) suggested that mixed valence copper bis( $\mu$ -oxido) intermediates are involved in the active site.<sup>[74]</sup>

## 1. Introduction

Due to its electrophilic character bis( $\mu$ -oxido) species are able to perform aromatic hydroxylation.<sup>[26]</sup> Holland *et al.* demonstrated the internal  $sp^2$ -hydroxylation of an aromatic ligand.<sup>[75]</sup> Schönecker *et al.* enhanced this synthesis to a regio and stereo selective  $\gamma$ -hydroxylation of a non-activated  $CH_2$  group. Furthermore his method allowed the conversion of substrates which can be separated from the ligand *via* cleaving an imine bonding.<sup>[76]</sup> Based on these findings Becker *et al.* enhanced this “*clip-and-cleave*” concept to the hydroxylation of non-activated aliphatic CH bonds in aldehydes (Figure 12).<sup>[77–79]</sup> The method of ligand hydroxylation *via* this copper oxygen adduct includes promising advantages, since it is useful for the modification of steroids and the syntheses of chemical feedstocks like salicylaldehyde and other compounds.<sup>[79–82]</sup>

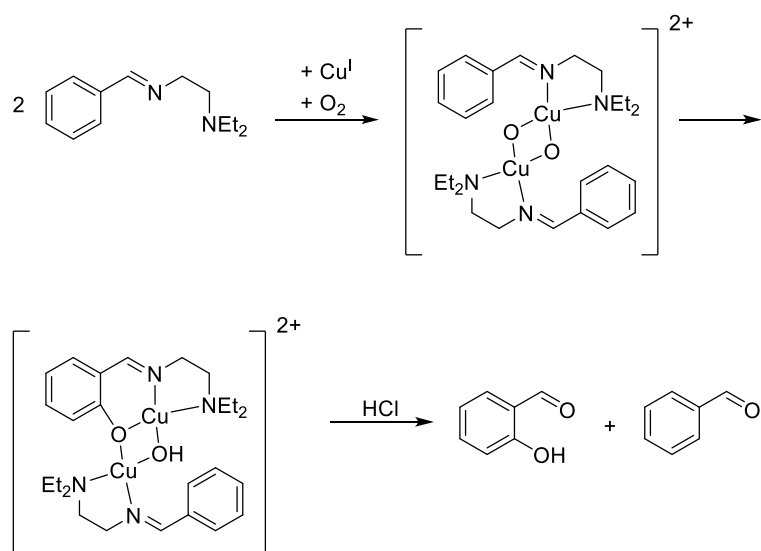


**Figure 12.** Mechanism of ligand hydroxylation via a bis( $\mu$ -oxido) intermediate. The products will be obtained by cleavage of the imine bond *via* acidic work-up. Redrawn according to reference.<sup>[78]</sup>

Before the first structures of the *side-on* oxygen species have been fully characterised, Karlin *et al.* reported on a *trans*  $\mu$ -1,2-peroxido copper complex utilizing tmpa ligand (see Figure 10, left).<sup>[83]</sup> Since there is no additional interaction between the antibonding  $\sigma^*$  orbital and the metal centre no attenuation of the O-O bonding occurs (Figure 13, left). The bond is even strengthened due to the donor interaction with the copper centre.<sup>[39]</sup>

Despite the enhancement of bond strengths and the nucleophilic character of the peroxido molecule, reactivity against CH-bonds was detected.<sup>[84]</sup> Lucas *et al.*

synthesized copper(I) *end-on* peroxido complexes with ligands derived from the tmpa structure. The activated species was directly dissolved into the substrate (toluene) at low temperatures (approximately  $-80\text{ }^{\circ}\text{C}$ ). Depending on electron-donating ability of the ligands and the geometry around the copper center, a conversion to benzaldehyde up to 40% was achieved.

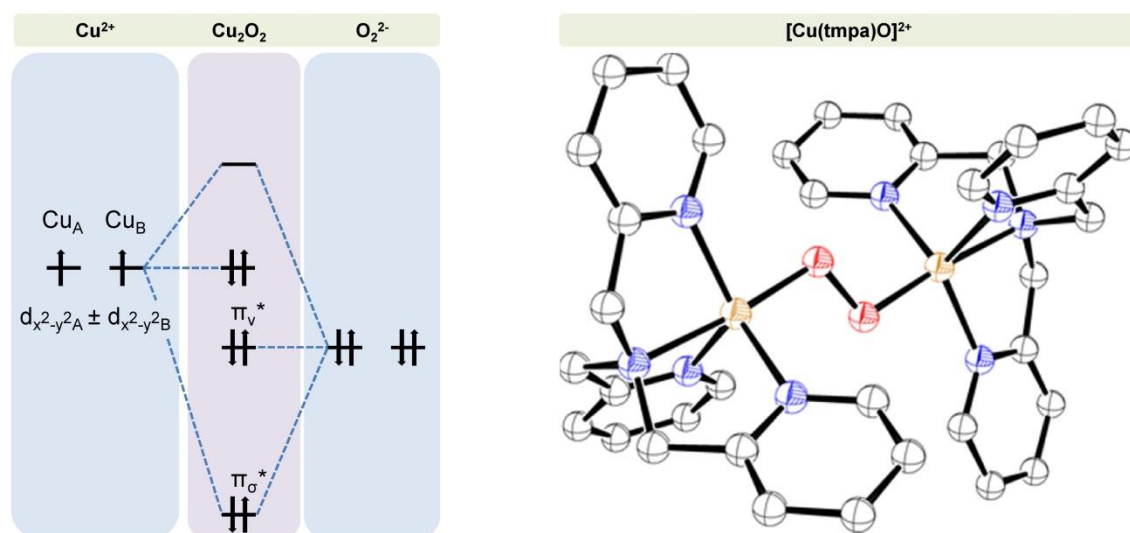


**Figure 13.** Left: electronic structure of the copper *end-on* peroxido species. EPR measurements revealed an antiferromagnetic coupling of the copper centres.<sup>[39]</sup> Right: crystal structure of  $[\text{Cu}(\text{tmpa})\text{O}]^{2+}$  *end-on* peroxido complex synthesized by the research group of Karlin.<sup>[83]</sup>

In 2004 Komiyama *et al.* succeeded in the stabilization of a solid copper *end-on* peroxido complex using sterically demanding substituents at a tren ligand.<sup>[85]</sup> Würtele *et al.* finally stabilized a solid copper *end-on* peroxido species by utilization of the sterically demanding anion tetraphenylborate.<sup>[86]</sup> It was directly obtained by treating the solid copper(I) complex with dioxygen. Suspending the solid in toluene at room temperature led to a conversion to benzaldehyde of 20%. As these oxygen species are nucleophiles the reactivity against toluene is noteworthy.<sup>[84]</sup> Karlin *et al.* offered two possible explanations (Figure 14): 1. Loss of the coordination of one ligand arm leads to the formation of a bis( $\mu$ -oxido) species which possesses the necessary electrophilicity.<sup>[87]</sup> 2. Decomposition into a copper(I) complex and another *end-on* superoxido species which is responsible for hydrogen abstraction and the subsequent benzaldehyde formation.<sup>[84]</sup> However, it was demonstrated an aromatic hydroxylation of electron-rich phenolates without the rearrangement of a *side-on* peroxido or *end-on* superoxido species is possible utilizing asymmetric *binuclear* complexes.<sup>[88]</sup>

## 1. Introduction

Selective CH-abstraction and subsequent hydroxylation is a challenging issue of current research. The targeted oxygenation of precursor molecules with molecular dioxygen is an important field of innovation within the scope of *green chemistry* to produce new and commercially crucial chemicals e.g. benzaldehyde.

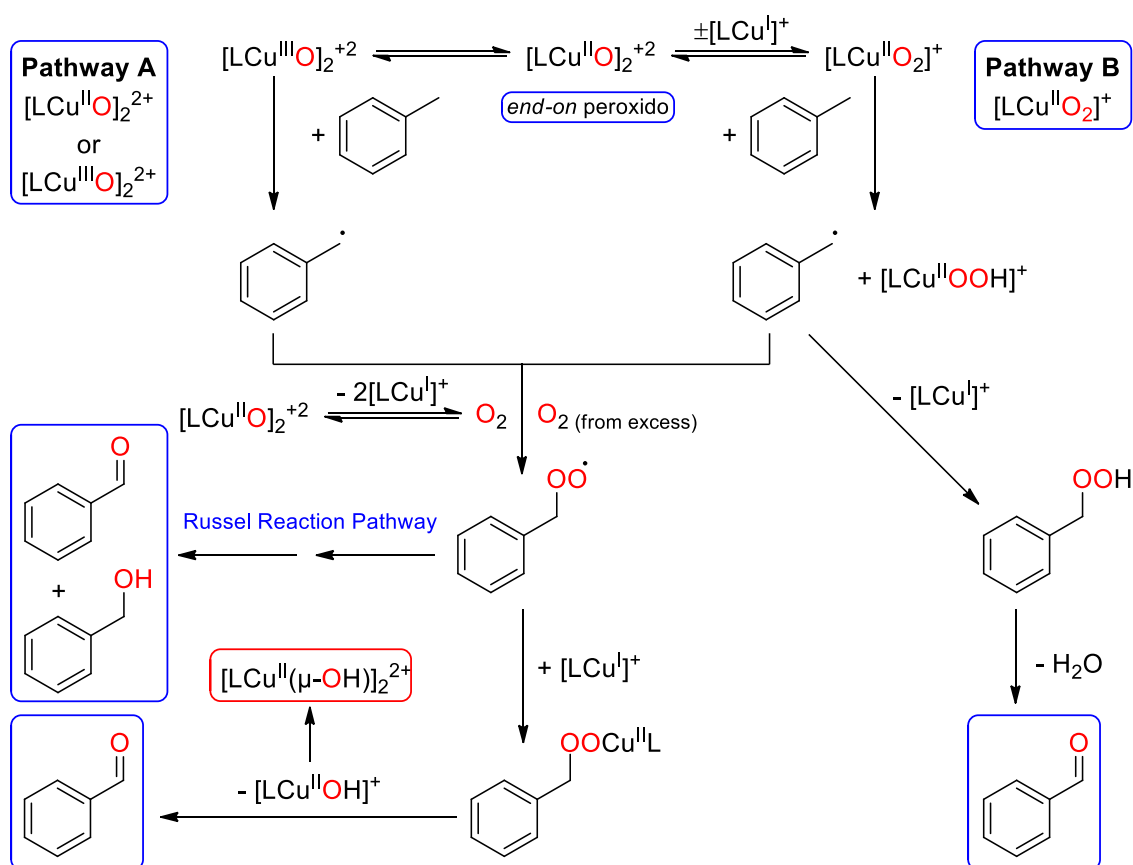


**Figure 14.** Mechanism describes two proposed pathways of toluene oxygenation through an *end-on* peroxido species: **A** hydrogen abstraction occurs *via* bis(μ-oxido) complex with subsequent bonding of molecular dioxygen. Toluene is generated either by disproportionation of the benzyl peroxy radical (Russell reaction) or by conducted reaction *via* copper(I) ligand (accessible due to equilibrium) and formation of bis(μ-hydroxido) complex. **B** Decomposition of complex liberates an active *end-on* superoxido species. Hydrogen abstraction with subsequent recombination with hydroperoxido radical leads to benzaldehyde and water. Original copper(I) complex will be released. Redrawn according to reference <sup>[84,87]</sup>

### 1.6 Benzaldehyde - Application and Production

The production of benzaldehyde and thus the selective oxygenation of toluene is an important field of research. Benzaldehyde is a crucial feedstock for important chemical processes: it is contained in many cosmetic products and foods.<sup>[89]</sup> Further it serves as a basic chemical for medicine (e.g. ephedrine) or flavour materials (e.g.

cinnamic aldehyde).<sup>[90,91]</sup> Next to vanillin, benzaldehyde is the second most produced flavour feedstock worldwide (~90.000 t/a).<sup>[92]</sup>

Benzaldehyde naturally occurs mostly chemically bonded in foods or some organic substances.<sup>[93]</sup> Liebig and Wöhler therefore succeeded in the first extraction from bitter almond oil.<sup>[94]</sup> Although the natural occurrence does not satisfy global demand, attempts are still being made to make these sources usable.<sup>[95]</sup> Today, most of the benzaldehyde is obtained by chlorination and subsequent hydrolysis of toluene or its direct oxidation *via* molybdenum oxides. Other methods like the Gattermann-Koch reaction are no longer industrially relevant (Figure 15).<sup>[90]</sup>

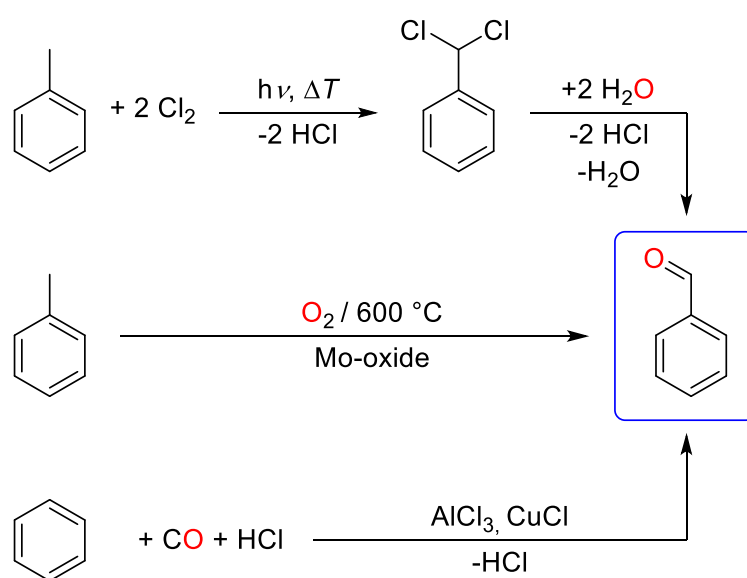


**Figure 15.** **Top:** chlorination of toluene with subsequent hydrolysis.<sup>[96]</sup> **Middle:** air-oxidation of toluene *via* Mo-oxide catalyst.<sup>[97]</sup> **Bottom:** Gattermann-Koch procedure, not very common anymore.<sup>[98]</sup>

Although these are well established industrial processes, they still have some disadvantages, such as high consumption of catalysts and the necessity of high pressure and temperature. Furthermore unselective oxidation causes a lot of side products and impurities. Several approaches to enhance the selective oxygenation of toluene have been reported over the last years e.g. with the utilization of different metal oxides or the treatment with high oxygen pressure without a catalyst in a gas-liquid reaction.<sup>[99,100]</sup> Selective conversions to benzaldehyde up to 30% using ammonium vanadate as a catalyst have recently been reported.<sup>[101]</sup> Furthermore, photocatalytic reactions using a titanium-oxide cluster have been described this year and thus indicate the current interest in this project.<sup>[102]</sup> Despite these efforts, the

main drawbacks remain with an unselective oxidation, a low substrate conversion, high catalyst costs and their consumption as well as a huge energy input and expensive chemicals. New approaches to a selective benzaldehyde synthesis are still being sought.

Based on the previously described superoxido complexes and their ability to selectively cleave CH-bonds, it appears promising to pursue this approach further with regard of benzaldehyde synthesis. In order to avoid the disadvantages described above (e.g. decomposition), as well as the dinuclear deactivation of the catalyst (Scheme 2), the possibility of immobilizing the complex on a solid surface appears to be a promising approach.

### 1.7 Immobilization of Active Species

Free (mobile) catalysts often suffer from self-decomposition, which leads to an increased consumption of material and thus to an increased use of resources and money. In addition, a low selectivity of the substrates is obtained and a work-up of starting materials, catalysts and products is necessary. Therefore, heterogeneous reactions are often preferred in industrial processes.<sup>[103,104]</sup> A catalytic system can be implemented by immobilizing active material on a solid surface. Substrate and products can be separated and purified much easier and an application into an automatic system (e.g. flow reactor) is possible.<sup>[105]</sup> However, this method still contains some disadvantages e.g. often less activity and higher costs.

In general, the headline *immobilization* contains a wide range of applications. Examples are the immobilization on gold nanoparticles for targeted distribution of medical substances or the preparation of an electrode surface to enhance its electrochemical properties.<sup>[106,107]</sup> In field of biological chemistry the immobilization of enzymes is well established.<sup>[108]</sup> In addition, applications of immobilized complexes for wastewater purification or CO<sub>2</sub> fixation are conceivable.<sup>[109,110]</sup> In this context, it becomes obvious why one often speaks of a *surface functionalization* instead of *immobilization*.

Many different ways have been described to perform an immobilization. A basic distinction is made between physical (adsorption) and chemical (covalent binding)

immobilization.<sup>[111]</sup> Szymańska *et al.* demonstrated the application of both options, within one system: they immobilized an enzyme either *via* a covalent bond or by means of a coordination of a histidine residue to a metal complex which has been immobilized beforehand.<sup>[108]</sup>

Bioinorganic chemistry is mostly limited to modeling the active centers of enzymes. As already described above, these *free* complexes suffer from the disadvantages of *free* catalysts (e.g. self-decomposition). A firm attachment to a solid surface, however, is intended to prevent these disadvantages by mimicking the solid protein framework around the catalytic centre of an enzyme. In an enzyme, the protein environment protects the active site from a dinuclear deactivation or self-decomposition and furthermore stabilizes the active species. The immobilization of model substances by various methods have already been reported.<sup>[103]</sup> For example Aratani *et al.* described a simple way of immobilization by cation exchange with a catalytic active manganese tmpa complex on mesoporous silica–alumina.<sup>[112]</sup> Another way of binding complexes by means of electrostatic interaction is to functionalize a surface beforehand with negatively charged linker molecules. With such an arrangement, Liu *et al.* succeeded in stabilizing a copper bis( $\mu$ -oxido) complex on silica nanoparticles, which was also able to selectively oxidize toluene.<sup>[113]</sup>

Another widespread method of surface functionalization is the direct covalent binding of the active material on a surface. A basic distinction is made between three methods (Figure 16):<sup>[114]</sup> the first category is what is known as *grafting*. A molecule (mostly complex) modified with a surface linker is immobilized on a pre-synthesized surface material. With this method, the research group of Mishra successfully immobilized a cobalt complex on mesoporous silica in 2014. This complex was able to activate molecular dioxygen and to selectively oxidize *n*-alkanes.<sup>[115]</sup> Another possibility for covalent immobilization is the *co-condensation (one-pot reaction)*. For this purpose, active species prepared with surface linker molecules are condensed together with the starting materials (tetraethylorthosilicate (TEOS)) of the surface to be synthesized. First studies were published by Lim *et al.*<sup>[116]</sup> The third method is a special form of *co-condensation*: the preparation of *periodic mesoporous organosilicas* (PMOs). Again the active species are equipped with a linker molecule and react in an *one-pot reaction* together with the starting material TEOS. However,

## 1. Introduction

the active materials must have multiple ends for condensation with the surface material in order to form a common network. Using this method, Suspène *et al.* incorporated a complex by means of a modified tren ligand in a mesoporous material.<sup>[117]</sup>

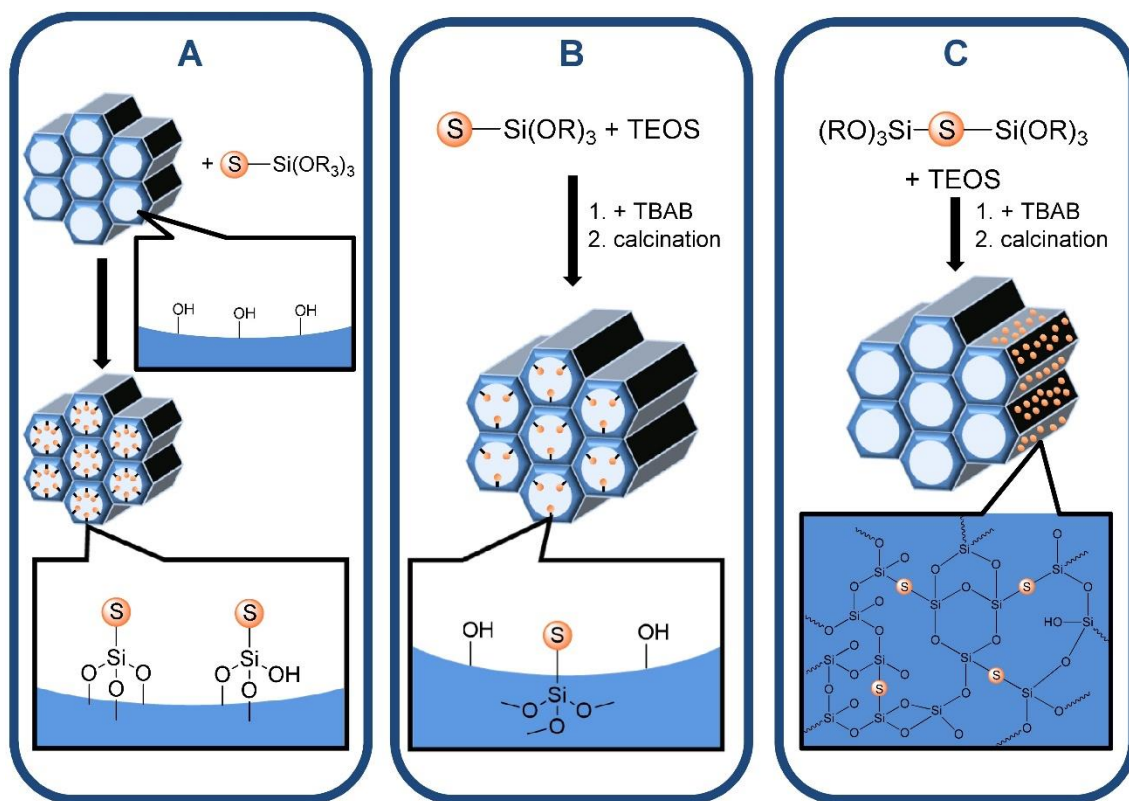


**Figure 16.** Three methods of covalent immobilization of an active species (S), pictured as orange ball. **A:** grafting **B:** co-condensation (one-pot reaction) **C:** periodic mesoporous organosilicas (PMO). Redrawn and modified according to reference <sup>[114]</sup>

Which of the three methods mentioned above are suitable depends on various factors (e.g. substrate, sensitivity of active material). Disadvantages such as pore blocking, but also advantages such as a homogeneous distribution of the complex, must be taken into account when choosing the appropriate method.

Another important factor is the choice of surface material. A distinction is made between organic and inorganic substances. An example of an organic surface material is polystyrene, which can be functionalized by using *click chemistry*.<sup>[118]</sup> However, such organic materials have some disadvantages such as swelling, reaction with solvents and poor mechanical stability. This is one reason why inorganic surfaces are mainly used. Suitable inorganic surface materials are, for

example, metal oxides (e.g. iron and aluminium oxides) which provide hydroxyl groups on their surface for condensation with the most common organic linker molecules.<sup>[119,120]</sup> The most common surface material, however, is silica gel (SiO<sub>2</sub>), due to the higher number of advantages over other organic and inorganic materials: a great resistance against organic solvents, no swelling, thermal resistance. Furthermore, it is one of the most commercially distributed surface materials and therefore less expensive (than e.g. noble metals, dotted metal oxides) and a large variety of several linker molecules exists.<sup>[120,121]</sup> Moreover, there is the option of simple configuration the silica into a desired shape in advance. For example, the pre-synthesized silica can be made into the shape of a monolith.<sup>[122,123]</sup> Another advantage is the determination of the porosity during the synthesis of the silica. In combination with the specific shape, the material can be optimally adapted to the respective application, e.g. in a flow reactor.

A further important aspect of the surface functionalization is the choice of an appropriate linker molecule. In addition to the correct linker moiety for attaching an active species, the anchor group for covalent bonding to the surface must also be considered. The choice of the linker depends on the type of reaction that should be performed (*grafting*, *co-condensation*, *PMOs*). Linkers with two or three anchor groups are mostly used for *PMOs* and *co-condensations*, whereas linkers with one single anchor group are preferred for distal distribution (*grafting*) on a surface. Regardless of the selected linker molecule, undesirable side reaction, e.g. dimerization and cross-linking, can occur before the condensation.<sup>[124]</sup> Adequate reaction conditions (e.g. no moisture) are essential.

### 2. Research Goals

Main motivation of this work was the selective oxygenation of toluene to benzaldehyde. For this purpose, molecular dioxygen should be activated by copper model complexes based on biological enzymes. The ligand systems of the various copper complexes were modified in order to obtain a suitable oxygen adduct. Furthermore, adjustments to known catalytic procedures had to be carried out to optimize the process. The results to be presented were based on previous work on toluene oxidation by Würtele *et al.*, with the aid of a *binuclear copper end-on peroxido* complexes, using tetradentate tripodal ligands based on the tmpa system.<sup>[86]</sup> However, since tmpa is comparatively difficult to modify, the ligand uns-penp ((2-aminoethyl)bis(2-pyridylmethyl)amine) (Figure 17) was used, which possesses a terminal amine group which is easier to functionalize.<sup>[125]</sup>

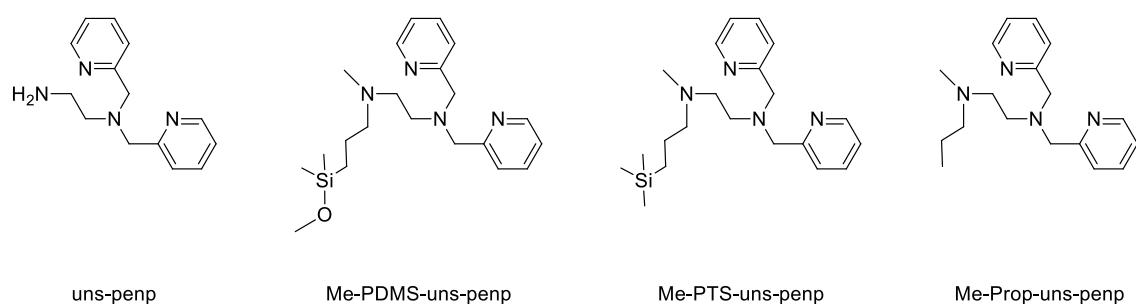
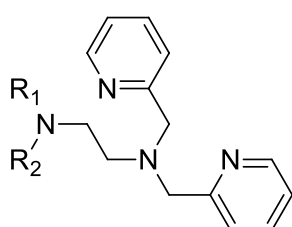


**Figure 17.** Basic ligand uns-penp (left) and its derivatives synthesized for immobilization and comparison reactions. Me-PDMS-uns-penp contains a single anchor group for covalent immobilization on a silica surface. The other two ligands have sterically and chemically similar substituents. They are used to compare mobile reactions with dioxygen and the catalytic properties with the immobilized system.

**Chapter 3** describes the functionalization of the uns-penp ligand for a covalent immobilization on a silica surface. Since the previous work using tmpa or uns-penp shows only a low conversion to benzaldehyde (15-20%) and a decomposition of the active species, the catalytic process should be improved by immobilization. Silica should imitate the rigid protein framework, which in biological models prevents self-decomposition of the enzyme and the deactivation of the active oxygen complex through a binuclear reaction (see Scheme 2). A mononuclear *end-on* superoxido complex prepared in this way, according to the proposed reactions in PHM and D $\beta$ M, should have a higher reactivity and selectivity towards the methyl group of toluene. Furthermore, by functionalizing pre-synthesized silica monoliths, the suitability for use

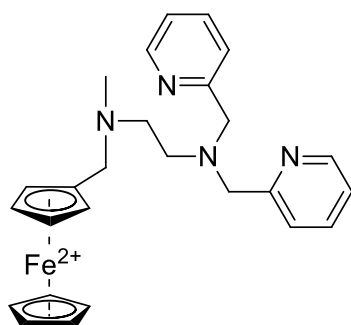
in a flow reactor was to be tested. Finally, the immobilized activated complex was compared with free model substances (see Figure 17) with regard to its catalytic properties.

**Chapter 4** focuses on the derivatization of the uns-penp ligand at the terminal nitrogen position to obtain various oxygen species, in addition to the known *end-on* peroxido complexes. Results from Chapter 3 served as a fundament, since simple modifications of the uns-penp ligand already revealed an impact on the reactivity towards dioxygen. Influences of small derivatizations by means of simple aliphatic residues on oxygen activation were to be investigated. A distinction was made between symmetrical (two identical residues) and unsymmetrical (two different residues) substituents. In addition, an uns-penp ligand with the redox active group ferrocene was synthesized in order to investigate the influence of another attached complex. Figure 18 gives an overview of the synthesized derivatives. The reactivity towards dioxygen of all synthesized complexes was investigated in solution and in the solid state. Adequate electrochemical, crystallographic and spectroscopic analyses were executed to determine the impact of *simple derivatization* on the oxygen activation.



symmetric:

uns-penp;  $R_1=R_2=H$   
 Me<sub>2</sub>uns-penp;  $R_1=R_2=Me$   
 Et<sub>2</sub>uns-penp;  $R_1=R_2=Et$   
 Prop<sub>2</sub>uns-penp;  $R_1=R_2=Prop$   
 iProp<sub>2</sub>uns-penp;  $R_1=R_2=iProp$



asymmetric:

Me-Et-uns-penp;  $R_1=Me; R_2=Et$   
 Me-Prop-uns-penp;  $R_1=Me; R_2=Prop$   
 Et-Prop-uns-penp;  $R_1=Et; R_2=Prop$   
 Me-iProp-uns-penp;  $R_1=Me; R_2=iProp$   
 Et-iProp-uns-penp;  $R_1=Et; R_2=iProp$

redox active:

Ferrocene-Me-uns-penp;  $R_1=Me; R_2=methylferrocene$

**Figure 18.** The uns-penp derivation products are distinguished by the symmetry of their substituents. The range of the attached aliphatic groups is between one and three carbon units.

**3. Immobilization of a copper complex based on the tripodal ligand (2-aminoethyl)bis(2-pyridylmethyl)amine (uns-penp)**

This work has been published in

*Zeitschrift für Anorganische und Allgemeine Chemie*

Tim Brückmann, Jonathan Becker, Kevin Turke, Bernd Smarsly,  
Morten Weiß, Roland Marschall, and Siegfried Schindler

*Z. Anorg. Allg. Chem.* **2021**, 647, 560 –571

<https://doi.org/10.1002/zaac.202100022>

# Immobilization of a copper complex based on the tripodal ligand (2-aminoethyl)bis(2-pyridylmethyl)amine (uns-penp)

Tim Brückmann,<sup>[a]</sup> Jonathan Becker,<sup>[a]</sup> Kevin Turke,<sup>[b]</sup> Bernd Smarsly,<sup>[b]</sup> Morten Weiß,<sup>[c]</sup> Roland Marschall,<sup>[c]</sup> and Siegfried Schindler<sup>\*[a]</sup>

Dedicated to the 60th birthday of Prof. Dr. Christoph Janiak

A new derivative of the ligand (2-aminoethyl)bis(2-pyridylmethyl)amine (uns-penp), capable for covalent immobilization on silica, was synthesized. Silica powder for column chromatography and mesoporous monoliths served as surface material. Functionalized silica was sufficiently characterized with reflectance UV/Vis and FTIR techniques. Copper(I) was successfully complexed with the immobilized ligand and exhibits reversible reactivity towards dioxygen at low temperatures. Suspending the oxygen species with toluene at low temperatures led to selective oxygenation to benzaldehyde, determined by GC-MS.

Copper(I) complexes with the ligands Me-PTS-uns-penp and Me-Prop-uns-penp were prepared and characterized to model the reaction behavior towards dioxygen in solution. Additionally, solid copper peroxido complexes with these ligands were obtained by precipitation with the sterically demanding anion tetraphenylborate. Furthermore, these complexes could be obtained in a reversible reaction by treating corresponding copper(I) complexes with dioxygen. With all oxygenated copper complexes catalytic oxidation of toluene was observed.

## Introduction

Benzaldehyde is an industrially important chemical and thousands of tons are produced per year. It is used for a wide range of products such as dyes, drugs, cosmetics and foods.<sup>[1]</sup> It has been first synthesized by Wöhler and Liebig and since then several ways of commercial fabrication have been established.<sup>[2]</sup> The Gattermann-Koch synthesis, the chlorination of toluene with subsequent hydrolysis of the intermediate product and the direct oxygenation, catalyzed by transition metal oxides, are

currently the most common procedures<sup>[3–5]</sup> However, these synthetic routes show some noticeable drawbacks: on the one hand, toxic reactants and catalysts are required and on the other hand, a range of side products due to overoxidation are formed. Furthermore, the huge consumption of energy and the necessary steps for product separation should be mentioned. Efforts to improve the industrial process have been reported, e.g. Gast et al. reported a catalyst-free method for direct oxygenation by treating toluene with dioxygen at high pressures and temperatures.<sup>[6]</sup> However, again no selective oxygenation could be achieved. With regard to sustainable chemistry, it would be desirable to synthesize benzaldehyde directly without waste/side products by selective oxidation of toluene at room temperature using a catalyst and dioxygen/air as the sole oxidant. Several copper containing enzymes exist which are capable to selectively oxygenate organic substrates under mild conditions, for example dopamine- $\beta$ -monooxygenase (D $\beta$ M), peptidylglycine- $\alpha$ -hydroxylating monooxygenase (PHM) or tyrosinase.<sup>[7]</sup> Modelling the reactivity of the copper enzymes with low molecular weight complexes therefore is a worthwhile approach to succeed in an optimized process for the synthesis of benzaldehyde. Different “dioxygen adduct” complexes as active species can form when a copper(I) compound is reacted with dioxygen. Some examples are shown in Figure 1.<sup>[8]</sup>

Copper(I) complexes with the tetradentate ligand tris(2-methylpyridyl)amine (tmpa) as well as its derivatives (Figure 2) react with dioxygen to form a trans- $\mu$ -1,2-peroxido species (Figure 1b). The molecular structures for the two complexes [LCu(O<sub>2</sub>)CuL]<sup>2+</sup> (L=tmpa and Me<sub>6</sub>tren, Figure 2) have been reported previously.<sup>[7,8]</sup> While this binding motif has not been observed in nature so far (side-on,  $\mu$ - $\eta^2$ - $\eta^2$ -peroxido, Figure 1e, is here preferred) it turned out that complexes of this type are

[a] T. Brückmann, J. Becker, Prof. Dr. S. Schindler  
Institut für Anorganische und Analytische Chemie  
Justus-Liebig-Universität  
Heinrich-Buff-Ring 17  
35392 Gießen, Germany  
E-mail: siegfried.schindler@anorg.chemie.uni-giessen.de

[b] K. Turke, B. Smarsly  
Institut für Physikalische Chemie  
Justus-Liebig-Universität  
Heinrich-Buff-Ring 17  
35392 Gießen, Germany

[c] M. Weiß, R. Marschall  
Fakultät für Biologie, Chemie und Geowissenschaften  
Universität Bayreuth  
Universitätsstraße 30  
95447 Bayreuth, Germany

Supporting information for this article is available on the WWW under <https://doi.org/10.1002/zaac.202100022>

© 2021 The Authors. *Zeitschrift für anorganische und allgemeine Chemie* published by Wiley-VCH GmbH. This is an open access article under the terms of the Creative Commons Attribution Non-Commercial License, which permits use, distribution and reproduction in any medium, provided the original work is properly cited and is not used for commercial purposes.

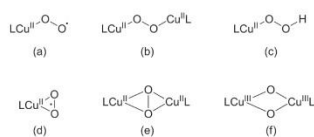


**Figure 1.** Examples of copper "dioxygen adduct" species: (a) *end-on* superoxido, (b) *trans-μ-1,2-peroxido*, (c)  $\eta^1$ -hydroperoxido, (d) *side-on* superoxido, (e)  $\mu$ - $\eta^2$ : $\eta^2$ -peroxido, (f) *bis(μ-oxido)*.

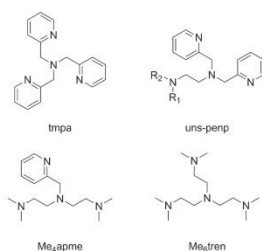


**Figure 2.** Tripodal ligand tmpa and derivatives: uns-penp ( $R_1=R_2=H$ ), Me<sub>6</sub>apme and Me<sub>6</sub>tren.

capable to catalytically oxidize toluene selectively to benzaldehyde.<sup>[9,10]</sup> Karlin and co-workers demonstrated that this reaction could be performed in solution at low temperatures with yields of up to 40%.<sup>[10]</sup> The anion tetrakis(pentafluorophenyl)-borate was applied to achieve higher solubility to perform the reaction under homogeneous conditions. Around the same time, it was observed that it is possible to dramatically stabilize some of the *trans-μ-1,2-peroxido* copper complexes with (some) tripodal ligands in the solid state by using tetraphenylborate as an anion.<sup>[9]</sup> These complexes were stable up to temperatures of +100 °C in the solid state and therefore seemed to be promising for heterogeneous catalytic oxidation of toluene. While this turned out to be correct, yields still remained rather low and did not exceed 20% for the copper/tmpa system that turned out to be most suitable for this application.

With regard to these findings, it was decided to immobilize tripodal copper complexes to optimize the catalytic system. As a sustainable carrier material, mesoporous silica was chosen that has been thoroughly investigated during the last years. It has been used to a large extent as grafting material and therefore has a number of advantages.<sup>[11,12]</sup> Due to its wide application, various linking reagents are available on the market, suitable for a wide range of functionalization. Furthermore, it is resistant against organic solvents in contrast to organic surface materials such as polystyrene. Its thermal resistance and low costs are important features as well.<sup>[13,14]</sup> Additionally, the generally high surface area is an advantage and the pore structure can be tailored towards the application.

The major goal would be to covalently graft an active complex onto a silica surface of a so-called silica monolith

(Figure 3). Its mesoporous structure in a network of macro pores are features of such a monolith for an application in a flow reactor. While the meso pores containing a large surface for a maximum of immobilization a regular network of macro pores is advantageous for the mass flow of the substrate through the monolith. This would allow the construction of a flow reactor in which the substrate and oxidant (dioxygen/air) would be combined in a solvent and passed through the monolith. As a consequence, the reaction would be clean (no fragments of catalyst decay) and only very few separation steps would be necessary. Moreover, after the oxygenation the complex could be easily reactivated by a reducing agent.

## Results and Discussion

In general, there are two established immobilization/grafting processes to obtain functionalized silica: 1. The whole ligand gets incorporated into the silica framework in form of its metal complex. For this purpose, a mixture of the "linkable" complex with a tetraalkoxysilane is hydrolyzed in basic media, leading to a solid silica compound containing the active material. For example, Suspène et al. used a tren-based ligand system (Figure 4a) incorporated into a mesoporous silica framework. The immobilization thus allowed stabilization of a copper oxygen adduct compound that was reversibly formed.<sup>[15]</sup> In a slightly different way a copper(II) tmpa complex has been incorporated into mesoporous silica-alumina (Al-MCM-41) and the obtained material had been used for catalytic hydroxylation of benzene to phenol using hydrogen peroxide as an oxidant.<sup>[16]</sup>

2. Alternatively and more common is the approach to covalently graft the active materials onto an actual silica surface, usually silica gel. In addition, it is possible to precast the surface material into a suitable shape for further applications such as a monolith that could be used in a flow reactor (Figure 3). Two different synthetic routes can be applied to achieve this: a) first the linker will be attached to the silica surface and in a second step it will be reacted with the actual ligand prior to adding a metal salt to form the final active

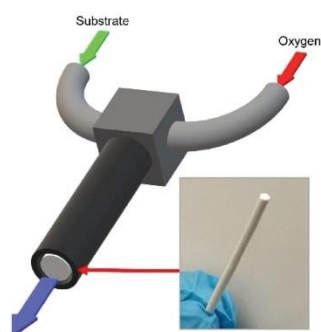


**Figure 3.** Functionalized silica monolith placed into a flow-reactor. Small picture at the right shows the silica monolith.

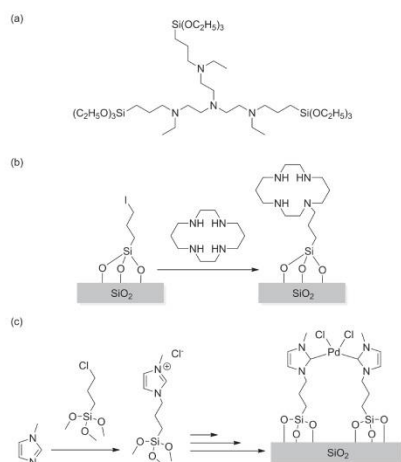


**Figure 4.** (a) tren derivative for incorporation into silica framework,<sup>[15]</sup> (b) approach with pre-condensed linker on silica surface with subsequent attachment of a ligand,<sup>[17]</sup> (c) approach with pre-combination of a linker with the ligand and subsequent condensation.<sup>[18]</sup>

material. This has been accomplished e.g. for the attachment of the macrocyclic ligand cyclam (Figure 4b) to coordinate cobalt ions and further bonding to an enzyme.<sup>[17]</sup> However, problems have been observed using this method with amines that can strongly bind to the surface of the silica and then are not available anymore for combination with the linker.<sup>[19]</sup> For that reason it seems preferable to apply method b) attaching the linker with the ligand prior to grafting on the surface of the silica. For example, this method was applied for covalently grafting palladium complexes onto a silica surface to perform Heck reactions (Figure 4c).<sup>[18]</sup>

Based on the previous results we chose (2-aminoethyl)bis(2-pyridylmethyl)amine (uns-penp, Figure 2, R=H) as a ligand for the combination with a suitable linker for the attachment at the terminal amine group. The ligand uns-penp has been first reported by Mandel et al. and has the advantage that it can be easily modified.<sup>[20]</sup> A kinetic study has been performed in the past on the reaction of  $[\text{Cu}(\text{Me}_2\text{-uns-penp})]^+$  (Me<sub>2</sub>-uns-penp, Figure 2, R=Me) with dioxygen.<sup>[21]</sup> Very similar to copper(I) complexes with tmpa or Me<sub>6</sub>tren as ligands it reacts according to equation 1 (L=Me<sub>2</sub>-uns-penp) in a first step to an *end-on* superoxido complex prior to its reaction with a second copper (I) unit to form a dinuclear *end-on* peroxido complex (Figure 1).



The hydrogen atoms of uns-penp need to be substituted by organic groups to obtain persistent peroxido complexes. If amine hydrogen atoms are present in the ligand system, hydrogen peroxide can be formed that would lead to quite

different reaction behaviour, usually involving radical pathways initiated by hydroperoxido complexes. Therefore, prior to modify uns-penp with silyl linker groups, one of the amine hydrogen atoms was substituted by a methyl group leading to Me-uns-penp (Figure 5).

## Syntheses

The preparation of Me-uns-penp is a bit more of a challenge in contrast to the facile synthesis of uns-penp or Me<sub>2</sub>-uns-penp. While a reductive alkylation reaction with formaldehyde allowed access to it, yields were very low and a large number of side products were obtained.<sup>[22]</sup> A different synthetic approach based on selective protecting and deprotecting reactions of the fundamental methyl-ethylene diamine structure, followed by reductive alkylation performed according to the literature allowed to obtain Me-uns-penp in satisfying yields.<sup>[23,24]</sup>

To enable Me-uns-penp for condensation and for covalent bonding on a silicon dioxide surface several silica linkers are commercially available that allow a large number of different possible reactions.<sup>[25]</sup> Alkoxy silane linkers are commonly used for immobilisation on silica surfaces: on the one hand they can be managed quite well to obtain sufficient grafting quantities, on the other hand a lot of derivatives, suitable for a large number of different reactions are known and available.<sup>[26]</sup> In here, application of a silane linker containing an alkyl group with a terminal halide suitable for amine attachment was chosen. As the most common silane linkers contain more than one alkoxy group at the silicon atom, there is the possibility of self-condensation between the linkers/ligands (frameworking) in the presence of moisture as shown in Figure 6.<sup>[27]</sup> This effect can easily suppress a statistical distribution of the immobilized compounds on the surface of the solids and a distal grafting of the complexes would not be possible.<sup>[19]</sup> The commercially available mono alkoxy linker (3-chloropropyl)dimethylmethoxy silane (CPDMS) was chosen as suitable starting material for immobilization. A comparison of both linker molecules is shown in Figure 6.

The substitution at the precursor ligand led to the product (2-methyl-(3-propyl)dimethyl-methoxysilane-aminoethyl)bis-(2-pyridylmethyl)amine (Me-PDMS-uns-penp, (Figure 5). However, this silane linker as well can undergo self-condensation. In

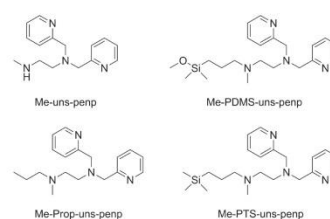


**Figure 5.** Precursor ligand Me-uns-penp and its derivatives for immobilization and solution experiments.

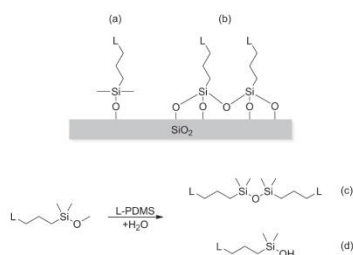


**Figure 6.** Top) Different grafting behaviour of the silane linker, L is the chosen ligand, (a) mono alkoxy silane linker units that are not capable of frameworking. It allows a roughly statistical distribution on a flat surface (b) frameworking of poly alkoxy silane linker units caused by self-condensation with subsequent immobilization. Bottom) Reaction of moisture with a mono alkoxy linker attached to a ligand (c) dimerization caused by self-condensation. (d) exchange of alkoxy anchor groups with hydroxyl groups.

contrast to its multi alkoxy silane derivatives, there is no prior frameworking but dimerization could still occur that would exclude the ability for grafting. (Figure 6c).<sup>[27]</sup> Furthermore, the loss of the alkoxy group and a subsequent exchange with a hydroxyl group could be observed (Figure 6d).

Therefore, all chemicals were properly dried and all preparations were carried out under inert conditions in a glove box. As the terminal carbon-chlorine bond of the CPDMS linker does not feature a sufficient reactivity towards the secondary amine of the Me-uns-penp ligand, an exchange through a better leaving group through a Finkelstein reaction was necessary.<sup>[28]</sup> The halide exchange as well as the linker attachment at the ligand were performed in a one-pot reaction in acetonitrile similar to reactions described previously.<sup>[15,29]</sup> Controlling the reaction via ESI-MS, after linker addition was completed, revealed that besides the product mass peak, dimerization and hydroxyl exchange of the silane group had occurred (bottom of Figure 6). A separation via column chromatography or by distillation did not lead to a satisfying yield of pure product. However, the mixture could be purified by cleaving the dimeric silanol by adding one equivalent of sodium methoxide and an excess of dimethyl carbonate.<sup>[30]</sup> Afterwards ESI-MS showed only the desired product mass. Even the hydroxy groups were converted under the basic conditions leading to the methoxy silane product. This step must be specifically highlighted as it represents the "bottle neck" reaction, which was fundamental for a pure product that precedes a reproducible grafting result and therefore to successfully apply it in catalysis. The overall synthetic procedure is presented in Figure 7.

Prior to immobilization of Me-PDMS-uns-penp a test reaction was performed if this modified uns-penp ligand system is still capable to support formation of copper "dioxygen adduct" complexes that could become useful for catalytic oxidations. Due to the extreme sensitivity of Me-PDMS towards moisture two analogues of this ligand, Me-PTS-uns-penp and

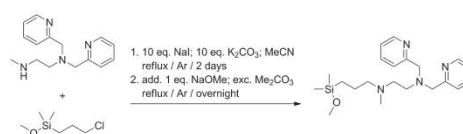


**Figure 7.** Synthesis of Me-PDMS-uns-penp ligand in a one-pot reaction: 1. linker attachment with prior halide exchange 2. side products were converted back into the desired species.

Me-Prop-uns-penp (Figure 5) were prepared. Copper(I) complexes from both ligands were synthesized and molecular structures of both complexes,  $[\text{Cu}(\text{Me-PTS-uns-penp})]\text{BPh}_4$  and  $[\text{Cu}(\text{Me-Prop-uns-penp})]\text{BPh}_4$  are presented in Figure 8 (Crystallographic data are reported in the Supporting Information).

It could be confirmed by low temperature stopped-flow measurements, that both copper(I) complexes reacted with dioxygen according to equation 1 described above. Time resolved spectra of the reaction of  $[\text{Cu}(\text{Me-PTS-uns-penp})]\text{BPh}_4$  with dioxygen in acetone are presented in Figure 9 and is very

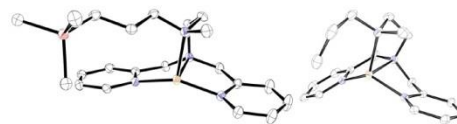


**Figure 8.** Molecular structures of the cations of  $[\text{Cu}(\text{Me-PTS-uns-penp})]\text{BPh}_4$  (left) and  $[\text{Cu}(\text{Me-Prop-uns-penp})]\text{BPh}_4$  (right). Ellipsoids set at 50% probability; the anions, H atoms, and solvent molecules are omitted for clarity. Carbon: black; nitrogen: blue; silicon: red; copper: brown.

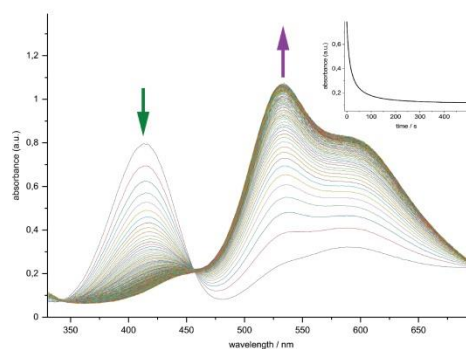


**Figure 9.** Time resolved spectra of the reaction of  $[\text{Cu}(\text{Me-PTS-uns-penp})]\text{BPh}_4$  with dioxygen in acetone at  $-81.0\text{ }^\circ\text{C}$  ( $[\text{complex}] = 2.0 \times 10^{-4}\text{ M}$ ,  $[\text{O}_2] = 4.4 \times 10^{-3}\text{ M}$ , total time: 250 s). At 414 nm the spectra shows the decreasing intensity of the superoxido intermediate. 535 nm shows the increasing intensity of the final peroxide complex. Time trace at the upper right shows decomposition of the superoxido species.

similar to the reaction of  $[\text{Cu}(\text{Me-Prop-uns-penp})\text{BPh}_4]$  with dioxygen (reported in the Supporting Information). Furthermore, the reaction behavior is in excellent agreement with previous reports on other copper complexes with tripodal ligands.<sup>[21,31–33]</sup> The decomposition of the copper superoxido complex can be followed by the decrease of the absorbance maxima at 414 nm (Figure 9, inset). The disappearance of this band and an increase of a band with a maximum at 532 nm is the formation of the consecutive reaction to the dinuclear copper peroxido complex (eq. 1).

While it is difficult to crystallize either an *end-on* superoxido or *end-on* peroxido intermediate complex (only a few examples have been reported in the literature)<sup>[19,34–37]</sup> it is quite easy to obtain and crystallize related copper(II) chlorido complexes as a model compounds for these intermediates.<sup>[38]</sup> Herein it was possible to crystallize  $[\text{Cu}(\text{Me-Prop-uns-penp})\text{Cl}]\text{ClO}_4$  and its molecular structure is shown in Figure 10. Crystallographic data are reported in the Supporting Information.

In contrast to other structurally characterized copper(II) complexes with uns-penp derivatives as ligands the copper centre in  $[\text{Cu}(\text{Me-Prop-uns-penp})\text{Cl}]\text{ClO}_4$  is not coordinated in a square pyramidal manner but in a trigonal bipyramidal geometry with a  $\tau$  value of 0,83.<sup>[39]</sup>

An essential intention of this work was to obtain an *end-on* superoxido copper complex by suppressing the consecutive formation of the dinuclear copper peroxido complex according to equation 1. This would allow a better modelling of the active site of dopamine- $\beta$ -monooxygenase (DBM) and peptidylglycine- $\alpha$ -hydroxylating monooxygenase (PHM) and might result in a more active species with higher yields in catalytic toluene oxidation. While an *end-on* superoxido copper complex can be stabilized with a sterically more demanding ligand it furthermore should be possible to achieve this stabilization through distal immobilization of the mononuclear copper units on a silica surface.<sup>[34,40]</sup> Therefore, the application of a trialkoxy silane linker was inapplicable due to its tendency towards frameworking.<sup>[32]</sup> Ligands attached in such a pre-grafted framework may possess distances that would be too short to exclude formation of peroxido complexes.

This strategy has been applied successfully in the past for a mononuclear cobalt imine complex. Investigations with "model" complexes for the actual silyl-based units allowed in the process structural characterization of an *end-on* superoxido cobalt complex.<sup>[41]</sup> Immobilization then proved the ability of this complex unit to catalytically oxidise *n*-alkanes.<sup>[42]</sup>

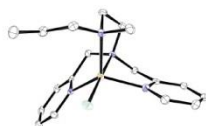


**Figure 10.** Molecular structure of the cation of  $[\text{Cu}(\text{Me-Prop-uns-penp})\text{Cl}]\text{ClO}_4$ . Ellipsoids set at 50% probability; the anions, H atoms, and solvent molecules are omitted for clarity. Carbon: black; nitrogen: blue; silicon: red; copper: brown.

## Immobilization

Common silica powder used in column chromatography (Kieselgel 60 M) was prepared for surface functionalization by refluxing it in concentrated hydrochloric acid for 24 hours and subsequent drying at 150 °C according to the literature.<sup>[18,43]</sup> This procedure insured sufficient supply of silanol groups, which serve as anchor positions for ligand condensation. Besides, it removes potential impurities such as grease and side products of the fabrication process. Physisorption measurements with nitrogen of the activated silica gel determined a specific BET (Brunauer-Emmett-Teller) surface area of 348 m<sup>2</sup>/g (Table S1, Supporting Information). As described above, the spatially separated immobilization of the ligands should prevent the formation of dinuclear peroxido copper complexes. To manage the required distance, an immobilization of only one ligand molecule per 4 nm<sup>2</sup> was attempted. Geometrical basis of this surface concentration is the distance of 0.738 nm between the silicon atom of the propylene arm and the coordinating nitrogen atom, positioned between both methyl pyridyl residues, into a Cu(I) complex with the Me-PTS-uns-penp ligand. A schematic drawing is pictured in Figure 11.

A statistical distribution of the ligand at the surface was assumed by the applied concentration of the reaction suspension containing ligand and the surface material. In accordance with the Zhuravlev model, a number between 4.6 and 4.9 OH groups per nm<sup>2</sup> exists on silica.<sup>[44]</sup> Therefore, an adequate amount of silanol groups is available for this assumption. Quantification of the resulting reaction solution via transmission UV/Vis spectroscopy shows that almost all molecules were successfully grafted on the silica surface (94%, Figure S4, Supporting Information). However, applying twice the ligand concentration led to a grafting of only 83% (Figure S4, Supporting Information). Despite the fact that more hydroxyl groups should be available the silica surface seems to be completely functionalized/saturated. One of the reasons for that effect may be the sterical hindrance of the ligand itself that

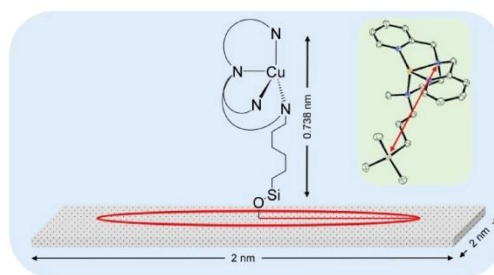


**Figure 11.** Schematic drawing of the immobilized copper(I) complex with the Me-PDMS-uns-penp ligand. The double-arrow illustrates the distance between the silicon anchor and the axial nitrogen atom. The red circle is an assumption of the rotational effect on the surface. The inset shows the molecular structure of the cation of  $[\text{Cu}(\text{I})(\text{Me-PTS-uns-penp})\text{BPh}_4]$ .

makes a further/additional consumption of the silanol groups through immobilization impossible. In addition, pores, which were blocked by an immobilized ligand at the entrance, cannot be accessed by ligand molecules anymore. Physisorption measurements of the functionalized material resulted in a reduction of the BET area with regard to the starting surface: Me-PDMS-uns-penp grafted an area of 47 m<sup>2</sup>/g, a loss of 14%. Applying twice the concentration as described above grafting of 72 m<sup>2</sup>/g (−21%) was detected confirming the results of the UV/Vis quantification.

FTIR measurements using diffuse reflectance technique DRIFTS reveal an immobilization on the silica gel with the Me-PDMS-uns-penp ligand (Figure 12). Comparison with untreated silica shows a decrease in intensity of the silanol band (3734 cm<sup>−1</sup>). Spectra with an enlarged area of interest are shown in the Supporting Information. Furthermore, the bands with low intensity between 2965 and 2907 cm<sup>−1</sup> as well as between 1470 and 1430 cm<sup>−1</sup> indicate the presence of an aliphatic group. The bands of the pyridyl groups with high wavenumbers cannot be seen due to the huge silanol absorption, however, the bands between 1600 and 1570 cm<sup>−1</sup> are visible. Bands at 1245 cm<sup>−1</sup> and 837 cm<sup>−1</sup> are slightly visible. They indicate the Si–CH<sub>3</sub>

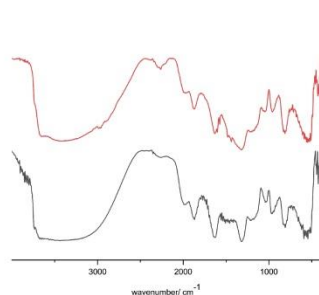


**Figure 12.** DRIFTS measurements of pure (black line, bottom) and functionalized (red line, top) silica gel. The band at 3734 cm<sup>−1</sup> is missing for the functionalized sample what indicates a successful immobilization.

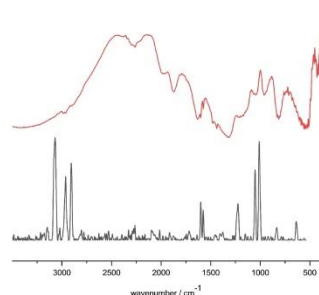


**Figure 13.** Comparison of DRIFTS spectra (red line, top) of functionalized silica gel with Raman spectra (black line, bottom).

groups, assigned to the presence of the ligand. The additional Raman spectra underline the successful covalent bonding (Figure 13). Some of the data obtained from the DRIFT spectra became clearer from the Raman measurements: the pyridyl band at 3068 cm<sup>−1</sup> became much more visible and the band of the Si–CH<sub>3</sub> groups is more distinct as well (1245 cm<sup>−1</sup>). The missing band of the Si–OCH<sub>3</sub> group at 1085 cm<sup>−1</sup> is an indication of the covalent Si–O–Si bonding on the silica surface.<sup>[45]</sup> Treatment of silica with the model ligand Me-PTS-uns-penp did not lead to comparable spectra, which proved the necessity of an anchor group to perform a successful immobilization.

A comparison of the surface investigation with the ATR spectra of the free model ligand Me-PTS-uns-penp is reported in the Supporting Information. Diffuse reflectance UV/Vis measurements showed two absorption maxima at 205 and 260 nm what is supposed to be a  $n/\pi \rightarrow \pi^*$  transition of the pyridyl part of the ligand (Figure 14).<sup>[46]</sup>

As described above monoliths based on mesoporous silica were applied as well to test for further applications in a flow reactor. Monoliths were synthesized by sol-gel procedures (“Nakanishi process”) as described previously.<sup>[47–49]</sup> In contrast to the procedure applied with silica powder described above the monoliths were not treated with concentrated HCl because these rough conditions could cause damage to the cylindrical shape. No further purification for the monoliths was performed to avoid deformation. The monoliths were dried at 150 °C overnight. They were obtained with a specific surface of 360 m<sup>2</sup>/g. Complexing experiments revealed that only the mantle of the monolith was functionalized due to the immobilization procedure: to functionalize its surface the monolith was placed into a special Schlenk tube with a double bottom to separate the stirring bar from the fragile structure (Figure S10, Supporting Information). UV/Vis quantification of the solution after the reaction showed almost complete ligand consumption (detailed spectra of the surface investigation are reported in the Supporting Information).

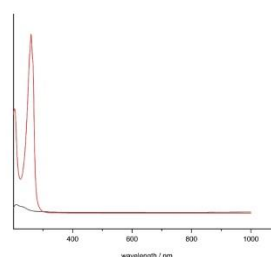


**Figure 14.** Diffuse reflectance UV/Vis measurements: Pure (black line) and functionalized silica (red line). Functionalized species shows a clear band at 205 and 260 nm caused by  $\pi \rightarrow \pi^*$  transition of the pyridyl groups of the ligand.

## Complexation

To determine the actual complexation ability of the grafted ligands and therefore a quantification of the desired catalytic properties, an excess of Cu(II) triflate was suspended into acetonitrile under inert conditions with a defined amount of functionalized silica gel. The silica powder apparently showed a change in colour from colourless to a light blue colour which is evidence of its complexation ability. However, a determination of the consumption of copper ions via UV/Vis measurements was not possible due to the low extinction coefficients in solution. Investigations with diffuse-reflectance UV/Vis revealed the ligand  $\pi \rightarrow \pi^*$  transition as described above together with a shoulder at 288 nm and a broad maximum around 700 nm, typically for  $d-d$  transitions of copper(II) ions (Figure 15).<sup>[50]</sup> Longer exposition with the complexation solution (stirring for ca. one hour) led to a green powder. The green product showed an additional maximum at 421 nm. Most likely the copper complexes reacted with free OH-silyl groups to form copper silicate bonds (Cu–O–Si) after deprotonation. Exposure to air yielded again a blue coloured solid after a couple of days that is comparable in appearance with the blue coloured immobilized complex described above. Treating immobilized copper(II) triflate in acetonitrile with sodium methoxide what act as an analogue of the proposed Si–O species immediately led to a green powder. Washing the sample with acetonitrile caused a colour change to a blue colour as well, which is evidence for a ligand exchange at the fifth coordination position at the copper centre.

Copper(I) complexes with triflate or hexafluorophosphate as anions were attached in the same way as the copper(II) salt leading to light yellow air sensitive powders similar to a previous report on the copper(I) complex with the ungrafted ligand Me<sub>2</sub>uns-penp.<sup>[9]</sup>

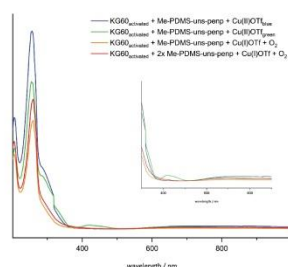


**Figure 15.** Comparison of copper complexes on functionalized silica: blue and green lines show the spectra of the blue and green coloured Cu(II)triflate complexes. The orange coloured spectrum shows the absorbance of the immobilized copper(I) triflate complex after its reaction with dioxygen. The red line shows the spectrum of the immobilized copper complex on a ligand-saturated silica surface.

## Reactivity towards Oxygen

As described above, time resolved UV/Vis spectra obtained in solution for the oxygenation of the complexes [Cu(I)(Me-PTS-uns-penp)BPh<sub>4</sub>] and [Cu(I)(Me-Prop-uns-penp)BPh<sub>4</sub>] showed the formation of transient superoxido and peroxido complexes. Therefore, it was assumed that these reactions could take place in the solid state as well, similar to findings reported previously.<sup>[9]</sup> The sterically demanding anion tetraphenylborate allowed precipitation of peroxido copper complexes from solution that turned out to be extremely stable.<sup>[9]</sup> In comparison with these compounds the new complexes reported in here were much less stable in the solid state. Overnight, the characteristic blue/purple colour of the 1,2-peroxido species had faded and a grey coloured solid remained. Reflectance UV/Vis spectra revealed – as expected – the lack of the absorbance of a peroxide species (Figure-S11 + S12, Supporting Information). In contrast and as reported before, the complex with the symmetric substituted Me<sub>2</sub>uns-penp as a ligand kept the blue colour quite persistently.<sup>[9]</sup>

The blue coloured copper peroxido complexes could also be obtained by exposure of the corresponding solid copper(I) complexes towards dioxygen. However, treating the solid model compounds [Cu(I)(Me-PTS-uns-penp)BPh<sub>4</sub>] and [Cu(I)(Me-Prop-uns-penp)BPh<sub>4</sub>] with dioxygen turned the yellow coloured complexes into green coloured solids instead (Figure S13, Supporting Information). While the colour change indicated the formation of an *end-on* superoxido copper complex UV/Vis spectra did not really support this. Reflectance UV/Vis spectra showed a single maximum around 330 nm (Figure S14, Supporting Information) and not at around 410–440 nm where it would have been expected for a superoxido species.<sup>[51,52]</sup> Keeping the complexes under an argon atmosphere the green colour changed back into a light yellow coloured solid within days. The colour change could be accelerated by moderate heat (~50 °C) under an argon flow within minutes (Figure S15, Supporting Information). The green colour however, could be reestablished by treating the complexes again with dioxygen, therefore demonstrating reversible reactivity. Further characterization of the green coloured solid has been unsuccessful so far. In contrast, the copper(I) complex with Me<sub>2</sub>uns-penp as ligand exhibits two maxima at 318 nm and 540 nm after exposure to dioxygen (Figure S14, Supporting Information) clearly showing the formation of the blue/purple dinuclear peroxido complex [(Me<sub>2</sub>uns-penp)Cu(O<sub>2</sub>)Cu[(Me<sub>2</sub>uns-penp)]<sup>2+</sup>.<sup>[9]</sup>

Immobilized [Cu(uns-penp)<sub>2</sub>](OTf) as well shows a strong sensitivity towards dioxygen: at room temperature the yellow powder immediately turned irreversibly into a light blue coloured solid, resembling the copper(II) product complex described above with the same spectroscopic features (Figure 15, orange and blue spectra). In contrast when the complex was reacted with dioxygen at –80 °C a dark green solid was formed. Flushing the reaction vessel with argon led back to the yellow coloured copper(I) complex. This process can be repeated for several times (Figure 16) until the compound is warmed under dioxygen that again led to the irreversible formation of the blue compound (Figure 15, orange spectre).

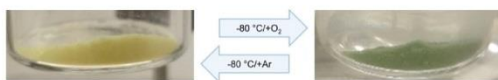


**Figure 16.** Reversible reaction of the immobilized copper(I) complex with dioxygen at low temperatures ( $-80^{\circ}\text{C}$ ).

Attempts to reactivate this compound, most likely a copper(II) species, by reducing it with ascorbate as described previously were not successful.<sup>[53]</sup>

Due to the instability of the “oxygen adduct” complex at moderate temperatures no spectroscopic characterization could be obtained so far. Due to the green colour of the compound the formation of a *end-on* superoxido complex is proposed. Efforts to obtain the proposed superoxido species by addition of  $\text{K}\text{O}_2$  (in combination with cryptand[2.2.2]) to an immobilized copper(II) complex, according to a procedure described by Bailey et al. failed.<sup>[54]</sup>

The monolith was treated in the same way as the functionalized silica powder and showed the same reactivity towards dioxygen at low temperatures.

### Catalysis

In general, all catalytic reactions were performed heterogeneously. For this purpose, the solid copper complex was suspended in a defined volume of toluene. In case of the model complexes, oxygen treated solid  $[\text{Cu}(\text{Me-Prop-uns-penp})]\text{BPh}_4$  and  $[\text{Cu}(\text{Me-PTS-uns-penp})]\text{BPh}_4$  were suspended with toluene and stirred at room temperature. Due to the sensitivity at moderate temperatures of the immobilized copper oxygen species,  $[\text{Cu}(\text{uns-penp}_{\text{immob}})]^+$ , it was treated with dioxygen at  $-80^{\circ}\text{C}$ , covered with toluene and kept at this temperature for 120 h. Afterwards the toluene layer was separated by applying a PTFE syringe filter (pore size  $20\ \mu\text{m}$ ). The products were determined by GC-MS technique. GC-MS data and a more detailed description of the procedure are reported in the Supporting Information. Table 1 shows the results and reaction conditions. Obviously, all compounds exhibit a catalytic activity towards the oxidation of toluene. The catalytic activity of the

“free” complexes  $[\text{Cu}(\text{Me-Prop-uns-penp})]\text{BPh}_4$  and  $[\text{Cu}(\text{Me-PTS-uns-penp})]\text{BPh}_4$  is in accordance with the results for  $[\text{Cu}(\text{Me}_2\text{uns-penp})\text{O}_2](\text{BPh}_4)_2$  (that reached a conversion to benzaldehyde of 15%) reported previously by Würtele et al.<sup>[6]</sup>

It should be pointed out however, that the proposed green coloured copper superoxido complexes  $[(\text{Me-Prop-uns-penp})\text{Cu}(\text{O}_2)]\text{BPh}_4$  and  $[(\text{Me-PTS-uns-penp})\text{Cu}(\text{O}_2)]\text{BPh}_4$  do not seem to be involved in the catalytic oxygenation process in contrast to our expectations. Deep blue solids, obviously the peroxido complexes  $[\text{Cu}(\text{Me-Prop-uns-penp})\text{O}_2](\text{BPh}_4)_2$  and  $[\text{Cu}(\text{Me-PTS-uns-penp})\text{O}_2](\text{BPh}_4)_2$  were formed once the corresponding copper(I) complexes were suspended in toluene under dioxygen. This effect was not observed if the treatment with toluene was carried out under an argon atmosphere. Under these conditions the green compound turned back into the yellow coloured copper(I) complex instead and no oxygenation reactions could be detected.

Processing the catalytic reaction with preformed  $[\text{Cu}(\text{Me-Prop-uns-penp})\text{O}_2](\text{BPh}_4)_2$  and  $[\text{Cu}(\text{Me-PTS-uns-penp})\text{O}_2](\text{BPh}_4)_2$  led to similar conversion of 18% and 14%, respectively (Table 1). However, here as well no oxygenation of toluene was observed under an argon atmosphere, clearly indicating the necessity of the presence of dioxygen.

Conversion was also achieved with the immobilized species  $[\text{Cu}(\text{uns-penp}_{\text{immob}})]^+$ , however, yields were rather low. The silica approach delivers a slightly higher conversion to benzaldehyde by comparison with the monolith (Table 1). The reason for this could be the nearby positioning of the ligands on the surface of the monolith that can lead to peroxide formation/deactivation. Even though there is no huge influence of the anions detected with regard to the conversion it turned out that the immobilized oxygenated complex with  $\text{PF}_6^-$  as an anion was much more stable towards decomposition. Even at moderate temperatures, the green colour of the oxygenated complex with this anion can be observed for a short time while the complex with triflate already decomposed immediately.

### Conclusions and Outlook

We succeeded with the immobilization of a copper complex system that is known to oxygenate toluene selectively to benzaldehyde, however in only moderate yields. Superoxido

**Table 1.** Results of the catalytic reaction of free and immobilized copper oxygen complexes into toluene.

Catalyst <sup>[a]</sup>	Duration	Temperature	Conversion <sup>[b]</sup>
$[\text{Cu}(\text{uns-penp}_{\text{immob}})]_{\text{silica}}\text{OTf}$	120 h	$-80^{\circ}\text{C}$	3%
$[\text{Cu}(\text{uns-penp}_{\text{immob}})]_{\text{silica}}\text{PF}_6$	120 h	$-80^{\circ}\text{C}$	5%
$[\text{Cu}(\text{uns-penp}_{\text{immob}})]_{\text{monolith}}\text{OTf}$	120 h	$-80^{\circ}\text{C}$	1%
$[\text{Cu}(\text{Me-Prop-uns-penp})]\text{BPh}_4$ <sup>[c]</sup>	70 h	r.t.	21%
$[\text{Cu}(\text{Me-PTS-uns-penp})]\text{BPh}_4$ <sup>[c]</sup>	70 h	r.t.	18%
$[\text{Cu}(\text{Me-Prop-uns-penp})]\text{BPh}_4$ <sup>[d]</sup>	70 h	r.t.	18%
$[\text{Cu}(\text{Me-PTS-uns-penp})]\text{BPh}_4$ <sup>[d]</sup>	70 h	r.t.	14%

[a] Active oxygenated species were prepared according to the description in the experimental section [b] conversion to benzaldehyde [c] the oxygen species were formed by exposure of the corresponding solid copper(I) complexes with dioxygen [d] copper peroxido adducts were obtained by precipitation at low temperatures.

and peroxido copper complexes have been assigned previously as active catalytic species. Unfortunately, the intention to model the active site of the peptidylglycine- $\alpha$ -hydroxylating monooxygenase (PHM), an *end-on* copper superoxido species, through immobilization was not really successful. While we observed green solids when reacting corresponding copper(I) complexes with dioxygen, indicating the formation of such species, it was not possible to obtain analytical data to support this, mainly due to the lability of these complexes. Furthermore, it was observed that oxygenation reactions still seemed to be mainly caused by the blue/purple dinuclear copper peroxido complexes instead. The expectation that an immobilized copper superoxido complex might result in a more active species with higher yields in catalytic toluene oxidation therefore were not fulfilled. However, it is quite important that it could be shown that the immobilized complexes are capable to bind dioxygen reversible at low temperature and that they are still able to selectively oxidize toluene to benzaldehyde, despite the low yields. A big advantage here lies in the fact that GC-MS measurements showed a pure product solution without any detectable side products. This is in contrast to the applied solid model complexes for the immobilized species where different side products were observed (e.g. products of the decomposition of the anion  $\text{BPh}_4^-$ ). Despite the problems and the low yields encountered, in principle we were successful to demonstrate that the approach to immobilize active copper complexes in silica have their potential for future applications in catalytic oxygenation reactions. Optimization of the catalytic system is still necessary (probably tridentate ligands might be better than the tripodal ligands applied herein) and most likely a system should be developed that allows the immobilization of neutral copper(I) complexes to avoid problems with anions.

## Experimental Section

### Materials and Methods

All chemicals were purchased from commercial suppliers. Extra dry solvents were refluxed under argon over drying agents prior to transfer into the glove box. All reaction vessels were dried under vacuum with a hot air gun. NaI and  $\text{K}_2\text{CO}_3$  were dried in vacuum at 250 °C and stored under argon.  $[\text{Cu}(\text{MeCN})_4]^+$  salts were synthesized according to the literature.<sup>[24]</sup> Storage and preparation of air sensitive compounds were carried out in an argon glove box (MBraun, Garching, Germany; water and dioxygen < 0.1 ppm). NMR measurements were performed with a Bruker Avance II 400 MHz (AV II 400) and Bruker Avance III HD 400 MHz (AV III 400). Solid UV/Vis spectra were recorded using a Perkin Elmer Lambda 750 UV/Vis-NIR spectrometer using a Harrick praying mantis. All shown spectra were converted applying the Kubelka–Munk equation. FTIR measurements were performed using a Bruker Alpha spectrometer equipped with either a DRIFT or an ATR module. Raman spectroscopy was executed on a SENTERRA dispersive Raman microscope (Bruker optics) equipped with a Nd:YAG laser ( $\lambda_{\text{exc}} = 532 \text{ nm}$ ). For determination of the specific surface for silica gel and monoliths, the Brunauer-Emmett-Teller method (BET) was used. A Hi-Tech SF-615X2 low-temperature stopped-flow unit equipped with a diode array spectrophotometer (Hi-Tech, Salisbury, UK) was used for kinetic measurements in solution. A two-syringe setup was used. A

detailed description has been reported previously.<sup>[21]</sup> UV/Vis spectra in solution were obtained with an Agilent 8453 spectrometer. GC-MS measurements were performed using an Agilent Technologies 5977B with a 7820 A GC system. Crystallographic structure determination is described in the Supporting Information.

### Syntheses

***N,N*-Boc-methylethylenediamine:** The protected precursor was synthesized according to the literature:<sup>[23]</sup> *N*-methylethylenediamine (2.00 g, 27.7 mmol) was dissolved in 50 mL dichloromethane. The solution was cooled to 0 °C in an ice bath and a solution of ethyl trifluoroacetate (3.83 g, 27.7 mmol) in 50 mL dichloromethane was added dropwise over a period of 40 minutes under argon. After the addition was complete, the resulting mixture was stirred for another 60 minutes at room temperature. Finally, the solvent was removed under vacuum. The colourless oil obtained, soon turned into a white solid. The product was dissolved in another 100 mL of dichloromethane. Di-*tert*-butyldicarbonate (5.89 g, 27.7 mmol) in 10 mL dichloromethane was added to the product solution at 0 °C under argon. The reaction mixture was stirred for 90 minutes at room temperature and quenched with 30 mL of a saturated sodium hydrogen carbonate solution and 30 mL of ethyl acetate subsequently. The aqueous phase was extracted three times with ethyl acetate. The combined organic layer was washed with brine, dried over  $\text{MgSO}_4$ , filtrated and concentrated with a rotary evaporator. The resulting oil slowly turned into a white solid. The product was placed into a vessel with 75 mL methanol and 25 mL of a 2–3 mol/L sodium hydroxide solution and stirred at room temperature for two hours. Methanol was removed and the aqueous layer was extracted three times with ethyl acetate. The combined organic layer was washed with brine, dried over magnesium sulphate, filtrated and the solvent was removed in vacuum. The crude product was obtained as a pale yellow oil (3.74 g, 21.5 mmol, 79%) and was used without further purification. <sup>1</sup>H-NMR (400 MHz,  $\text{CDCl}_3$ , 24 °C,  $\delta$  [ppm]): 3.31 (br, 2 H,  $\text{NH}_2$ ), 2.88 (s, 5 H,  $\text{NCH}_2/\text{CH}_2$ ), 2.63 (s, 2 H,  $\text{CH}_2$ ), 1.46 (s, 9 H,  $\text{C}(\text{CH}_3)_3$ ) ESI-MS (*m/z*):  $[\text{M} + \text{H}]^+$ : 175.15;  $[\text{M} + \text{Na}]^+$ : 197.13;  $[2 \text{M} + \text{H}]^+$ : 349.28;  $[2 \text{M} + \text{Na}]^+$ : 371.47;

**(2-methylaminoethyl)bis(2-pyridylmethyl)amine (Me-uns-penp):** Reductive alkylation was performed similar to published procedures.<sup>[24]</sup> *N,N*-Boc-methylethylenediamine was dissolved in 60 mL dichloroethane, 2-pyridinecarboxaldehyde (4.82 g, 45.1 mmol) and sodium triacetoxyborohydride (13.63 g, 64.4 mmol) were added. The solution was stirred overnight under argon. Afterwards the reaction suspension was quenched with 60 mL of 2 mol/L NaOH solution and extracted three times with dichloromethane. The organic layers were combined, washed with brine, dried over  $\text{MgSO}_4$ , filtrated and the solvent was removed in vacuum. The obtained brown oil was treated with 100 mL of half concentrated hydrochloric acid. The brown solution was refluxed overnight. NaOH solution (6 mol/L) was slowly added up to a pH of 14 while cooling in an ice bath. The resulting solution was extracted three times with dichloromethane, washed with brine, dried over  $\text{MgSO}_4$ , filtrated and the solvent was removed in vacuum. Kugelrohr distillation led to a pure product which was stored in the glove box (3.11 g, 56%). Overall yield 45% (respectively 2.00 g *N*-methylethylenediamine). <sup>1</sup>H-NMR (400 MHz,  $\text{CDCl}_3$ , 24 °C,  $\delta$  [ppm]): 8.53 (d, 2 H, py-H), 7.65 (td, 2 H, py-H); 7.48 (d, 2 H, py-H), 7.14 (t, 2 H, py-H), 3.85 (s, 4 H, py- $\text{CH}_2$ ), 2.75 (t, 2 H,  $\text{NCH}_2\text{CH}_2\text{N}(\text{CH}_2\text{py})_2$ ), 2.67 (t, 2 H,  $\text{NCH}_2\text{CH}_2\text{N}(\text{CH}_2\text{py})_2$ ), 2.31 (s, 2 H,  $\text{NCH}_2$ ) <sup>13</sup>C-NMR (101 MHz,  $\text{CDCl}_3$ , 24 °C,  $\delta$  [ppm]): 159.6, 149.0, 136.4, 122.9, 121.9, 64.4, 60.8, 53.9, 49.4, 36.3 ESI-MS (*m/z*):  $[\text{M} + \text{H}]^+$ : 257.18;  $[\text{M} + \text{Na}]^+$ : 279.16

**(2-methyl-(3-propyl)dimethyl-methoxysilane-aminoethyl)bis(2-pyridylmethyl)amine (Me-PDMS-uns-penp):** Alkylation of an amine via  $\text{S}_{\text{N}}2$  reaction and halide exchange into acetonitrile has been

reported previously.<sup>15,29</sup> The preparation was carried out in an argon box: Me-uns-penp (0,85 g, 3.32 mmol) was dissolved in 40 mL of acetonitrile and transferred into a 100 mL two-neck Schlenk flask. NaI (5.00 g, 33.4 mmol) and K<sub>2</sub>CO<sub>3</sub> (5.00 g, 36.2 mmol) were added. When the Schlenk Flask was removed from the argon box it immediately was covered with aluminium foil. While applying an argon counter flow (3-chloropropyl)dimethylmethoxysilane (650 µL, 0.69 g, 4.14 mmol) was added via an Eppendorf pipet. The reaction mixture was refluxed under argon at 90 °C for two days. The reaction progress was controlled by sampling the mixture above the free neck of the flask for ESI-MS measurements. After there was no further mass of the precursor ligand detected, dimethyl carbonate (0,5 mL, 0,47 g, 5,19 mmol) and sodium methoxide (0,18 g, 3,33 mmol) dissolved in 3.5 mL of dry methanol were added under argon to transform the side products into the desired product.<sup>30</sup> The reaction was continued overnight. Afterwards the solvent was removed by transferring it into a cold trap. The resulting solid was treated with dry pentane under argon. The suspension was separated via an equipped pre-dried Schlenk frit, end-capped with a flask suitable for Kugelrohr distillation. After transferring the pentane into a cold trap, the crude product was purified via Kugelrohr distillation and then stored in an argon box (0,66 g, 51 %). <sup>1</sup>H-NMR (400 MHz, CDCl<sub>3</sub>, 24 °C, δ [ppm]): 8.48 (d, 2 H, py-H), 7.60 (td, 2 H, py-H); 7.51 (d, 2 H, py-H), 7.09 (t, 2 H, py-H), 3.83 (s, 4 H, py-CH<sub>2</sub>), 3.36 (s, 3 H, SiOCH<sub>3</sub>), 2.67 (t, 2 H, NCH<sub>2</sub>CH<sub>2</sub>N(CH<sub>2</sub>py)<sub>2</sub>), 2.52 (t, 2 H, NCH<sub>2</sub>CH<sub>2</sub>N(CH<sub>2</sub>py)<sub>2</sub>), 2.24 (t, 2 H, NCH<sub>2</sub>CH<sub>2</sub>CH<sub>2</sub>Si), 2.12 (s, 3 H, NCH<sub>3</sub>), 1.41 (m, 2 H, NCH<sub>2</sub>CH<sub>2</sub>CH<sub>2</sub>Si), 0.48 (t, 2 H, NCH<sub>2</sub>CH<sub>2</sub>CH<sub>2</sub>Si), 0.04 (s, 6 H, Si(CH<sub>3</sub>)<sub>2</sub>). <sup>13</sup>C-NMR (101 MHz, CDCl<sub>3</sub>, 24 °C, δ [ppm]): 160.0, 149.1, 136.4, 122.9, 121.9, 61.6, 61.0, 55.8, 52.3, 50.4, 42.6, 21.0, 13.5, -2.6 ESI-MS (m/z): [M + H]<sup>+</sup>: 387.26; [M + Na]<sup>+</sup>: 409.24 IR (ATR, ν<sup>-</sup> [cm<sup>-1</sup>]): 3052 (w), 3009 (w) 2933 (m), 2827 (m), 1589 (s), 1570 (m), 1427 (m), 1433 (s), 1362 (m), 1305 (w), 1250 (s), 1188 (m), 1146 (m), 1085 (vs), 1047 (s), 1015 (m), 994 (m), 981 (m), 882 (m), 836 (vs), 757 (vs), 729 (s), 634 (w), 615 (m), 470 (w), 404 (s)

**(2-methyl-(3-propyl)trimethylsilane-aminoethyl)bis(2-pyridylmethyl)-amine (Me-PTS-uns-penp):** Me-uns-penp (0.75 g, 2.9 mmol) was dissolved in 30 mL acetonitrile, mixed with K<sub>2</sub>CO<sub>3</sub> (4.9 g, 35.5 mmol) and (3-chloropropyl)trimethylsilane (0.55 mL, 0.49 g, 3.2 mmol) and covered with aluminium foil. The suspension was heated to reflux for two days under argon. The solvent was removed by rotary evaporation and the residue was treated with diethyl ether and filtered. The obtained solution was concentrated and the crude product was purified via Kugelrohr distillation (0.65 g; 60%). The product was stored in absence of oxygen and moisture in an argon box. <sup>1</sup>H-NMR (400 MHz, CDCl<sub>3</sub>, 24 °C, δ [ppm]): 8.50 (d, 2 H, py-H), 7.62 (td, 2 H, py-H); 7.52 (d, 2 H, py-H), 7.11 (t, 2 H, py-H), 3.84 (s, 4 H, py-CH<sub>2</sub>), 2.68 (t, 2 H, NCH<sub>2</sub>CH<sub>2</sub>N(CH<sub>2</sub>py)<sub>2</sub>), 2.53 (t, 2 H, NCH<sub>2</sub>CH<sub>2</sub>N(CH<sub>2</sub>py)<sub>2</sub>), 2.24 (t, 2 H, NCH<sub>2</sub>CH<sub>2</sub>CH<sub>2</sub>Si), 2.13 (s, 3 H, NCH<sub>3</sub>), 1.37 (m, 2 H, NCH<sub>2</sub>CH<sub>2</sub>CH<sub>2</sub>Si), 0.37 (t, 2 H, NCH<sub>2</sub>CH<sub>2</sub>CH<sub>2</sub>Si), -0.07 (s, 9 H, Si(CH<sub>3</sub>)<sub>3</sub>). <sup>13</sup>C-NMR (101 MHz, CDCl<sub>3</sub>, 26 °C, δ [ppm]): 160.1, 149.2, 136.5, 123.0, 122.0, 62.0, 61.1, 55.84, 55.7, 52.4, 42.8, 21.9, 14.4, -1.5 ESI-MS (m/z): [M + H]<sup>+</sup>: 371.26 IR (ATR, ν<sup>-</sup> [cm<sup>-1</sup>]): 3051 (w), 3009 (w) 2950 (m), 2795 (m), 1589 (s), 1570 (m), 1472 (s), 1433 (s), 1362 (m), 1303 (m), 1247 (s), 1172 (m), 1146 (m), 1121 (m), 1047 (m), 1016 (m), 994 (m), 982 (m), 835 (vs), 775 (vs), 691 (m), 634 (w), 613 (m), 513 (w), 472 (w), 404 (w)

**(2-methyl-propyl-aminoethyl)bis(2-pyridylmethyl)amine (Me-Prop-uns-penp):** Me-uns-penp (1.00 g, 3.9 mmol) was mixed with *n*-iodopropane (0.7 g, 4.1 mmol) and K<sub>2</sub>CO<sub>3</sub> (2.5 g, 18.1 mmol) in 20 mL of acetonitrile. The mixture was stirred under argon at 50 °C for two days. The solvent was removed by rotary evaporation and the residue was dissolved in diethyl ether and filtered. Removing the solvent *in vacuo* and purification via Kugelrohr distillation yielded the product as a yellow oil (0,65 g, 56%). The product was stored in the absence of oxygen and moisture in an argon box. <sup>1</sup>H-

NMR (400 MHz, CDCl<sub>3</sub>, 23 °C, δ [ppm]): 8.49 (d, 2 H, py-H), 7.61 (td, 2 H, py-H); 7.52 (d, 2 H, py-H), 7.10 (t, 2 H, py-H), 3.83 (s, 4 H, py-CH<sub>2</sub>), 2.67 (t, 2 H, NCH<sub>2</sub>CH<sub>2</sub>N(CH<sub>2</sub>py)<sub>2</sub>), 2.52 (t, 2 H, NCH<sub>2</sub>CH<sub>2</sub>N(CH<sub>2</sub>py)<sub>2</sub>), 2.21 (t, 2 H, NCH<sub>2</sub>CH<sub>2</sub>CH<sub>2</sub>), 2.14 (s, 3 H, NCH<sub>3</sub>), 1.40 (m, 2 H, NCH<sub>2</sub>CH<sub>2</sub>CH<sub>2</sub>), 0.80 (t, 2 H, NCH<sub>2</sub>CH<sub>2</sub>CH<sub>2</sub>). <sup>13</sup>C-NMR (101 MHz, CDCl<sub>3</sub>, 24 °C, δ [ppm]): 160.0, 149.1, 136.4, 122.9, 122.0, 61.0, 60.24, 55.7, 52.26, 42.7, 20.5, 12.0 ESI-MS (m/z): [M + H]<sup>+</sup>: 299.22 IR (ATR, ν<sup>-</sup> [cm<sup>-1</sup>]): 3063 (w), 3009 (w), 2958(m), 2933 (m), 2873 (m), 2801 (m), 1676 (w), 1589 (s), 1570 (s), 1472 (s), 1433 (s), 1362 (m), 1305 (m), 1249 (m), 1216 (m), 1147 (m), 1122 (m), 1083 (m), 1047 (s), 994 (s), 892 (m), 842 (m), 755 (vs), 613 (s), 516 (m), 468 (m)

**Me-uns-penp<sub>immob</sub>(silica gel):** Silica gel for column chromatography (Kieselgel 60 M, Macherey-Nagel, Germany) was prepared by refluxing it in concentrated hydrochloric acid for 24 h followed by washing it with demineralized water for neutralisation.<sup>43</sup> Me-PDMS-uns-penp (56 mg, 0.14 mmol) was dissolved in dry toluene, suspended with 1.00 g of prepared silica gel and stirred for at least 30 minutes. The condensation on the silica surface was performed at 130 °C under argon for 24 h.<sup>55</sup> Additionally, the functionalized powder was filtered with a glass frit pore 4, washed with toluene, ethanol and diethyl ether. The material was transferred into an argon box, suspended in 10 mL of acetonitrile and 0.5 mL trimethylamine and stirred for ten minutes. The powder was washed again with acetonitrile, diethyl ether and dried in vacuum. The final functionalized silica gel was kept under argon in a glove box. IR (DRIFTS, ν<sup>-</sup> [cm<sup>-1</sup>]): 2963, 2910, 1601, 1575, 1482, 1439, Raman (raman shift, ν<sup>-</sup> [cm<sup>-1</sup>]): 3069 (s), 2962 (s), 2906 (s), 1661 (m), 1575 (m), 1224 (m), 1053 (s), 1010 (s), 833 (w), 636 (w), 486 (w) UV/Vis (diffuse reflectance, λ [nm]): 205, 260

**Me-uns-penp<sub>immob</sub>(monolith):** A silica monolith (108 mg), pre-dried at 150 °C, was placed in a Schlenk reactor (Figure S10, Supporting Information) and covered with 60 mL of dry toluene with Me-PDMS-uns-penp (8.0 mg, 0.03 mmol). The reactor was heated to reflux for 24 h under argon.<sup>55</sup> The monolith was placed into a petri dish and first covered with toluene, then with ethanol and finally with diethyl ether for 15 minutes each. Further preparation took place in an argon box. The monolith was treated with 1.0 mL trimethylamine in 20 mL acetonitrile for ten minutes. Afterwards the monolith was treated again with first acetonitrile and finally with diethyl ether each for 10 minutes. The monolith was dried in vacuum and stored in a glove box. IR (DRIFTS, ν<sup>-</sup> [cm<sup>-1</sup>]): 2961, 1601, 1573, 1480, 1439 Raman (raman shift, ν<sup>-</sup> [cm<sup>-1</sup>]): 3079 (w), 3069 (w), 2964 (w), 2909 (w), 1228 (w), 1052 (w), 1009 (vw) UV/Vis (diffuse reflectance, λ [nm]): 205, 260

**[Cu(Me-uns-penp<sub>immob</sub>(silica gel))(SO<sub>3</sub>CF<sub>3</sub>)<sub>2</sub>]:** 200 mg of Me-uns-penp<sub>immob</sub> were suspended in a solution of 100 mg copper(II) trifluoromethanesulfonate in 10 mL acetonitrile and stirred for one hour. Blue powder can be obtained by interrupting the reaction after ten minutes. The green product obtained after approximately one hour of complexation reaction. Both products were washed properly with acetonitrile and diethyl ether. After drying in vacuum, products were stored under argon. UV/Vis (diffuse reflectance, λ [nm]): 205, 260, 288, (421 for the green product)

**[Cu(Me-uns-penp<sub>immob</sub>(silica gel))]X (X: SO<sub>3</sub>CF<sub>3</sub><sup>-</sup>, PF<sub>6</sub><sup>-</sup>):** 50 mg of [Cu(MeCN)<sub>2</sub>]X was dissolved in dry acetonitrile under inert conditions. 100 mg functionalized silica were suspended in the copper solution. After one hour the yellow solid was removed from the suspension, washed several times with acetonitrile and diethyl ether and dried in vacuum. The silica appears as a yellow solid and was stored under argon. UV/Vis (diffuse reflectance, λ [nm]): 205, 260, 288

**[Cu(Me-uns-penp<sub>immob</sub>(monolith))]SO<sub>3</sub>CF<sub>3</sub>:** The functionalized monolith was placed into a petri dish und covered with a solution

of 50 mg  $[\text{Cu}(\text{MeCN})_4] \text{SO}_3\text{CF}_3$  dissolved in 20 mL acetonitrile. After ten minutes, the monolith was kept in acetonitrile and diethyl ether, each time for ten minutes, to remove the remaining copper salt. After drying in vacuum the monolith had turned into a yellow colour. UV/Vis (diffuse reflectance,  $\lambda$  (nm)): 205, 260, 288

Cu(I) and Cu(II) complexes with the derivatives of uns-penp described below were prepared under argon similar to published procedures for related complexes.<sup>19,24)</sup>

**[Cu(Me-PTS-uns-penp)]BPh<sub>4</sub>**: A solution of  $[\text{Cu}(\text{MeCN})_4]\text{PF}_6$  (0.19 g, 0.51 mmol) in 2 mL acetone was added dropwise with stirring to a solution of Me-PTS-uns-penp (0.20 g, 0.54 mmol) in 0.5 mL acetone. Additionally, sodium tetraphenylborate (0.19 g, 0.56 mmol) was added to the yellow coloured complex solution. The final solid was obtained by adding the solution into approximately 40 mL of pentane. The yellow compound was filtered of, washed with diethyl ether and dried in vacuum. Single crystals for X-ray diffraction were obtained by diffusion of diethyl ether.

**[Cu(Me-Prop-uns-penp)]BPh<sub>4</sub>**: A solution of  $[\text{Cu}(\text{MeCN})_4]\text{PF}_6$  (0.24 g, 0.64 mmol) in 2 mL acetone was added dropwise to a stirred solution of Me-Prop-uns-penp (0.20 g, 0.67 mmol) in 0.5 mL acetone. Additionally sodium tetraphenylborate. (0.24 g, 0.70 mmol) was added to the yellow coloured complex solution. The final solid was obtained by adding the solution into approximately 40 mL of diethyl ether. The yellow compound was filtered of, washed with diethyl ether and dried in vacuum. Single crystals for X-ray diffraction were obtained by ether diffusion.

**[Cu(Me-Prop-uns-penp)Cl]ClO<sub>4</sub>**: Me-Prop-uns-penp (50 mg, 0.16 mmol) was dissolved into 4 mL of methanol.  $\text{CuCl}_2 \cdot 2\text{H}_2\text{O}$  (14 mg, 0.08 mmol) and of  $\text{Cu}(\text{ClO}_4)_2 \cdot 6\text{H}_2\text{O}$  (31 mg, 0.08 mmol) were added. After brief stirring suitable crystals for X-ray analysis could be obtained by slow evaporation of the solvent.

**Supporting Information** (see footnote on the first page of this article): Additional information about time resolved stopped flow measurements, calibration values via UV/Vis measurement, BET values, spectra of surface investigations, schematic drawing of the monolith reactor, additional results of oxygen treatment, GC-MS and crystallographic data.

## Acknowledgements

Financial support is gratefully acknowledged by the Deutsche Forschungsgemeinschaft (DFG SPP1740, SCHI 377/13-2). Open access funding enabled and organized by Projekt DEAL.

**Keywords:** immobilization · monolith · copper complex · tripodal ligands · superoxido complex

- [1] A. Andersen, *Int. J. Toxicol.* **2006**, *25 Suppl 1*, 11–27.
- [2] F. Wöhler, J. von Liebig, *Ann. der Pharm.* **1832**, *3*, 249,282.
- [3] E. Breitmaier, G. Jung in *Organische Chem*, Thieme Verlag, Stuttgart, **2009**, Vol. 6, p.318.
- [4] F. Wang, J. Xu, X. Li, J. Gao, L. Zhou, R. Ohnishi, *Adv. Synth. Catal.* **2005**, *347*, 1987–1992.
- [5] E. V. Boikov, M. V. Vishnetskaya, A. N. Emel'yanov, I. S. Tomskii, N. V. Shcherbakov, *Russ. J. Phys. Chem. A* **2008**, *82*, 2233–2237.
- [6] S. Gast, J. H. Matthies, U. S. Tuttlies, U. Nieken, *Chem. Eng. Technol.* **2017**, *40*, 1445–1452.

- [7] E. I. Solomon, D. E. Heppner, E. M. Johnston, J. W. Ginsbach, J. Cirera, M. Qayyum, M. T. Kieber-Emmons, C. H. Kjaergaard, R. G. Hadt, L. Tian, *Chem. Rev.* **2014**, *114*, 3659–3853.
- [8] L. M. Mirica, X. Ottenwaelder, T. D. P. Stack, *Chem. Rev.* **2004**, *104*, 1013–1045.
- [9] C. Würtele, O. Sander, V. Lutz, T. Waitz, F. Tuczek, S. Schindler, *J. Am. Chem. Soc.* **2009**, *131*, 7544–7545.
- [10] H. R. Lucas, L. Li, A. A. N. Sarjeant, M. A. Vance, E. I. Solomon, K. D. Karlin, *J. Am. Chem. Soc.* **2009**, *131*, 3230–3245.
- [11] F. Hoffmann, M. Cornelius, J. Morell, M. Fröba, *Angew. Chem. Int. Ed.* **2006**, *45*, 3216–3251; *Angew. Chem.* **2006**, *118*, 3290–3328.
- [12] M. Ferré, R. Pleixats, M. Wong Chi Man, X. Cattoën, *Green Chem.* **2016**, *18*, 881–922.
- [13] P. K. Jal, S. Patel, B. K. Mishra, *Talanta* **2004**, *62*, 1005–1028.
- [14] S. Sun, Y. Cao, J. Feng, P. Wu, *J. Mater. Chem.* **2010**, *20*, 5605–5607.
- [15] C. Suspène, S. Brandès, R. Guillard, *Chem. Eur. J.* **2010**, *16*, 6352–6364.
- [16] M. Yamada, K. D. Karlin, S. Fukuzumi, *Chem. Sci.* **2016**, *7*, 2856–2863.
- [17] K. Szymańska, K. Odrozek, A. Zniszczoł, G. Torrello, V. Resch, U. Hanefeld, A. B. Jarzębski, *Catal. Sci. Technol.* **2016**, *6*, 4882–4888.
- [18] B. Karimi, D. Enders, *Org. Lett.* **2006**, *8*, 1237–1240.
- [19] L. D. White, C. P. Tripp, *J. Colloid Interface Sci.* **2000**, *232*, 400–407.
- [20] J. B. Mandel, C. Maricondi, B. E. Douglas, *Inorg. Chem.* **1988**, *27*, 2990–2996.
- [21] M. Weitzer, M. Schatz, F. Hampel, F. W. Heinemann, S. Schindler, *Dalton Trans.* **2002**, 686–694.
- [22] G. C. Kuang, J. R. Allen, M. A. Baird, B. T. Nguyen, L. Zhang, T. J. Morgan, C. W. Levenson, M. W. Davidson, L. Zhu, *Inorg. Chem.* **2011**, *50*, 10493–10504.
- [23] C. Komiya, K. Aihara, K. Morishita, H. Ding, T. Inokuma, A. Shigenaga, A. Otaka, *J. Org. Chem.* **2016**, *81*, 699–707.
- [24] M. Schatz, M. Leibold, S. P. Foxon, M. Weitzer, F. W. Heinemann, F. Hampel, O. Walter, S. Schindler, *Dalton Trans.* **2003**, 1480–1487.
- [25] J. W. Park, Y. J. Park, C. H. Jun, *Chem. Commun.* **2011**, *47*, 4860–4871.
- [26] B. Arkles, *Gelst, Inc.* **2014**, 1–76.
- [27] D. Huebner, V. Koch, B. Ebeling, J. Mechau, J. E. Steinhoff, P. Vana, *J. Polym. Sci. Part A* **2015**, *53*, 103–113.
- [28] H. Finkelstein, *Ber. Dtsch. Chem. Ges.* **1910**, *43*, 1528.
- [29] L. Li, W. Liu, H. Zeng, X. Mu, G. Cosa, Z. Mi, C. J. Li, *J. Am. Chem. Soc.* **2015**, *137*, 8328–8331.
- [30] E. Suzuki, M. Akiyama, Y. Ono, *J. Chem. Soc. Chem. Commun.* **1992**, 136–137.
- [31] M. Weitzer, S. Schindler, G. Brehm, S. Schneider, E. Hörmann, B. Jung, S. Kaderli, A. D. Zuberbühler, *Inorg. Chem.* **2003**, *42*, 1800–1806.
- [32] S. Schindler, *Eur. J. Inorg. Chem.* **2000**, 2311–2326.
- [33] M. Schatz, M. Becker, F. Thaler, F. Hampel, S. Schindler, R. R. Jacobson, Z. Tyeklar, N. N. Murthy, P. Ghosh, Q. Chen, et al., *Inorg. Chem.* **2001**, *40*, 2312–2322.
- [34] C. Würtele, E. Gaoutchenova, K. Harms, M. C. Holthausen, J. Sundermeyer, S. Schindler, *Angew. Chem. Int. Ed.* **2006**, *45*, 3867–3869; *Angew. Chem.* **2006**, *118*, 3951–3954.
- [35] R. R. Jacobson, Z. Tyeklar, A. Farooq, K. D. Karlin, S. Liu, J. Zubieta, A. Farooq, R. R. Jacobson, Z. Tyeklar, K. D. Karlin, et al., *J. Am. Chem. Soc.* **1988**, *110*, 3690–3692.
- [36] T. Hoppe, S. Schaub, J. Becker, C. Würtele, S. Schindler, *Angew. Chem.* **2013**, *125*, 904–907; *Angew. Chem. Int. Ed.* **2013**, *52*, 870–873.

- [37] S. Fujinami, A. Hashimoto, K. Komiyama, S. Nagatomo, T. Kitagawa, M. Suzuki, H. Hayashi, H. Furutachi, *Bull. Chem. Soc. Jpn.* **2004**, *77*, 59–72.
- [38] M. Becker, F. W. Heinemann, S. Schindler, *Chem. A Eur. J.* **1999**, *5*, 3124–3129.
- [39] A. W. Addison, T. N. Rao, *J. Chem. Soc. Dalton Trans.* **1984**, 1349–1356.
- [40] Y. Kobayashi, K. Ohkubo, T. Nomura, M. Kubo, N. Fujieda, H. Sugimoto, S. Fukuzumi, K. Goto, T. Ogura, S. Itoh, *Eur. J. Inorg. Chem.* **2012**, 4574–4578.
- [41] F. Carré, R. J. P. Corriu, E. Lancelle-Beltran, A. Mehdi, C. Reyé, R. Guillard, J. Sýkora, A. Van Der Lee, *J. Chem. Soc. Dalton Trans.* **2003**, *3*, 3211–3215.
- [42] K. Machado, P. B. Tavares, C. Freire, G. S. Mishra, *Polyhedron* **2014**, *69*, 119–126.
- [43] E. M. Soliman, *Anal. Lett.* **1997**, *30*, 1739–1751.
- [44] L. T. Zhuravlev, *Colloid. Silica Fundam. Appl.* **2005**, *173*, 261–266.
- [45] G. Socrates, *Infrared and Raman Characteristic Group Frequencies. Tables and Charts*, Vol. 3, Wiley-VCH, Weinheim, **2001**.
- [46] M. Hesse, H. Meier, B. Zeeh in *Spektroskopische Methoden in Der Organischen Chemie*, Vol. 8, Thieme Verlag, Stuttgart, **2012**.
- [47] R. Meinus, R. Ellinghaus, K. Hormann, U. Tallarek, B. M. Smarsly, *Phys. Chem. Chem. Phys.* **2017**, *19*, 14821–14834.
- [48] K. Nakanishi, N. Soga, *J. Am. Ceram. Soc.* **1991**, *74*, 2518–2530.
- [49] T. Hara, S. Mascotto, C. Weidmann, B. M. Smarsly, *J. Chromatogr. A* **2011**, *1218*, 3624–3635.
- [50] L. Jianmin, Z. Yugeng, *Cryst. Res. Technol.* **1991**, *26*, 331–337.
- [51] D. Maiti, D.-H. Lee, K. Gaoutchenova, C. Würtele, M. C. Holthausen, A. A. Narducci Sarjeant, J. Sundermeyer, S. Schindler, K. D. Karlin, *Angew. Chem.* **2008**, *120*, 88–91.
- [52] C. E. Elwell, N. L. Gagnon, B. D. Neisen, D. Dhar, A. D. Spaeth, G. M. Yee, W. B. Tolman, *Chem. Rev.* **2017**, *117*, 2059–2107.
- [53] C. C. Liu, T. S. Lin, S. I. Chan, C. Y. Mou, *J. Catal.* **2015**, *322*, 139–151.
- [54] W. D. Bailey, N. L. Gagnon, C. E. Elwell, A. C. Cramblitt, C. J. Bouchev, W. B. Tolman, *Inorg. Chem.* **2019**, *58*, 4706–4711.
- [55] A. S. Amarasekara, O. S. Owereh, *Catal. Commun.* **2010**, *11*, 1072–1075.

Manuscript received: January 16, 2021

Revised manuscript received: February 17, 2021

Accepted manuscript online: February 17, 2021



**4. Characterization of copper complexes with derivatives of the ligand (2-aminoethyl)bis(2-pyridylmethyl)amine (uns-penp) and their reactivity towards oxygen**

This work has been published in

*Journal of Inorganic Biochemistry*

Tim Brückmann, Jonathan Becker, Christian Würtele, Marcel Seuffert, Dominik Heuler, Klaus Müller-Buschbaum, Morten Weiß, Siegfried Schindler,

*J. Inorg. Biochem.* **2021**, 223, 111544

<https://doi.org/10.1016/j.jinorgbio.2021.111544>



Contents lists available at ScienceDirect

Journal of Inorganic Biochemistry

journal homepage: [www.elsevier.com/locate/jinorgbio](http://www.elsevier.com/locate/jinorgbio)

## Characterization of copper complexes with derivatives of the ligand (2-aminoethyl)bis(2-pyridylmethyl)amine (uns-penp) and their reactivity towards oxygen

Tim Brückmann<sup>a</sup>, Jonathan Becker<sup>a</sup>, Christian Würtele<sup>a</sup>, Marcel Thomas Seuffert<sup>a</sup>, Dominik Heuler<sup>a</sup>, Klaus Müller-Buschbaum<sup>a</sup>, Morten Weiß<sup>b</sup>, Siegfried Schindler<sup>a,\*</sup>

<sup>a</sup> Institut für Anorganische und Analytische Chemie, Justus-Liebig-Universität, Heinrich-Buff-Ring 17, 35392 Giessen, Germany

<sup>b</sup> Fakultät für Biologie, Chemie und Geowissenschaften, Universität Bayreuth, Universitätsstrasse 30, 95447 Bayreuth, Germany

### ARTICLE INFO

#### Keywords:

Copper complex  
Tripodal ligands  
Dioxygen activation  
Peroxido complex  
Superoxido complex  
Stopped-flow

### ABSTRACT

A series of copper(I) complexes with ligands derived from the tripodal ligand (2-aminoethyl)bis(2-pyridylmethyl)amine (uns-penp) have been structurally characterized and their redox chemistry analyzed by cyclic voltammetry. While the redox potentials of most of the complexes were similar their reactivity towards dioxygen was quite different. While the complex with a ferrocene derived ligand of uns-penp reacted in solution at low temperatures in a two-step reaction from the preliminary formed mononuclear *end-on* superoxido complex to a quite stable dinuclear peroxido complex it did not react with dioxygen in the solid state. Other complexes also did not react with dioxygen in the solid state while some showed a reversible formation to a green compound, indicating formation of an *end-on* superoxido complex that unfortunately so far could not be characterized. In contrast, copper complexes with the Me<sub>2</sub>uns-penp and Et-iProp-uns-penp formed dinuclear peroxido complexes in a solid-state reaction. While the reaction of dioxygen with the [Cu(Me<sub>2</sub>uns-penp)BPh<sub>4</sub>] was quite slow an instant reaction took place for [Cu(Et-iProp-uns-penp)BPh<sub>4</sub>]. Very unusual, it turned out that crystals of the copper(I) complex that could be structurally characterized still were crystalline when reacted with dioxygen. Therefore, it was possible to solve the structure of the corresponding dinuclear peroxido complex directly from the same batch of crystals. The crystalline structures of the copper(I) and copper(II) complex revealed that the reason for this is the fact, that the copper(I) complex is kind of preorganized for the uptake of dioxygen and does not really change in its overall structure when being oxidized.

### 1. Introduction

Copper plays an important role in organic life. Due to its accessible I/II redox pair and biological availability it is mostly present in enzymatic processes of electron transfer, dioxygen transport and oxidation/oxygenation of organic substrates [1]. During the last decades, quite some understanding had been gained for the reactions of copper(I) complexes with dioxygen and a large number of different so called “dioxygen adduct” complexes could be identified. Some structurally characterized examples of these complexes are presented in Fig. 1. Some of these complexes are found in the active site of copper enzymes, mainly monooxygenases, such as e. g. **a** (Fig. 1) in peptidylglycine  $\alpha$ -hydroxylating monooxygenase (PHM) and dopamine- $\beta$ -mono-oxygenase (D $\beta$ M) or **e** in tyrosinase. While actually, so far, only these two

species, an *end-on*  $\eta^1$ -superoxido (**a**) and a *side-on*  $\eta^2$ -peroxido copper complex (**e**), have been detected in biological systems, this does not mean that the other complexes in Fig. 1 are less interesting [2]. For example, bis( $\mu$ -oxido) copper complexes **f** (which in some cases can be in an equilibrium with the *side-on*  $\eta^2$ : $\eta^2$ -peroxido copper complex **e**) proved to be quite useful in selective hydroxylation reactions (only two selected examples are given in the references) [3,4]. Furthermore, we as well as Karlin and co-workers had observed that *trans*- $\mu$ -1,2-peroxido complexes **b** are capable to catalytically oxidize toluene selectively to benzaldehyde [5,6]. There is high interest to transfer this type of reaction from the lab into industry where such oxygenations are usually done at higher temperatures, sometimes in the presence of quite toxic chemicals and often accompanied by undesired side products. In contrast, copper complexes that model the reactivity of the natural

\* Corresponding author.

E-mail address: [siegfried.schindler@anorg.chemie.uni-giessen.de](mailto:siegfried.schindler@anorg.chemie.uni-giessen.de) (S. Schindler).

<https://doi.org/10.1016/j.jinorgbio.2021.111544>

Received 17 April 2021; Received in revised form 5 July 2021; Accepted 12 July 2021

Available online 16 July 2021

0162-0134/© 2021 Elsevier Inc. All rights reserved.

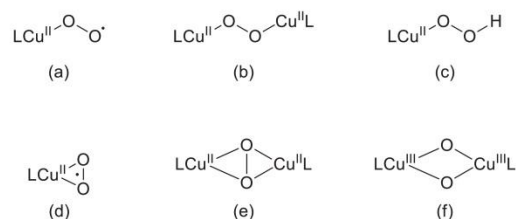
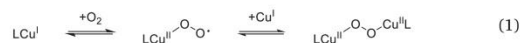


Fig. 1. Examples of copper "dioxygen adduct" species: (a) *end-on* superoxido, (b) *trans-μ-1,2-peroxido*, (c)  $\eta^1$ -hydroperoxido, (d) *side-on* superoxido, (e)  $\mu$ - $\eta^2$ : $\eta^2$ -peroxido, (f) bis( $\mu$ -oxido).

enzymes should catalyze these reactions under ambient conditions with dioxygen from air as the sole oxidant, with high yields and with fewer side products.

The first structurally characterized "dioxygen adduct" complex, [(tmpa)Cu(O<sub>2</sub>)Cu(tmpa)](PF<sub>6</sub>)<sub>2</sub> (tmpa = tris(2-methylpyridyl)-amine, Fig. 2), a **b** system was reported by Karlin and co-workers [7]. The formation of this complex had been investigated in great detail and low temperature stopped-flow measurements allowed the brief observation of a short-lived *end-on* superoxido complex (a) in a first reaction step according to the Eq. (1) [8,9]. Due to the consecutive reaction to the dinuclear peroxido complex this labile intermediate could only be spectroscopically (UV–vis data) characterized.



Following up on these results it was possible, with the copper(I) complex and the tripodal ligand tris(2-dimethylaminoethyl)amine (Me<sub>6</sub>tren, Fig. 2), to observe the same reactivity (Eq. (1)), however here it was possible to obtain a resonance Raman spectrum of the intermediate with a characteristic peak at 1122 cm<sup>-1</sup> for the vibration frequency of <sup>16</sup>O–<sup>16</sup>O [10].

With the tren system it seemed easy to modify the ligand system accordingly to finally stabilize an *end-on* superoxido copper enough for a full characterization. Instead, this turned out to be a journey for many years with some of the efforts by us only been published recently [11]. However, by applying the tren derivative tris(tetramethylguanidino) tren (TMG<sub>3</sub>tren, Fig. 2) as a ligand the corresponding *end-on* superoxido complex, [(TMG<sub>3</sub>tren)Cu(O<sub>2</sub>)]SbF<sub>6</sub>, was formed in a reversible reaction and was stabilized to the point that it could finally be structurally characterized [12,13]. While this complex so far is still the only example of a structurally characterized *end-on* superoxido copper complex and can be regarded as a decent model complex for PHM and DβM, it lacks their reactivity (due to the increased stability). However, most recently in a cooperation with Karlin and co-workers it could be shown that a copper(I) complex with a sulfur derivative of TMG<sub>3</sub>tren can model this reactivity [14,15].

From all these findings over the last 20 years it became clear that slight ligand modifications of the tripodal ligand system (chelate ring size, donor atoms, alkyl groups) in combination with solvent and selected anions can have a huge influence on the reaction of the

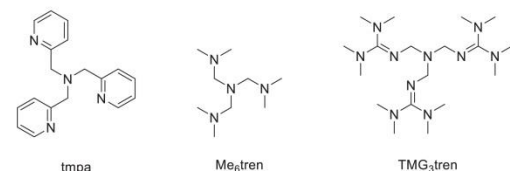


Fig. 2. Tripodal ligands tmpa, Me<sub>6</sub>tren and TMG<sub>3</sub>tren.

corresponding copper(I) complexes with dioxygen.

With regard to these findings we have started a thorough investigation on copper complexes with derivatives of the ligand (2-aminoethyl)bis(2-pyridylmethyl)amine (uns-penp, Fig. 3), that can be viewed as a combination of the ligands tmpa and tren. The advantage of this ligand is the possibility to easily modify the amine arm to test for the influence of different substituents or to prepare it for an immobilization [16]. To get a better picture of the influence of the amine arm modification on the reactivity of the corresponding copper(I) complexes with dioxygen we in here now present a systematic study with the ligands presented in Fig. 3.

## 2. Experimental

### 2.1. Materials and methods

All chemicals were purchased from commercial suppliers. Extra dry solvents were refluxed under argon over a drying agent prior to taking them into the glove box. [Cu(MeCN)<sub>4</sub>]<sup>+</sup> salts were synthesized according to literature methods [17]. Storage and preparation of air sensitive compounds was carried out in a glove box under an argon atmosphere (Braun, Garching, Germany; water and dioxygen <0.1 ppm). NMR measurements were performed with a Bruker Avance II 400 MHz (AV II 400) and Bruker Avance III HD 400 MHz (AV III 400). Electrospray ionization-MS (ESI-MS) measurements were performed on a Bruker microTOF mass spectrometer. UV–Vis investigations in solution were performed with an Agilent 8453 spectrometer, equipped with a cryostat CoolSpek UV USP-203-B (Unisoku Co., Ltd., Osaka, Japan). Solid state UV–Vis spectra were recorded using a Perkin Elmer Lambda 750 UV–Vis-NIR spectrometer equipped with a Harrick praying mantis. All shown spectra were converted into absorption by the Kubelka–Munk equation [18]. A Hi-Tech SF-61SX2 low-temperature stopped-flow unit equipped with a diode array spectrophotometer (Hi-Tech, Salisbury, UK) was used for kinetic measurements in solution. A two-syringe setup was applied to perform the experiments. Detailed descriptions on the setup and the procedure have been reported previously [19]. Raman spectroscopy was executed on a SENTERRA dispersive Raman microscope (Bruker optics) equipped with a Nd:YAG laser ( $\lambda_{\text{exc}} = 532$  nm). Cyclic voltammetry measurements (CV) were performed with an e-corder 410 High Resolution Laboratory Data Recorder, connected with an EA163 Potentiostat (eDAQ, Denistone East, Australia). Powder X-ray diffraction (PXRD) was carried out on a STOE STADI P diffractometer (Darmstadt, Germany), equipped with a DECTRIS MYTHEN 1 K detector and a Ge(111) monochromator. Cu K $\alpha$  radiation ( $\lambda = 1.5406$  Å) was used in Debye–Scherrer geometry. Samples were filled under an argon

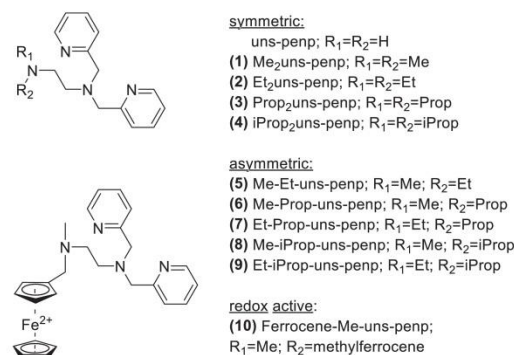


Fig. 3. Ligands L, derivatives of uns-penp derivatives and abbreviations (Me = methyl; Et = ethyl; Prop = propyl; iProp = isopropyl).

atmosphere into glass capillaries (Hilgenberg  $\varnothing = 0.5$  mm) and sealed prior to the measurements. The WinXPOW program package (V3.05, STOE & Cie GmbH 2011, Darmstadt, Germany) was used for data collection. Details on single crystal characterization are reported in the Supporting Information.

## 2.2. Reactivity towards oxygen

The reactions of the complexes with dioxygen were carried out either in solution or in the solid state. For reactions in solution, the complexes were dissolved in dry and dioxygen free acetone. For time resolved stopped-flow UV-Vis measurements the solutions were reacted at low temperatures with dioxygen saturated acetone. The solvent was saturated by passing dioxygen for 15 min through a syringe filled with dry acetone [20]. For other UV-Vis measurements the complex solutions were cooled to low temperatures using a cryo unit. The solutions were subsequently flushed with dioxygen. For solid state reactions, the crystalline complexes were treated with gaseous dioxygen.

## 2.3. Cyclic voltammetry measurements

The cyclic voltammetry measurements were carried out in a conventional, three-electrode setup (working, counter, and reference electrode) [21]. As working electrode, a glassy carbon electrode and as counter electrode a Pt/Ti wire were used. As reference served an Ag/AgCl electrode. The cell was prepared under an inert atmosphere. 0.1 mol/L dried tetrabutylammonium tetrafluoroborate solution in dry acetonitrile was used as electrolyte; the scanning rate was 50 mV/S. Complex concentrations of 1 mmol/L was used. During the measurements the vessel was flushed continuously with dinitrogen through a syringe to avoid air exposure.

## 2.4. Syntheses

Syntheses were performed according to procedures reported in the literature for the asymmetric uns-penp derivatives and furthermore for the basic ligand uns-penp and its derivatives [22,23].

### 2.4.1. (2-methylaminoethyl)bis(2-pyridylmethyl)amine (Me-uns-penp)

2.0 g *N*-methylthylenediamine (27.7 mmol) were dissolved in 50 mL dichloromethane (DCM). The solution was cooled to 0 °C with an ice bath and a solution of 3.83 g ethyltrifluoroacetate (27.7 mmol) in 50 mL DCM was added dropwise over a period of 40 min under argon. After the addition was complete, the resulting mixture was stirred for another 60 min at room temperature. The solvent, as well as the ethanol from the reaction were removed using a rotary evaporator. The obtained colorless oil crystallized as a white solid briefly afterwards. To attach a butoxycarbonyl (Boc) protecting group the product was dissolved in 100 mL of DCM. 5.89 g of di-*tert*-butyldicarbonate (Boc<sub>2</sub>O) in 10 mL DCM were added to the product solution at 0 °C under argon. The reaction mixture was stirred for 90 min at room temperature and then quenched with 30 mL of saturated Na<sub>2</sub>CO<sub>3</sub> solution and 30 mL of ethyl acetate. After gas formation stopped the aqueous phase was extracted three times with ethyl acetate. The combined organic layers were washed with brine, dried over MgSO<sub>4</sub>, filtrated and concentrated using a rotary evaporator. The resulting oil crystallized as a white solid after a few minutes. The product was placed into a vessel with 75 mL methanol and 25 mL of a 2–3 M NaOH solution and stirred at room temperature for two hours. Finally, methanol was removed and the aqueous layer was extracted three times with ethyl acetate. The combined organic layers were washed with brine, dried over MgSO<sub>4</sub>, filtrated and the solvent was removed under vacuum. The crude product was a pale, yellow colored oil (3.74 g, 21.5 mmol, 79%). The product was used for the following syntheses without further purification and characterization. *N,N*-Boc-methylethylenediamine was dissolved in 60 mL 1,2-dichloroethane (DCE). 4.82 g 2-pyridinecarboxaldehyde (45.1 mmol) and 13.63

sodium triacetoxyborohydride (STAB) (64.4 mmol) were added. The solution was stirred overnight under argon. Then the reaction suspension was quenched with 60 mL of 2 M NaOH solution and extracted three times with DCM. The organic layers were combined, washed with brine, dried over MgSO<sub>4</sub>, filtrated and the solvent was removed under vacuum. The resulting brown oil was treated with 100 mL half concentrated hydrochloric acid (intense gas formation was observed). The brown solution was heated to 130 °C and kept under reflux overnight. The solution was made basic by adding dropwise 6 M NaOH solution while simultaneously cooling the solution in an ice bath. The solution obtained was extracted three times with DCM, washed with brine, dried over MgSO<sub>4</sub>, filtrated and the solvent was removed under vacuum. Distillation via Kugelrohr lead to a pure product which was stored under an argon atmosphere (3.11 g, 56%). Overall yield 45% (respectively 2.0 g *N*-methylthylenediamine). <sup>1</sup>H NMR (400 MHz, CDCl<sub>3</sub>, 24 °C,  $\delta$  [ppm]): 8.53 (d, 2H, py-H), 7.65 (td, 2H, py-H); 7.48 (d, 2H, py-H), 7.14 (t, 2H, py-H), 3.85 (s, 4H, py-CH<sub>2</sub>), 2.75 (t, 2H, NCH<sub>2</sub>CH<sub>2</sub>N(CH<sub>2</sub>py)<sub>2</sub>), 2.67 (t, 2H, NCH<sub>2</sub>CH<sub>2</sub>N(CH<sub>2</sub>py)<sub>2</sub>), 2.31 (s, 2H, NCH<sub>2</sub>). <sup>13</sup>C NMR (101 MHz, CDCl<sub>3</sub>, 24 °C,  $\delta$  [ppm]): 159.6, 149.0, 136.4, 122.9, 121.9, 64.4, 60.8, 53.9, 49.4, 36.3 ESI-MS (*m/z*): [M + H]<sup>+</sup>: 257.18; [M + Na]<sup>+</sup>: 279.16

### 2.4.2. (2-ethylaminoethyl)bis(2-pyridylmethyl)amine (Et-uns-penp)

2.0 g of *N*-ethylethylenediamine (22.7 mmol) were dissolved in 50 mL DCM. The solution was cooled to 0 °C with an ice bath and a solution of 3.22 g ethyltrifluoroacetate (22.7 mmol) in 50 mL DCM was added dropwise over a period of 40 min under argon. After the addition was complete, the mixture obtained was stirred for another 60 min at room temperature. The solvent, as well as the ethanol from the reaction were removed using a rotary evaporator. The derived colorless oil crystallized as a white colored solid briefly afterwards. The product was dissolved in 100 mL of DCM. 4.95 g of Di-*tert*-butyldicarbonate in 5 mL DCM were added to the product solution at 0 °C under argon. The reaction mixture was stirred for 90 min at room temperature and then quenched with 30 mL of saturated Na<sub>2</sub>CO<sub>3</sub> solution and 30 mL of ethyl acetate. After the gas formation had stopped, the aqueous phase was extracted three times with ethyl acetate. The combined organic layers were washed with brine, dried over MgSO<sub>4</sub>, filtrated and concentrated using a rotary evaporator. The oil obtained crystallized as a white solid after a few moments. The product was placed into a vessel with 75 mL methanol and 25 mL of a 2–3 M NaOH solution and stirred at room temperature for two hours. Finally, methanol was removed and the aqueous layer was extracted three times with ethyl acetate. The combined organic layers were washed with brine, dried over MgSO<sub>4</sub>, filtrated and the solvent was removed under vacuum. The obtained crude product was a pale yellow colored oil (3.97 g, 21.1 mmol, 93%). The product was used for the following syntheses without further purification and characterization. *N,N*-Boc-ethylethylenediamine was dissolved in 60 mL DCE. 4.52 g 2-pyridinecarboxaldehyde (42.2 mmol) and 13.41 STAB (63.3 mmol) were added. The solution was stirred overnight under argon. Then the reaction suspension was quenched with 60 mL of 2 M NaOH solution and extracted three times with DCM. The organic layers were combined, washed with brine, dried over MgSO<sub>4</sub>, and after filtration the solvent was removed under vacuum. The obtained brown colored oil was treated with 100 mL half concentrated hydrochloric acid (intense gas formation was observed). The brown solution was heated to 130 °C and refluxed overnight. The solution was made basic by adding dropwise 6 M NaOH solution by simultaneous cooling it in an ice bath. The resulting solution was extracted three times with DCM, washed with brine, dried over MgSO, filtrated and the solvent was removed under vacuum. Distillation via Kugelrohr lead to a pure product which was stored under an argon atmosphere (3.49 g, 61%). Overall yield 57% (in respect to starting material *N*-ethylethylenediamine). <sup>1</sup>H NMR (400 MHz, CDCl<sub>3</sub>, 23 °C,  $\delta$  [ppm]): 8.48 (d, 2H, py-H), 7.60 (td, 2H, py-H), 7.43 (d, 2H, py-H), 7.09 (t, 2H, py-H), 3.81 (s, 4H, py-CH<sub>2</sub>), 2.75–2.62 (m, 4H, NCH<sub>2</sub>CH<sub>2</sub>N), 2.45 (q, 2H, NCH<sub>2</sub>CH<sub>3</sub>), 1.00 (t, 3H, NCH<sub>2</sub>CH<sub>3</sub>). <sup>13</sup>C NMR (101 MHz, CDCl<sub>3</sub>, 24 °C,  $\delta$  [ppm]):  $\delta$  159.7, 149.0, 148.5, 136.5, 136.4,

122.9, 122.1, 121.9, 120.4, 64.3, 60.8, 54.2, 47.1, 44.0, 15.3. **ESI-MS** ( $m/z$ ):  $[M + H]^+$ : 271.19;  $[M + Na]^+$ : 293.17

**2.4.2.1. Symmetric uns-penp derivatives.** The preparation of symmetric uns-penp derivatives Me<sub>2</sub>uns-penp and Et<sub>2</sub>uns-penp were reported previously [24,25]. Furthermore, the synthesis of the ligand iProp<sub>2</sub>uns-penp was performed according to these descriptions. The ligand Prop<sub>2</sub>uns-penp was synthesized from uns-penp. The terminal primary amine was subsequently modified via an S<sub>N</sub>2 reaction [23,26].

#### 2.4.3. Me<sub>2</sub>uns-penp (1)

*N,N*-dimethylethylenediamine (2.0 g, 22.7 mmol) was dissolved in 30 mL of DCE. 2-pyridincarboxaldehyde (4.86 g; 45.4 mmol) and STAB (14.43 g; 68.1 mmol) were added. The foamy mixture was stirred at room temperature overnight under an argon atmosphere. The reaction was quenched with 30 mL of 2 M NaOH solution and extracted three times with DCM. The combined organic layers were washed with brine and dried over MgSO<sub>4</sub>. The crude product was obtained by removing the solvent. The pure product was obtained by purification via Kugelrohr distillation. The light brown colored oil was stored under an argon atmosphere (4.83 g, 79%). <sup>1</sup>H NMR (400 MHz, CDCl<sub>3</sub>, 26 °C, δ [ppm]): 8.48 (d, 2H, py-H), 7.60 (td, 2H, py-H), 7.49 (d, 2H, py-H), 7.09 (t, 2H, py-H), 3.82 (s, 4H, py-CH<sub>2</sub>), 2.69–2.63 (t, 2H, NCH<sub>2</sub>CH<sub>2</sub>N(CH<sub>2</sub>py)<sub>2</sub>), 2.45 (t, 2H, NCH<sub>2</sub>CH<sub>2</sub>N(CH<sub>2</sub>py)<sub>2</sub>), 2.13 (s, 6H, N(CH<sub>3</sub>)<sub>2</sub>). <sup>13</sup>C NMR (101 MHz, CDCl<sub>3</sub>, 28 °C, δ [ppm]): 149.8, 149.2, 149.0, 136.9, 136.7, 136.3, 122.9, 122.4, 122.3, 122.2, 121.9, 120.4, 60.53, 45.8, 45.61, 5.5, 21.8. **ESI-MS** ( $m/z$ ):  $[M + H]^+$ : 270.18.

#### 2.4.4. Et<sub>2</sub>uns-penp (2)

*N,N*-diethylethylenediamine (2.0 g, 17.2 mmol) was dissolved in 30 mL of DCE. 2-pyridincarboxaldehyde (3.69 g; 34.4 mmol) and STAB (10.94 g; 51.6 mmol) were added. The foamy mixture was stirred at room temperature overnight under argon. The reaction was quenched with 30 mL of 2 M NaOH solution and extracted three times with DCM. The combined organic layers were washed with brine and dried over MgSO<sub>4</sub>. The crude product was obtained by removing the solvent. The pure product was obtained by purification via Kugelrohr distillation. The light brown colored oil was stored under an argon atmosphere (3.04 g, 59%). <sup>1</sup>H NMR (400 MHz, CDCl<sub>3</sub>, 26 °C, δ [ppm]): 8.50 (d, 2H, py-H), 7.62 (td, 2H, py-H), 7.53 (d, 2H, py-H), 7.11 (t, 2H, py-H), 3.85 (s, 4H, py-CH<sub>2</sub>), 2.67 (t, 2H, NCH<sub>2</sub>CH<sub>2</sub>N(CH<sub>2</sub>py)<sub>2</sub>), 2.60 (t, 2H, NCH<sub>2</sub>CH<sub>2</sub>N(CH<sub>2</sub>py)<sub>2</sub>), 2.44 (q, 4H, N(CH<sub>2</sub>CH<sub>3</sub>)<sub>2</sub>), 0.93 (t, 6H, N(CH<sub>2</sub>CH<sub>3</sub>)<sub>2</sub>). <sup>13</sup>C NMR (101 MHz, CDCl<sub>3</sub>, 26 °C, δ [ppm]): 160.0, 149.0, 136.3, 122.8, 121.9, 61.0, 52.3, 50.9, 47.5, 47.4, 11.8. **ESI-MS** ( $m/z$ ):  $[M + H]^+$ : 298.22.

#### 2.4.5. Prop<sub>2</sub>uns-penp (3)

The precursor ligand uns-penp was synthesized according to the literature and purified via Kugelrohr distillation [23]. The such purified uns-penp (1.0 g; 4.1 mmol) was dissolved in 20 mL acetonitrile. K<sub>2</sub>CO<sub>3</sub> (4.1 g; 30.0 mmol) and 1-iodopropane (1.50 g; 8.8 mmol) were added to the solution. The mixture was stirred overnight at 50 °C under an argon atmosphere. Afterwards the solvent was removed. The residue was treated with diethylether, filtrated and the solvent was removed. Kugelrohr distillation led to a pure product that was stored under an argon atmosphere (0.90 g; 67%). <sup>1</sup>H NMR (400 MHz, CDCl<sub>3</sub>, 24 °C, δ [ppm]): 8.48 (d, 2H, py-H), 7.61 (td, 2H, py-H), 7.52 (d, 2H, py-H), 7.10 (t, 2H, py-H), 3.83 (s, 4H, py-CH<sub>2</sub>), 2.61 (m, 4H, NCH<sub>2</sub>CH<sub>2</sub>N), 2.27 (t, 4H, N(CH<sub>2</sub>CH<sub>2</sub>CH<sub>3</sub>)<sub>2</sub>), 1.34 (m, 4H, N(CH<sub>2</sub>CH<sub>2</sub>CH<sub>3</sub>)<sub>2</sub>), 0.77 (t, 6H, N(CH<sub>2</sub>CH<sub>2</sub>CH<sub>3</sub>)<sub>2</sub>). <sup>13</sup>C NMR (101 MHz, CDCl<sub>3</sub>, 27 °C, δ [ppm]): 160.1, 149.1, 136.4, 122.9, 121.9, 61.1, 56.8, 52.4, 20.4, 12.0. **ESI-MS** ( $m/z$ ):  $[M + H]^+$ : 327.26;  $[M + Na]^+$ : 349.24.

#### 2.4.6. iProp<sub>2</sub>uns-penp (4)

*N,N*-diisopropylethylenediamine (1.0 g, 6.9 mmol) was dissolved in

50 mL DCE. 2-pyridincarboxaldehyde (1.48 g; 13.8 mmol) and STAB (4.41 g; 20.8 mmol) were added. The foamy mixture was stirred at room temperature overnight under argon. The reaction was quenched with 50 mL of 2 M NaOH solution and extracted three times with DCM. The combined organic layers were washed with brine and dried over MgSO<sub>4</sub>. The crude product was obtained by removing the solvent. The pure product was obtained by purification via Kugelrohr distillation. The light brown colored oil was stored under an argon atmosphere (1.63 g, 72%). <sup>1</sup>H NMR (400 MHz, CDCl<sub>3</sub>, 23 °C, δ [ppm]): 8.50 (d, 2H, py-H), 7.62 (td, 2H, py-H), 7.56 (d, 2H, py-H), 7.11 (t, 2H, py-H), 3.84 (s, 4H, py-CH<sub>2</sub>), 2.88 (m, 4H, NCH(CH<sub>3</sub>)<sub>2</sub>), 2.55 (s, 4H, NCH<sub>2</sub>CH<sub>2</sub>N), 0.89 (d, 12H, NCH(CH<sub>3</sub>)<sub>2</sub>). <sup>13</sup>C NMR (101 MHz, CDCl<sub>3</sub>, 24 °C, δ [ppm]): 160.2, 149.0, 136.3, 122.7, 121.8, 61.1, 56.4, 49.1, 43.6, 20.6. **ESI-MS** ( $m/z$ ):  $[M + H]^+$ : 327.26;  $[M + Na]^+$ : 349.24.

**2.4.6.1. Asymmetric uns-penp derivatives.** The asymmetric ligands are based on the priorly synthesized precursor ligands with a secondary amine at the terminal position. The second alkyl residue was added via a simple S<sub>N</sub>2 reaction in an established procedure [26]. However, the Ferrocene residue was connected via reductive alkylation [23].

#### 2.4.7. Me-Et-uns-penp (5)

Me-uns-penp (1.0 g, 3.9 mmol) was dissolved in 20 mL acetonitrile. Bromoethane (0.74 g; 6.8 mmol) and K<sub>2</sub>CO<sub>3</sub> (2.5 g; 18.1 mmol) were added. The solution was stirred at 50 °C under argon for three days. The solvent was removed. The residue was treated with diethyl ether, and the solvent was removed after filtration. Kugelrohr distillation led to a pure product that was stored under an argon atmosphere (0.60 g; 54%). <sup>1</sup>H NMR (400 MHz, CDCl<sub>3</sub>, 23 °C, δ [ppm]): 8.49 (d, 2H, py-H), 7.61 (td, 2H, py-H), 7.52 (d, 2H, py-H), 7.10 (t, 2H, py-H), 3.83 (s, 4H, py-CH<sub>2</sub>), 2.68 (t, 2H, NCH<sub>2</sub>CH<sub>2</sub>N(CH<sub>2</sub>py)<sub>2</sub>), 2.52 (t, 2H, NCH<sub>2</sub>CH<sub>2</sub>N(CH<sub>2</sub>py)<sub>2</sub>), 2.33 (q, 2H, NCH<sub>2</sub>CH<sub>3</sub>), 2.12 (s, 3H, NCH<sub>3</sub>), 0.97 (t, 3H, NCH<sub>2</sub>CH<sub>3</sub>). <sup>13</sup>C NMR (101 MHz, CDCl<sub>3</sub>, 25 °C, δ [ppm]): 160.0, 149.1, 136.4, 123.0, 122.0, 61.0, 55.2, 52.3, 51.8, 42.1, 12.3. **ESI-MS** ( $m/z$ ):  $[M + H]^+$ : 285.21;  $[M + Na]^+$ : 307.19.

#### 2.4.8. Me-Prop-uns-penp (6)

Me-uns-penp (1.0 g, 3.9 mmol) was dissolved in 20 mL acetonitrile. 1-iodopropane (0.70 g; 4.1 mmol) and K<sub>2</sub>CO<sub>3</sub> (2.5 g; 18.1 mmol) were added. The solution was stirred at 50 °C under argon for two days. The solvent was removed. The residue was treated with diethyl ether, filtrated and the solvent was removed. Kugelrohr distillation led to a pure product that was stored under an argon atmosphere (0.65 g; 56%). <sup>1</sup>H NMR (400 MHz, CDCl<sub>3</sub>, 23 °C, δ [ppm]): 8.49 (d, 2H, py-H), 7.61 (td, 2H, py-H), 7.52 (d, 2H, py-H), 7.10 (t, 2H, py-H), 3.83 (s, 4H, py-CH<sub>2</sub>), 2.67 (t, 2H, NCH<sub>2</sub>CH<sub>2</sub>N(CH<sub>2</sub>py)<sub>2</sub>), 2.52 (t, 2H, NCH<sub>2</sub>CH<sub>2</sub>N(CH<sub>2</sub>py)<sub>2</sub>), 2.21 (t, 2H, NCH<sub>2</sub>CH<sub>2</sub>CH<sub>3</sub>), 2.14 (s, 3H, NCH<sub>3</sub>), 1.40 (h, 2H, NCH<sub>2</sub>CH<sub>2</sub>CH<sub>3</sub>), 0.80 (t, 2H, NCH<sub>2</sub>CH<sub>2</sub>CH<sub>3</sub>). <sup>13</sup>C NMR (101 MHz, CDCl<sub>3</sub>, 24 °C, δ [ppm]): 160.0, 149.1, 136.41, 122.9, 122.0, 61.0, 60.2, 55.7, 52.3, 42.7, 20.5, 12.0. **ESI-MS** ( $m/z$ ):  $[M + H]^+$ : 299.22.

#### 2.4.9. Et-Prop-uns-penp (7)

Et-uns-penp (1.0 g, 3.7 mmol) was dissolved in 20 mL acetonitrile. 1-iodopropane (0.87 g; 5.1 mmol) and K<sub>2</sub>CO<sub>3</sub> (2.5 g; 18.1 mmol) were added. The solution was stirred at 50 °C under an argon atmosphere for seven days. The solvent was removed. The residue was treated with diethyl ether, filtrated and the solvent was removed. Kugelrohr distillation led to a pure product that was stored under an argon atmosphere (0.75 g; 65%). <sup>1</sup>H NMR (400 MHz, CDCl<sub>3</sub>, 23 °C, δ [ppm]): 8.49 (d, 2H, py-H), 7.62 (td, 2H, py-H), 7.53 (d, 2H, py-H), 7.10 (t, 2H, py-H), 3.84 (s, 4H, py-CH<sub>2</sub>), 2.62 (m, 4H, NCH<sub>2</sub>CH<sub>2</sub>N), 2.42 (q, 2H, NCH<sub>2</sub>CH<sub>3</sub>), 2.28 (t, 2H, NCH<sub>2</sub>CH<sub>2</sub>CH<sub>3</sub>), 1.36 (h, 2H, NCH<sub>2</sub>CH<sub>2</sub>CH<sub>3</sub>), 0.80 (t, 2H, NCH<sub>2</sub>CH<sub>2</sub>CH<sub>3</sub>), 0.92 (t, 3H, NCH<sub>2</sub>CH<sub>3</sub>), 0.78 (t, 3H, NCH<sub>2</sub>CH<sub>2</sub>CH<sub>3</sub>). <sup>13</sup>C NMR (101 MHz, CDCl<sub>3</sub>, 26 °C, δ [ppm]): 160.1, 149.1, 136.4, 122.9, 121.9, 61.1, 56.13, 52.4, 51.7, 48.1, 20.4, 12.0, 11.9. **ESI-MS** ( $m/z$ ):  $[M$

+ H]<sup>+</sup>: 313.24, [M + Na]<sup>+</sup>: 335.22.

#### 2.4.10. Me-iProp-uns-penp (8)

Me-uns-penp (0.71 g, 2.8 mmol) was dissolved in 20 mL acetonitrile. 2-iodopropane (0.75 g; 4.4 mmol) and K<sub>2</sub>CO<sub>3</sub> (2.5 g; 18.1 mmol) were added. The solution was stirred at 50 °C under argon for four days. The solvent was removed. The residue was treated with diethylether, filtrated and the solvent was removed. Kugelrohr distillation led to a pure product that was stored under an argon atmosphere (0.51 g; 62%). <sup>1</sup>H NMR (400 MHz, CDCl<sub>3</sub>, 25 °C, δ [ppm]): 8.49 (d, 2H, py-H), 7.61 (td, 2H, py-H), 7.53 (d, 2H, py-H), 7.09 (t, 2H, py-H), 3.84 (s, 4H, py-CH<sub>2</sub>), 2.72 (h, 1H, NCH(CH<sub>3</sub>)<sub>2</sub>), 2.65 (t, 2H, NCH<sub>2</sub>CH<sub>2</sub>N(CH<sub>2</sub>py)<sub>2</sub>), 2.53 (t, 2H, NCH<sub>2</sub>CH<sub>2</sub>N(CH<sub>2</sub>py)<sub>2</sub>), 2.10 (s, 3H, NCH<sub>3</sub>), 0.91 (d, 2H, NCH(CH<sub>3</sub>)<sub>2</sub>). <sup>13</sup>C NMR (101 MHz, CDCl<sub>3</sub>, 26 °C, δ [ppm]): 160.1, 149.1, 136.4, 122.9, 121.9, 61.0, 53.8, 53.1, 51.3, 37.5, 18.0. ESI-MS (m/z): [M + H]<sup>+</sup>: 299.22, [M + Na]<sup>+</sup>: 321.21.

#### 2.4.11. Et-iProp-uns-penp (9)

Et-uns-penp (1.0 g, 3.7 mmol) was dissolved in 20 mL acetonitrile. 2-iodopropane (1.74 g; 10.2 mmol) and K<sub>2</sub>CO<sub>3</sub> (5.0 g; 36.2 mmol) were added. The solution was refluxed under argon for five days. The solvent was removed. The residue was treated with diethyl ether, filtrated and the solvent was removed. Kugelrohr distillation led to a pure product that was stored under an argon atmosphere (0.77 g; 67%). <sup>1</sup>H NMR (400 MHz, CDCl<sub>3</sub>, 23 °C, δ [ppm]): 8.49 (d, 2H, py-H), 7.62 (td, 2H, py-H), 7.54 (d, 2H, py-H), 7.10 (t, 2H, py-H), 3.84 (s, 4H, py-CH<sub>2</sub>), 2.84 (h, 1H, NCH(CH<sub>3</sub>)<sub>2</sub>), 2.61 (t, 2H, NCH<sub>2</sub>CH<sub>2</sub>N(Py)<sub>2</sub>), 2.54 (t, 2H, NCH<sub>2</sub>CH<sub>2</sub>N(Py)<sub>2</sub>), 2.38 (q, 2H, NCH<sub>2</sub>CH<sub>3</sub>), 0.90 (m, 9H, NCH<sub>2</sub>CH<sub>3</sub> and NCH(CH<sub>3</sub>)<sub>2</sub>). <sup>13</sup>C NMR (101 MHz, CDCl<sub>3</sub>, 23 °C, δ [ppm]): 160.1, 149.3, 149.1, 136.4, 122.9, 121.9, 61.1, 54.4, 50.8, 47.6, 44.9, 18.4, 14.1. ESI-MS (m/z): [M + H]<sup>+</sup>: 313.24, [M + Na]<sup>+</sup>: 335.22.

#### 2.4.12. Ferrocene-Me-uns-penp (10)

Me-uns-penp (0.50 g; 2.0 mmol) was dissolved in 20 mL DCE. Ferrocene aldehyde (0.46 g; 2.1 mmol) and STAB (0.94 g; 4.4 mmol) were added. The reaction mixture was stirred at room temperature under argon atmosphere overnight. The reaction was quenched with 30 mL of 2 M NaOH and extracted with DCM. The combined organic layers were washed with brine, dried over MgSO<sub>4</sub> and the solvent was removed. The product was purified by column chromatography on silica as stationary phase eluted with DCM/MeOH (95: 5 v/v, + 0.2 vol% DIPEA). The solvent of the collected fractions was removed and the obtained oil was transferred into a glove box. Subsequently the crude product was dissolved in dry diethylether and treated with a small amount of DIPEA. After stirring for a few minutes, the solution was separated via a syringe filter (0.2 μm) and the solvent and the residual DIPEA as well were removed under vacuum. ESI-MS (m/z): [M + H]<sup>+</sup>: 455.19.

Copper(I) complexes: All copper(I) complexes with tetraphenylborate as anion were obtained under inert conditions according to a general procedure described in the literature [5]. In case of [Cu(10)]BPh<sub>4</sub>, the copper(I) salt [Cu(MeCN)<sub>4</sub>]SO<sub>3</sub>CF<sub>3</sub> was used to prevent disproportionation.

#### 2.4.13. [Cu(Ligand)]BPh<sub>4</sub>

200 mg of the ligand were dissolved in a small amount of dry acetone. A solution of 0.95 eq [Cu(MeCN)<sub>4</sub>]PF<sub>6</sub> was dissolved in a small amount of dry acetone and added dropwise to the ligand solution while stirring. Afterwards, 1.05 eq NaBPh<sub>4</sub> was added. The complex was precipitated by dropwise addition into dry diethyl ether. The yellow solid was filtrated, washed with diethyl ether and dried under vacuum. Diffusion of diethyl ether led to crystals which were suitable for X-ray analysis (except for [Cu(iProp<sub>2</sub>uns-penp)]BPh<sub>4</sub>, detection via ESI-MS).

Copper(II) complexes: All copper(II) complexes with coordinating chloride and non-coordinating perchlorate as anion were obtained according to a general procedure described in the literature [23].

#### 2.4.14. [Cu(Ligand)Cl]ClO<sub>4</sub>

70 mg of the ligand was dissolved in 2 mL of methanol. A solution of 0.5 eq of copper(II)chloride dehydrate and 0.5 eq copper(II)perchlorate hexahydrate were dissolved in 4 mL of methanol. The blue solution containing the copper salts was added to the ligand solution. Slow evaporation yielded crystals suitable for X-ray analysis.

### 3. Results and discussion

#### 3.1. Syntheses and characterization

The ligands presented in Fig. 3 were synthesized without too many problems in acceptable yields according to published procedures. Symmetrical ligands Me<sub>2</sub>uns-penp, Et<sub>2</sub>uns-penp and iProp<sub>2</sub>uns-penp could be obtained from commercially available chemicals in a one step-reaction. Only for the synthesis of ligand Prop<sub>2</sub>uns-penp, uns-penp was needed as a precursor. The addition of the second alkyl residue for the unsymmetric ligands was performed under basic conditions in a S<sub>N</sub>2 reaction. The reaction duration of the synthesis of Et-iProp-uns-penp was striking. A reason for this might be the strong steric hindrance around the fully substituted nitrogen atom. This effect further explains the lack of an oversubstitution which was detected within all other S<sub>N</sub>2 reactions performed. All ligands needed to be purified by Kugelrohr distillation. Ferrocene aldehyde was attached to the Me-uns-penp ligand by reductive alkylation. Here purification via Kugelrohr distillation was not possible due to similar sublimation temperatures of the final ligand and the reactants. However, with column chromatography separation was achieved and after a final treatment with base under inert conditions the pure ligand was obtained.

The copper(I) complexes had to be synthesized under inert conditions in a glove box (argon) due to their high sensitivity towards air and moisture. However, it was possible to determine the molecular structures by SCXRD of the copper(I) complexes with all ligands in Fig. 3 with the exception of the copper(I) complex with iProp<sub>2</sub>uns-penp as a ligand. Therefore, [Cu(4)]BPh<sub>4</sub> was analyzed by ESI-MS instead. While molecular structures of [Cu(1)]BPh<sub>4</sub> and [Cu(6)]BPh<sub>4</sub> have been reported previously crystallographic data for [Cu(1)]BPh<sub>4</sub> have not been published yet (crystallographic data are reported in the Supporting Information, Tables SI-5 – SI-9) [16,27]. As an example for a copper(I) complex with a symmetric ligand arm, Fig. 4 shows the molecular structure of the cation of [Cu(1)]BPh<sub>4</sub> with its symmetry equivalent. As an example for a copper(I) complex with an asymmetric ligand arm, the molecular structure of the cation of [Cu(9)]BPh<sub>4</sub> (one complex cation and its symmetry equivalent to show their relative orientation) is

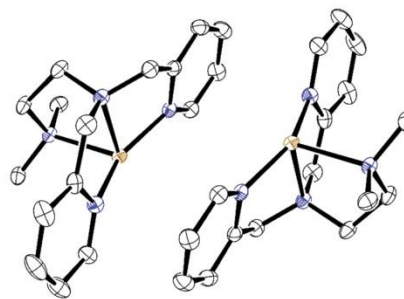


Fig. 4. Molecular structure of the cation of [Cu(1)]BPh<sub>4</sub> complex and its symmetry equivalent (–x, 1–y, 1–z). Ellipsoids set at 50% probability; the anions, H atoms, and solvent molecules are omitted for clarity. Carbon: black; nitrogen: blue; copper: brown. (For interpretation of the references to color in this figure legend, the reader is referred to the web version of this article.)

presented in Fig. 5. Furthermore, the molecular structure of the cation of the somewhat a bit more special copper(I) complex with the redox active ferrocene derivative as ligand, [Cu(10)]BPh<sub>4</sub> is shown in Fig. 6. The molecular structures of all copper(I) complexes as well as their crystallographic data are reported in the Supporting Information (Figs. SI-8 – SI-15 and Tables SI-5 – SI-44). These complexes are perfectly in line with the data already reported for related copper(I) complexes with tripodal ligands [19,28,29].

Due to the fact that usually “dioxygen adduct” copper complexes are only spectroscopically observed as reactive intermediates, molecular structures of these compounds are rare. However, to get an idea for the structure of these complexes, it is a good strategy to structurally characterize the corresponding copper(II) complexes with chloride anions as additional ligands (representing/modelling the binding of the oxygen atom) [28–30]. Copper(II) complexes with chloride could be structurally characterized and molecular structures of the cations of [Cu(2)Cl]ClO<sub>4</sub>, [Cu(3)Cl]ClO<sub>4</sub>, [Cu(5)Cl]ClO<sub>4</sub>, [Cu(7)Cl]ClO<sub>4</sub>, [Cu(8)Cl]ClO<sub>4</sub> and [Cu(9)Cl]ClO<sub>4</sub> as well as crystallographic data are reported in the Supporting Information (Figs. SI-16 – SI-22 and Tables SI-45 – SI-81). The molecular structure of [Cu(6)Cl]ClO<sub>4</sub> has been reported previously [16]. No crystals suitable for structural characterization of the copper(II) complex with the Ferrocene-Me-uns-penp (10) were obtained. Furthermore, efforts to crystallize and structurally characterize [Cu(4)Cl]ClO<sub>4</sub> were not successful. Instead, crystallization of the product from a solution of this complex showed that the (iProp)<sub>2</sub>-amine group obviously got detached from the ligand and that the remaining ligand part was oxidized. The molecular structure of this complex [Cu(11)Cl] (11 = dipicolinamide anion) is presented in the Supporting Information (Fig. SI-1). The molecular structure has already been reported previously [31,32]. While the mechanism of this reaction is not completely clear yet, it is more than likely that it follows a similar mechanism proposed for related copper complexes [33,34]. The reactivity of copper chloride towards organic substrates is beyond the scope of this work and was not investigated any further herein.

### 3.2. Cyclic voltammetry

To gain more information on the influence of the alternating residues at the terminal amine with regard to their redox potentials, cyclic voltammetry was performed in acetonitrile. The cyclic voltammograms for symmetric and asymmetric substituted ligands are shown in Figs. 7 and 8. The redox potentials are reported in Table 1. All complexes show a reversible Cu(I)/Cu(II) redox reaction and the potentials of nearly all copper(I) complexes are quite similar with a value of  $E_{1/2}$  close to 0.1 V.

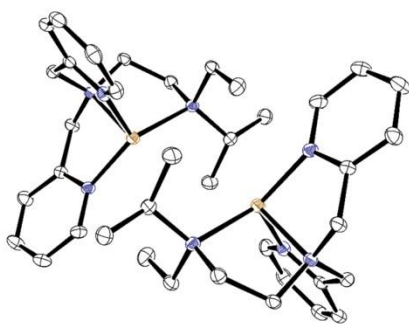


Fig. 5. Molecular structure of the cation of [Cu(9)]BPh<sub>4</sub> complex and its symmetry equivalent (2-x, 2-y, 1-z). Ellipsoids set at 50% probability; the anions, H atoms, and solvent molecules are omitted for clarity. Carbon: black; nitrogen: blue; copper: brown. (For interpretation of the references to color in this figure legend, the reader is referred to the web version of this article.)

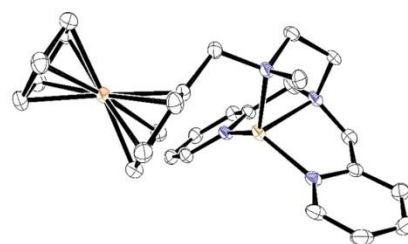


Fig. 6. Molecular structure of the cation of [Cu(10)]BPh<sub>4</sub> complex. Ellipsoids set at 50% probability; the anions, H atoms, and solvent molecules are omitted for clarity. Carbon: black; nitrogen: blue; iron: orange; copper: brown. (For interpretation of the references to color in this figure legend, the reader is referred to the web version of this article.)

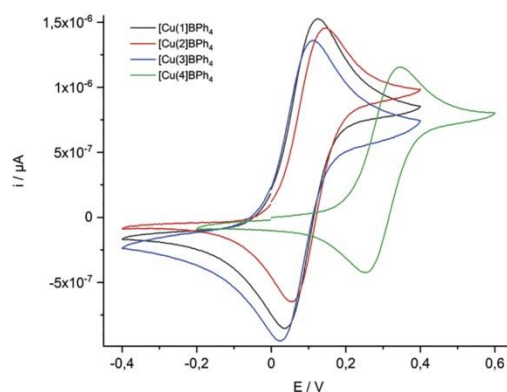


Fig. 7. Cyclic voltammograms of the copper(I) complexes with ligands 1, 2, 3 and 4 (symmetric uns-penp derivatives) in acetonitrile at room temperature. [complex] = 1 mmol/L; [electrolyte] ([NBu<sub>4</sub>]BF<sub>4</sub>) = 0.1 mol/L.

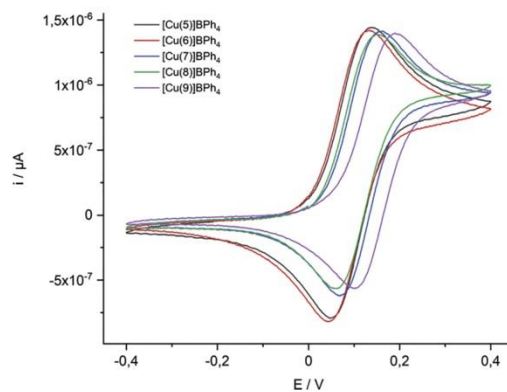


Fig. 8. Cyclic voltammograms of the copper(I) complexes with ligands 5, 6, 7, 8 and 9 (asymmetric uns-penp derivatives) in acetonitrile at room temperature. [complex] = 1 mmol/L; [electrolyte] ([NBu<sub>4</sub>]BF<sub>4</sub>) = 0.1 mol/L.

**Table 1**  
Potentials of the copper(I) complexes and ferrocene in comparison.

	$E_p^{red}$ [V]	$E_p^{ox}$ [V]	$E_{1/2}$ [V]	$\Delta E$ [mV]
[Cu(1)]BPh <sub>4</sub>	0.034	0.127	0.081	93
[Cu(2)]BPh <sub>4</sub>	0.055	0.147	0.101	92
[Cu(3)]BPh <sub>4</sub>	0.023	0.115	0.069	92
[Cu(4)]BPh <sub>4</sub>	0.254	0.348	0.301	94
[Cu(5)]BPh <sub>4</sub>	0.048	0.140	0.094	92
[Cu(6)]BPh <sub>4</sub>	0.043	0.132	0.088	89
[Cu(7)]BPh <sub>4</sub>	0.066	0.163	0.115	97
[Cu(8)]BPh <sub>4</sub>	0.059	0.152	0.106	93
[Cu(9)]BPh <sub>4</sub>	0.100	0.189	0.145	89
[Cu(10)]BPh <sub>4</sub>	0.014	0.130	0.072	116
	0.848	0.930	0.889	82
		1.270		
ferrocene	0.613	0.686	0.650	73

Not unexpected, [Cu(4)]BPh<sub>4</sub> has a much higher potential with  $E_{1/2} = 0.301$  V. Furthermore, the potential  $E_{1/2} = 0.145$  V of [Cu(9)]BPh<sub>4</sub> is somewhat higher with regard to the other complexes. This can be easily explained by the known fact that the *N*-donor atom can dissociate from the metal ion in the tripodal complex if the *R* groups become sterically too demanding. Acetonitrile that has been used for the CV measurements is a strongly competing ligand that additionally will enforce such a dissociation. So the CV of [Cu(4)]BPh<sub>4</sub> most likely shows the redox potential of the complex [Cu(4)(CH<sub>3</sub>CN)<sub>x</sub>]BPh<sub>4</sub> with a detached amine arm and therefore is quite different in comparison with the other complexes.

Complex [Cu(10)]BPh<sub>4</sub> was synthesized to integrate an internal redox indicator. It is treated separately because the modification of the uns-penp ligand is much bigger in comparison with the other ligands applied. The CV of this complex is presented in Fig. 9 and potentials are reported in Table 1. The redox potential of the copper complex is well in line with the other complexes and does not seem to be influenced by the directly bonded ferrocene unit. The potential of the ferrocene unit with 0.89 V is shifted to a more positive value compared with 0.65 V of the free ferrocene under these conditions. However, this again is expected because ferrocene derivatives such as ferrocene aldehyde show similar shifts in comparison with ferrocene [35].

### 3.3. Reactivity towards dioxygen

The reactivity of the copper(I) complexes with uns-penp and Me<sub>2</sub>uns-penp (1) towards dioxygen have been studied in great detail in the same way as with the ligands tmpa and Me<sub>6</sub>tren [9,10,19,23,36]. As described

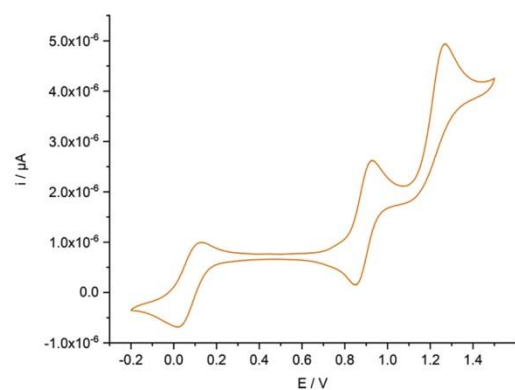


Fig. 9. Cyclic voltammogram of [Cu(10)]BPh<sub>4</sub> in acetonitrile at room temperature. [complex] = 1 mmol/L; [electrolyte] ([NBu<sub>4</sub>]BF<sub>4</sub>) = 0.1 mol/L.

in the introduction these complexes form quite stable *trans-μ*-1,2-peroxido copper complexes at low temperatures (Eq. (1)). The same behavior was observed for the copper complexes with ligands 2, 3 and 5–10. The UV–vis spectra of [Cu(1)]BPh<sub>4</sub>, [Cu(4)]BPh<sub>4</sub> and [Cu(9)]BPh<sub>4</sub> prior and after their reaction with dioxygen in acetone at –85 °C are presented in Fig. 10. The typical spectra of the dinuclear copper peroxido complexes with an absorbance maximum at around 530 nm and a shoulder around 600 nm are observed [37,38]. The UV–vis spectra of the other copper dioxygen “adduct” complexes are reported in the Supporting Information (Figs. SI-2 and SI-3).

Again, [Cu(4)]BPh<sub>4</sub> shows different reactivity, as can be seen in Fig. 10. Only a small and very broad maximum was observed that could be assigned to the corresponding *trans-μ*-1,2-peroxido copper complex, indicating an already decaying oxygen “adduct complex”. Time resolved UV–Vis spectra obtained in a stopped-flow measurement at –83 °C in acetone (Fig. 11) revealed a fast formation of the peroxido complex within 1.7 s at 550 nm according to Eq. (1) (briefly the superoxido intermediate can be seen as well with an absorbance maximum at 420 nm). Despite the low temperature, the peroxido complex is not stable and decomposes over two minutes (time trace shown in the inset in Fig. 11). This furthermore explains the observation from Fig. 10 and gives a hint towards the decomposition and oxidation of 4 described above.

Quite surprising was the fact that the copper(I) complex with the ferrocene unit, [Cu(10)]BPh<sub>4</sub>, also reacted according to Eq. (1) and formed a quite stable peroxido complex at low temperatures. Stopped-flow measurements at –81 °C are shown in Fig. 12 and nicely show the formation of this complex in the time resolved UV–vis spectra together with the decrease of the absorbance maxima of the superoxido complex at 410 nm (inset in Fig. 12).

### 3.4. Solid state reactions

As has been observed previously, by utilizing the anion tetraphenylborate, copper peroxido complexes with some tripodal ligands could be stabilized in the solid state to such an extent that it was possible to even heat them up to around a 100 °C and furthermore to use them for catalytic oxygenation of toluene [5,16]. To investigate the influence of the substitution at the terminal nitrogen atom, all solid copper(I) complexes with tetraphenylborate as anion were treated with dioxygen at room temperature. The results of the oxygen exposure of the complexes

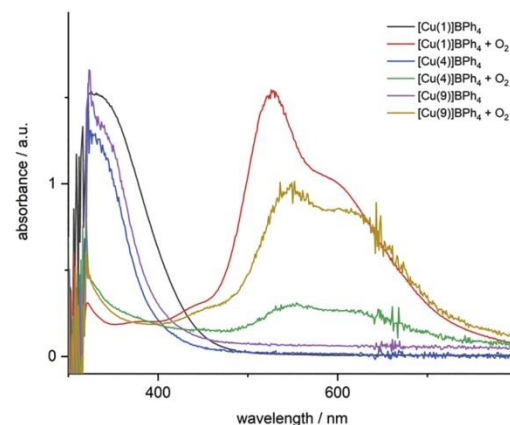
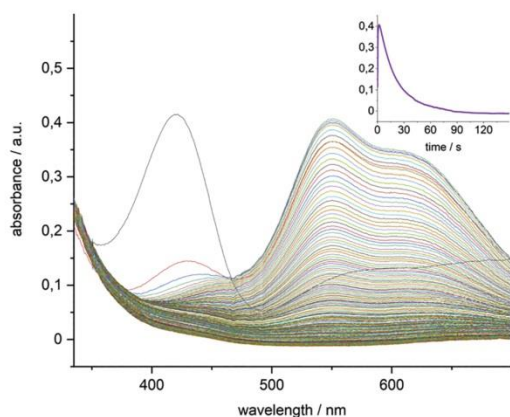
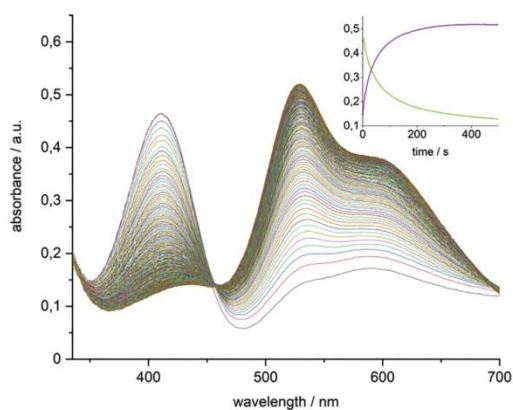


Fig. 10. UV–Vis of symmetric complexes [Cu(1)]BPh<sub>4</sub> and [Cu(4)]BPh<sub>4</sub> and the asymmetric complex [Cu(9)]BPh<sub>4</sub> in acetone at –85 °C. Spectra are shown before and after treatment with dioxygen.



**Fig. 11.** Time-resolved spectra of the reaction of  $[\text{Cu}(4)]\text{BPh}_4$  with dioxygen in acetone at  $-83\text{ }^\circ\text{C}$  ( $[\text{complex}] = 2.0 \times 10^{-4}\text{ M}$ ,  $[\text{O}_2] = 4.4 \times 10^{-3}\text{ M}$ , total time: 150 s). At 420 nm the spectra shows the decreasing intensity of the superoxido intermediate. At 550 nm the increasing intensity of the labile peroxido complex is visible. The time trace at the upper right shows the fast decomposition of the peroxido species.



**Fig. 12.** Time-resolved spectra of the reaction of  $[\text{Cu}(10)]\text{BPh}_4$  with dioxygen in acetone at  $-81\text{ }^\circ\text{C}$  ( $[\text{complex}] = 2.0 \times 10^{-4}\text{ M}$ ,  $[\text{O}_2] = 4.4 \times 10^{-3}\text{ M}$ , total time: 500 s). At 410 nm the spectra show the decreasing intensity of the superoxido intermediate. At 528 nm the increasing intensity of the final peroxido complex is visible. The time trace at the upper right shows the formation of the peroxido species with the parallel decomposition of the superoxido complex.

with symmetric uns-penp derivatives are shown in Fig. 13, the results with the asymmetric ligands in Fig. 14.

As was observed previously, the yellow colored powder of  $[\text{Cu}(1)]\text{BPh}_4$  turned slowly into the intensively purple colored peroxido complex (Fig. 13 a) when reacted with dioxygen [5,16]. A diffuse reflectance UV-vis spectrum of the peroxido complex  $[(1)\text{CuO}_2\text{Cu}(1)](\text{BPh}_4)_2$  is reported in the Supporting Information (Fig. SI-4). In contrast no reaction was observed for complexes with ligands 2, 3 and 4. Furthermore, solid  $[\text{Cu}(10)]\text{BPh}_4$  did not react with dioxygen under these conditions (not shown in the pictures).

In contrast all solid copper(I) complexes with asymmetric ligands

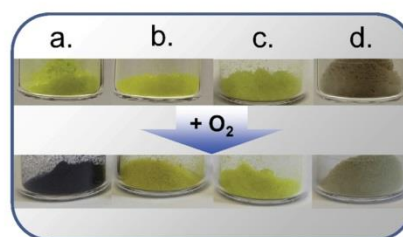


**Fig. 13.** Solid copper(I) complexes with symmetric uns-penp ligands after exposure with dioxygen; (a)  $[\text{Cu}(1)]\text{BPh}_4$ ; (b)  $[\text{Cu}(2)]\text{BPh}_4$ ; (c)  $[\text{Cu}(3)]\text{BPh}_4$ ; (d)  $[\text{Cu}(4)]\text{BPh}_4$ .

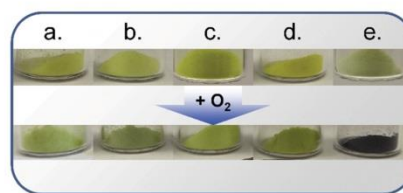


**Fig. 14.** Solid copper(I) complexes with asymmetric uns-penp ligands after exposure with dioxygen; (a)  $[\text{Cu}(5)]\text{BPh}_4$ ; (b)  $[\text{Cu}(6)]\text{BPh}_4$ ; (c)  $[\text{Cu}(7)]\text{BPh}_4$ ; (d)  $[\text{Cu}(8)]\text{BPh}_4$ ; (e)  $[\text{Cu}(9)]\text{BPh}_4$ .  $[\text{Cu}(10)]\text{BPh}_4$  did not show any reactivity in the solid state and was not considered.

5–9 exhibited a visible reaction with dioxygen. The yellow solids shown in Fig. 14 a-d reacted to a green solid (a bit difficult to see in the picture but very clear in the direct observation in the experiment). It is noticeable that these products kept their color and no further reaction to a purple/blue peroxido complex was observed. Reactions with the comparable complexes with tmpa and  $\text{Me}_2\text{uns-penp}$  also develop a green color shortly after exposure to dioxygen, which however, after some time, changed to a dark blue/purple color typical for a binuclear peroxido complex. The green color meanwhile is a hint for copper  $\eta^1$ -superoxo complex which is formed in a reversible reaction and is stable at room temperature [12,13,39,40]. Storing the  $[\text{Cu}(6)]\text{BPh}_4$  complex under argon atmosphere for a couple of days brought back the former yellow color. Treating the sample with oxygen led to the green colored compound again. Same results were obtained by heating the green solid up to  $50\text{ }^\circ\text{C}$  under an argon atmosphere. This effect was described previously by us within an investigation of the immobilization of copper complexes (with ligands derived from uns-penp) on silica surfaces [16].

$[\text{Cu}(9)]\text{BPh}_4$  (Fig. 14e) showed a different behavior, similar to the symmetric system with  $\text{Me}_2\text{uns-penp}$ . Here as well a binuclear peroxido complex was formed. Solid UV-Vis measurements supported this observation (see Supporting Information Fig. SI-4). But the formation works much faster than in the symmetric system. The first contact with dioxygen led immediately to the shown blue/purple color (video of this reaction is provided in the Supporting Information).

These results initiated a closer investigation to elucidate the differences between the symmetric and the asymmetric derivatizations of the ligands. Therefore the compounds  $[\text{Cu}(1)]\text{BPh}_4$ ,  $[\text{Cu}(3)]\text{BPh}_4$ ,  $[\text{Cu}(6)]\text{BPh}_4$  and  $[\text{Cu}(9)]\text{BPh}_4$  were investigated further.

Raman measurements of the oxygen treated copper(I) complexes are presented in Fig. 15. Especially the distinct band at  $830\text{ cm}^{-1}$  at the lower spectra of  $[\text{Cu}(1)]\text{BPh}_4$  demonstrates the formation of the trans- $\mu$ -1,2-peroxido complex [5]. Also the spectra of  $[\text{Cu}(9)]\text{BPh}_4$  contains this feature but with a relative small intensity. More striking is the presence of that band in the spectra of  $[\text{Cu}(6)]\text{BPh}_4$  which does not show

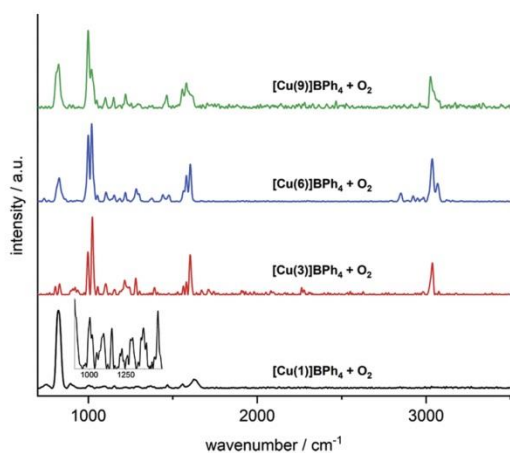


Fig. 15. Raman measurement of the complexes [Cu(1)]BPh<sub>4</sub>, [Cu(3)]BPh<sub>4</sub>, [Cu(6)]BPh<sub>4</sub> and [Cu(9)]BPh<sub>4</sub> after treatment with oxygen. The band around 830 cm<sup>-1</sup> indicates a peroxide species. The Inset shows the spectrum of [Cu(1)]BPh<sub>4</sub> magnified between 900 and 1750 cm<sup>-1</sup>.

an obvious conversion into a blue product. An explanation for this finding might be that a small amount of the batch is converted to the peroxido complex which cannot be seen by looking at the sample. The spectrum of the [Cu(3)]BPh<sub>4</sub> complex did not show any sign of a reaction with dioxygen. This correlates with the visual findings. The absorbance around 1020 cm<sup>-1</sup> is common for all complexes investigated. It is assigned as a ring and C–H stretching mode of the coordinated pyridine residues [41]. The inset shows a magnified region in the spectrum of complex [Cu(1)]BPh<sub>4</sub>. Due to the strong resonance of the peroxido ligand the intensities of the remaining bands almost disappear. Only by magnification at the corresponding wavelengths made visible.

To gain information about the change in the crystal structure of the solid compounds, powder XRD measurements under inert conditions before and after exposure with dioxygen were performed. Recorded diffractograms of [Cu(3)]BPh<sub>4</sub>, [Cu(6)]BPh<sub>4</sub> and [Cu(9)]BPh<sub>4</sub> compared with the corresponding diffraction patterns of the educts of the complex synthesis simulated from single crystal data are given in the Supporting Information (Fig. SI-5 – SI-7) to verify phase purity.

The diffractograms of the complex [Cu(1)]BPh<sub>4</sub> before and after the treatment with dioxygen as well as a comparison with a simulated pattern from single crystal data as well as patterns of the reagents are shown in Fig. 16. Small deviations of the simulated from the experimental diffraction pattern can be explained by different measurement temperatures of single crystal XRD and powder XRD. By comparing the patterns before and after the treatment with dioxygen, it is obvious that [Cu(1)]BPh<sub>4</sub> undergoes a transformation upon exposure to dioxygen, as the PXRD after the treatment strongly differs from the pattern before and also does not coincide with the simulated pattern anymore.

The results of the powder XRD measurements of [Cu(3)]BPh<sub>4</sub> with the symmetric ligand Prop<sub>2</sub>uns-penp are shown in Fig. SI-5. Comparing the simulated diffraction pattern of [Cu(3)]BPh<sub>4</sub> (black) with the recorded pattern (red), a slight shift of the reflections of the experimental diffractogram towards higher angles in 2θ can be noticed due to the different temperatures. Different to [Cu(1)]BPh<sub>4</sub>, a comparison of the experimental powder diffraction patterns before and after dioxygen exposure reveals good accordance for [Cu(3)]BPh<sub>4</sub>. This indicates that the lattice parameters do not differ significantly. In combination with the findings of Figs. 13 and 15, a reaction with oxygen seems to be unlikely.

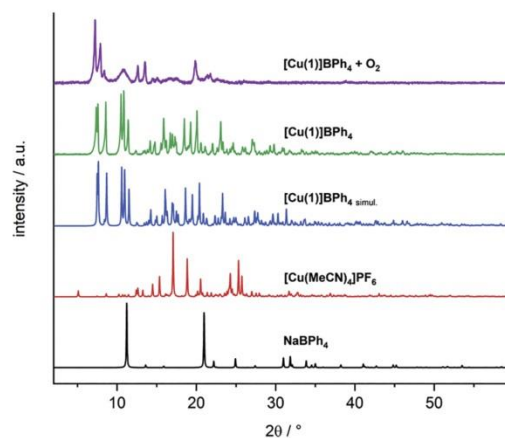


Fig. 16. Powder XRD patterns of [Cu(1)]BPh<sub>4</sub> measured before (green) and after the treatment with dioxygen (purple) in comparison to powder diffraction patterns of [Cu(1)]BPh<sub>4</sub> simulated from single crystal data (blue), NaBPh<sub>4</sub> (black) [42], and [Cu(MeCN)<sub>4</sub>]PF<sub>6</sub> (red) [43]. (For interpretation of the references to color in this figure legend, the reader is referred to the web version of this article.)

Comparable results were obtained from the investigation of the complex [Cu(6)]BPh<sub>4</sub> with the asymmetric ligand (see Supporting Information Fig. SI-6). Although there has been a change in color detected for the product, there is no observable change in the powder pattern and thus meaning no change in crystal structure and lattice. Due to these findings, an insertion of a dioxygen molecule would be unlikely, too, by means of the result of PXRD. Nonetheless, the single crystal measurement of [Cu(6)]BPh<sub>4</sub> indicates the structural possibility of a reaction with dioxygen. A change in color is observable upon dioxygen treatment, which indicates a suchlike insertion. A possible explanation for the discrepancy to powder XRD data is an insertion of dioxygen in low quantity only and not for the bulk material. Thus, in the measured powder diffraction pattern, only the majority phase is observable, which is the un-reacted complex [Cu(6)]BPh<sub>4</sub>, and still the color change can apply.

Quite surprisingly, the small crystals of [Cu(9)]BPh<sub>4</sub>, which were obtained by precipitation into diethylether during the common complexation and anion exchange reactions retain an adequate crystallinity after their reaction with dioxygen. The crystals were still suitable for single crystal X-ray analysis. Fig. 17 shows the molecular structure of the binuclear peroxido complex [(9)Cu(O<sub>2</sub>)Cu(9)](BPh<sub>4</sub>)<sub>2</sub> obtained this way. This complex is quite similar to the other three structurally characterized *end-on* peroxido copper complexes with the tripodal ligands tmpa, Bz<sub>3</sub>tren, Me<sub>6</sub>tren and a bit different to the copper complex with the macrocyclic ligand tet b [5,7,44,45]. Our previous efforts to accomplish the same solid state reaction with the copper Me<sub>6</sub>tren system had failed. After the reaction with dioxygen the complex had become amorphous and the peroxido complex had to be crystallized in a different way [5]. Crystallographic data of the complex [(9)Cu(O<sub>2</sub>)Cu(9)](BPh<sub>4</sub>)<sub>2</sub> are reported in the Supporting Information (Table SI-77-81).

Therefore, it was also possible to achieve the insertion of dioxygen into the bulk substance of [Cu(9)]BPh<sub>4</sub>. The experimental powder diffractograms of [Cu(9)]BPh<sub>4</sub> before and after dioxygen treatment in comparison to the powder diffraction patterns simulated from single crystal data are depicted in Fig. 18. In both cases, the measured diffraction patterns are in good accordance to the simulated patterns, indicating the structures, single crystal structure analysis as bulk products, too. However, there is a distinct change in structure detectable

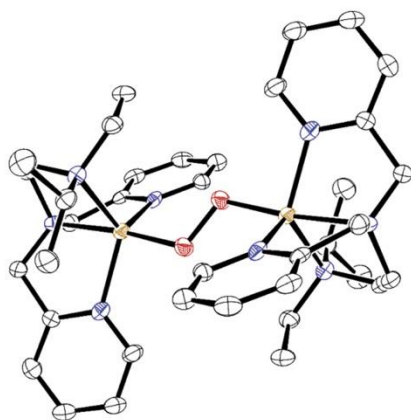


Fig. 17. Molecular structure of the cation of binuclear [(9)Cu(O<sub>2</sub>)Cu(9)](BPh<sub>4</sub>)<sub>2</sub>. Ellipsoids set at 50% probability; the anions, H atoms, and solvent molecules are omitted for clarity. Carbon: black; nitrogen: blue; oxygen: red; copper: brown. (For interpretation of the references to color in this figure legend, the reader is referred to the web version of this article.)

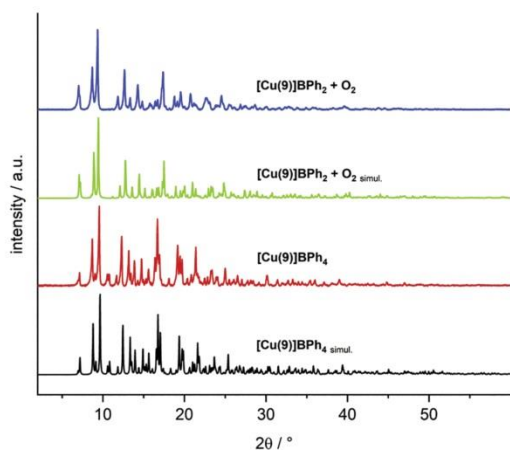


Fig. 18. Powder XRD patterns for [Cu(9)]BPh<sub>4</sub> before (red) and after the treatment with dioxygen (blue) compared with the powder diffraction patterns of [Cu(9)]BPh<sub>4</sub> and [Cu(9)O<sub>2</sub>](BPh<sub>4</sub>)<sub>2</sub> simulated from single crystal data (black). (For interpretation of the references to color in this figure legend, the reader is referred to the web version of this article.)

upon dioxygen treatment, as it can be seen by differences in number, intensities and positions of reflections between initial and [Cu(9)]BPh<sub>4</sub> flushed with dioxygen. In contrast to the proposed reactivity towards dioxygen of complex [Cu(6)]BPh<sub>4</sub>, a complete conversion of [Cu(9)]BPh<sub>4</sub> to the oxygenated product [Cu(9)O<sub>2</sub>](BPh<sub>4</sub>)<sub>2</sub> can be observed corroborated by comparison of simulated with experimental patterns.

Table 2 contains the values of the unit cells before and after exposure to oxygen. Comparison of the unit cells reveals only a slight expansion of the unit cell of the peroxido complex. The relative change is less than 2%.

Furthermore, there is a small deformation between two and three

Table 2

Cell parameters received from single crystal data of [Cu(9)]BPh<sub>4</sub> complex before and after oxygenation.

[Cu(9)]BPh <sub>4</sub>			
a / Å	11.3474(19)	α / °	94.310(5)
b / Å	13.161(2)	β / °	111.929(5)
c / Å	13.443(2)	γ / °	101.989(6)
[Cu(9)O <sub>2</sub> ](BPh <sub>4</sub> ) <sub>2</sub>			
a / Å	11.392(3)	α / °	97.027(7)
b / Å	12.911(3)	β / °	109.247(7)
c / Å	13.538(3)	γ / °	103.938(7)
Relative differences			
a / %	0.39%	α / %	2.80%
b / %	1.94%	β / %	2.45%
c / %	0.70%	γ / %	1.88%

degrees detectable. The complete structural parameters for the crystal structure are reported in the Supporting Information. This single crystal to single crystal transformation is most likely made possible due to the orientation of the copper center towards its symmetry equivalent in the crystal structure. Two copper ions are directly facing each other (Fig. 5). The distance between them decreases after the formation of the peroxido complex (5.591 Å to 4.475 Å), however, the relative orientation almost remains. This special geometry is not observed in the complexes with the other ligand derivatives. The metal centers in the crystal lattice of e. g. [Cu(1)]BPh<sub>4</sub> are orientated adversely towards each other (Fig. 4). The copper-copper distance is 12.230 Å. An end-on peroxido formation will therefore lead to a complete loss of crystallinity.

#### 4. Conclusion

Investigations on the reactivity of a series of copper(I) complexes [Cu(L)]BPh<sub>4</sub> towards dioxygen were performed to gain a better understanding of the steric influence of a tripodal ligand system. The ligand L, R<sup>1</sup>-R<sup>2</sup>-uns-penp (uns-penp = (2-aminoethyl)bis(2-pyridylmethyl) amine), was chosen because, while the bispicolylamine unit already stabilized the copper(I) unit, the additional amine arm could be easily modified. In combination with the same anion (tetraphenylborate is essential for stabilization of the complexes in the solid state) it could be shown that the redox potential Cu(I)/Cu(II) for nearly all complexes was quite similar. Therefore, only the different alkyl groups bound to the amine arm were responsible for different reactivities. While Me<sub>2</sub>uns-penp as a ligand still supported quite slow formation of a solid peroxido complex, symmetric substitution with two ethyl, propyl or isopropyl groups completely suppressed reactivity of the corresponding copper(I) complexes (in the solid state) towards dioxygen. Quite surprisingly, however, was the observation that copper(I) complexes with ligands with asymmetric substitution of the amine nitrogen, Me-Et-uns-penp (5), Me-Prop-uns-penp (6), Et-Prop-uns-penp (7), Me-iProp-uns-penp (8) and Et-iProp-uns-penp (9) clearly showed reactivity towards dioxygen in the solid state. Copper(I) complexes with ligands 5–8 reversibly formed a green compound that indicated formation of a mononuclear superoxido complex, however, so far and as described previously, we did not find a way to really characterize these products [16]. In contrast, [Cu(9)]BPh<sub>4</sub> instantly reacted with dioxygen to form a stable trans-μ-1,2-peroxido product complex that could be structurally characterized. A look at the crystal structures of the copper(I) complexes of all ligands clearly showed that [Cu(9)]BPh<sub>4</sub> is kind of preformed for the uptake of dioxygen and only has to undergo minor changes in the overall geometry when reacted to the copper(II) peroxido complex. Usually copper(I) complexes undergo a big change in coordination geometry/coordination number (bond lengths and angles) when oxidized to the corresponding copper(II) complexes. However, this is slightly different for copper complexes with tripodal ligands and thus allowed with the modification of the uns-penp ligand to find a perfect system for the fast uptake of dioxygen without a major structure change. Definitely

we could prove that slight modifications of the tripodal ligand system can have a large effect on the chemistry of the corresponding copper complexes.

#### Declaration of Competing Interest

The authors declare that they have no known competing financial interests or personal relationships that could have appeared to influence the work reported in this paper.

#### Acknowledgements

Prof. Dr. Roland Marschall (Fakultät für Biologie, Chemie und Geowissenschaften, Universität Bayreuth) is acknowledged for his support of the solid-state UV–vis measurements.

#### Appendix A. Supplementary data

Supplementary data to this article can be found online at <https://doi.org/10.1016/j.jinorgbio.2021.111544>.

#### References

- [1] E.I. Solomon, D.E. Heppner, E.M. Johnston, J.W. Ginsbach, J. Cirera, M. Qayyum, M.T. Kieber-Emmons, C.H. Kjaergaard, R.G. Hadt, L. Tian, Copper active sites in biology, *Chem. Rev.* 114 (2014) 3659–3853, <https://doi.org/10.1021/cr400327f>.
- [2] D.A. Quist, D.E. Diaz, J.J. Liu, K.D. Karlin, Activation of dioxygen by copper metalloproteins and insights from model complexes, *J. Biol. Inorg. Chem.* 22 (2017) 253–288, <https://doi.org/10.1007/s00775-016-1415-2>.
- [3] S. Herres-Pawlis, P. Verma, R. Haase, P. Kang, C.T. Lyons, E.C. Wasinger, U. Florke, G. Henkel, T.D.P. Stack, Phenolate hydroxylation in a bis( $\mu$ -oxo)dicopper(III) complex: lessons from the guanidine/amine series, *J. Am. Chem. Soc.* 131 (2009) 1154–1169, <https://doi.org/10.1021/ja807809x>.
- [4] A. Hoffmann, C. Citek, S. Binder, A. Goos, M. Rübhausen, O. Troepfner, I. Ivanovic-Burmazović, E.C. Wasinger, T.D.P. Stack, S. Herres-Pawlis, Catalytic Phenol hydroxylation with dioxygen: extension of the tyrosinase mechanism beyond the protein matrix, *Angew. Chemie - Int. Ed.* 52 (2013) 5398–5401, <https://doi.org/10.1002/anie.201301249>.
- [5] C. Würtele, O. Sander, V. Lutz, T. Waitz, F. Tucek, S. Schindler, Aliphatic C-H bond oxidation of toluene using copper peroxo complexes that are stable at room temperature, *J. Am. Chem. Soc.* 131 (2009) 7544–7545, <https://doi.org/10.1021/ja902327s>.
- [6] H.R. Lucas, L. Li, A.A.N. Sarjeant, M.A. Vance, E.I. Solomon, K.D. Karlin, Toluene and ethylbenzene aliphatic C-H bond oxidations initiated by a Dicopper(II)- $\mu$ -1,2-peroxo complex, *J. Am. Chem. Soc.* 131 (2009) 3230–3245, <https://doi.org/10.1021/ja807081d>.
- [7] R.R. Jacobson, Z. Tyeklar, A. Farooq, K.D. Karlin, S. Liu, J. Zubieta, A Cu<sub>2</sub>-O<sub>2</sub> complex. Crystal structure and characterization of a reversible dioxygen binding system, *J. Am. Chem. Soc.* 110 (1988) 3690–3692, <https://doi.org/10.1021/ja00219a071>.
- [8] S. Kaderli, N. Wei, K.D. Karlin, B. Jung, A.D. Zuberbühler, P. Niklaus, Kinetics and thermodynamics of formation of copper-Dioxygen adducts: oxygenation of mononuclear copper(I) complexes containing Tripodal Tetradentate ligands, *J. Am. Chem. Soc.* 115 (1993) 9506–9514, <https://doi.org/10.1021/ja00074a015>.
- [9] C.X. Zhang, S. Kaderli, M. Costas, E. Il Kim, Y.M. Neuhold, K.D. Karlin, A. D. Zuberbühler, Copper(I)-dioxygen reactivity of [(L)Cu]<sup>+</sup> (L) Tris(2-pyridylmethyl)amine: kinetic/thermodynamic and spectroscopic studies concerning the formation of Cu–O<sub>2</sub> and Cu<sub>2</sub>-O<sub>2</sub> adducts as a function of solvent medium and 4-pyridyl ligand substituent variations, *Inorg. Chem.* 42 (2003) 1807–1824, <https://doi.org/10.1021/ic0205684>.
- [10] M. Weitzer, S. Schindler, G. Brehm, S. Schneider, E. Hörmann, B. Jung, S. Kaderli, A.D. Zuberbühler, Reversible binding of dioxygen by the copper(I) complex with Tris(2-dimethylaminoethyl)amine (Me<sub>6</sub>Tren) ligand, *Inorg. Chem.* 42 (2003) 1800–1806, <https://doi.org/10.1021/ic025941m>.
- [11] J. Will, C. Würtele, J. Becker, O. Walter, S. Schindler, Synthesis, crystal structures and reactivity towards dioxygen of copper(I) complexes with tripodal aliphatic amine ligands, *Polyhedron*. 171 (2019) 448–454, <https://doi.org/10.1016/j.poly.2019.07.007>.
- [12] C. Würtele, E. Gaoutchenova, K. Harms, M.C. Holthausen, J. Sundermeyer, S. Schindler, Crystallographic characterization of a synthetic 1:1 end-on copper dioxygen adduct complex, *Angew. Chem. Int. Ed.* 45 (2006) 3867–3869, <https://doi.org/10.1002/anie.200600351>.
- [13] M. Schatz, V. Raab, S.P. Foxon, G. Brehm, S. Schneider, M. Reiher, M. C. Holthausen, J. Sundermeyer, S. Schindler, Combined spectroscopic and theoretical evidence for a persistent end-on copper Superoxo complex, *Angew. Chem. Int. Ed.* 43 (2004) 4360–4363, <https://doi.org/10.1002/anie.200454125>.
- [14] T. Hoppe, P. Josephs, N. Kempf, C. Wölper, S. Schindler, A. Neuba, G. Henkel, An approach to model the active site of Peptidylglycine- $\alpha$ -hydroxylating monooxygenase (PHM), *Z. Anorg. Allg. Chem.* 639 (2013) 1504–1511, <https://doi.org/10.1002/zaac.201300066>.
- [15] M. Bhadra, W.J. Transue, H. Lim, R.E. Cowley, J.Y.C. Lee, M.A. Siegler, P. Josephs, G. Henkel, M. Lerch, S. Schindler, A. Neuba, K.O. Hodgson, B. Hedman, E. I. Solomon, K.D. Karlin, A Thioether-ligated cupric superoxide model with hydrogen atom abstraction reactivity, *J. Am. Chem. Soc.* 143 (2021) 3707–3713, <https://doi.org/10.1021/jacs.1c00260>.
- [16] T. Brückmann, J. Becker, K. Turke, B. Smarsly, M. Weiß, R. Marschall, S. Schindler, Immobilization of a copper complex based on the tripodal ligand (2-aminoethyl)bis(2-pyridylmethyl)amine (uns-penp), *Z. Anorg. Allg. Chem.* 647 (2021) 560–571, <https://doi.org/10.1002/zaac.202100022>.
- [17] G.J. Kubas, B. Monzyk, A.L. Crumbliss, Tetrakis(acetonitrile)copper(I) Hexafluorophosphate, *Inorg. Synth.* 19 (1979) 90–92, <https://doi.org/10.1002/9780470132500.ch18>.
- [18] J.W. Gooch, Kubelka-Munk equation, in: J.W. Gooch (Ed.), *Encycl. Dict. Polym.*, Springer Verlag, New York, NY, 2007, pp. 559–560, [https://doi.org/10.1007/978-0-387-30160-0\\_6609](https://doi.org/10.1007/978-0-387-30160-0_6609).
- [19] M. Weitzer, M. Schatz, F. Hampel, F.W. Heinemann, S. Schindler, Low temperature stopped-flow studies in inorganic chemistry, *Dalton Trans.* (2002) 686–694, <https://doi.org/10.1039/b107927c>.
- [20] S.V. Kryatov, E.V. Rybak-Akimova, S. Schindler, Kinetics and mechanisms of formation and reactivity of non-heme Iron oxygen intermediates, *Chem. Rev.* 105 (2005) 2175–2226, <https://doi.org/10.1021/cr030709z>.
- [21] N. Elgrishi, K.J. Rountree, B.D. McCarthy, E.S. Rountree, T.T. Eisenhart, J. L. Dempsey, A practical Beginner's guide to cyclic voltammetry, *J. Chem. Educ.* 95 (2018) 197–206, <https://doi.org/10.1021/acs.jchemed.7b00361>.
- [22] C. Komiya, K. Aihara, K. Morishita, H. Ding, T. Inokuma, A. Shigenaga, A. Otaka, Development of an Intein-inspired amide cleavage chemical device, *J. Organomet. Chem.* 81 (2016) 699–707, <https://doi.org/10.1021/acs.joc.5b02399>.
- [23] M. Schatz, M. Leibold, S.P. Foxon, M. Weitzer, F.W. Heinemann, F. Hampel, O. Walter, S. Schindler, Synthesis and characterization of copper complexes of the ligand (2-aminoethyl)emph(bis)(2-pyridylmethyl)amine (uns-penp) and derivatives, *Dalton Trans.* (2003) 1480–1487.
- [24] G.J.P. Britovsek, J. England, A.J.P. White, Non-heme Iron(II) complexes containing tripodal tetradentate nitrogen ligands and their application in alkane oxidation catalysis, *Inorg. Chem.* 44 (2005) 8125–8134, <https://doi.org/10.1021/ic0509229>.
- [25] M. Balamurugan, R. Mayilmurugan, E. Suresh, M. Palaniandavar, Nickel(ii) complexes of tripodal 4N ligands as catalysts for alkane oxidation using m-CPBA as oxidant: ligand stereoelectronic effects on catalysis, *Dalton Trans.* 40 (2011) 9413–9424, <https://doi.org/10.1039/c1dt10902b>.
- [26] C. Suspène, S. Brandes, R. Guillard, Reversible coordination of Dioxygen by Tripodal Tetraamine copper complexes incorporated in a porous silica framework, *Chem. Eur. J.* 16 (2010) 6352–6364, <https://doi.org/10.1002/chem.200903148>.
- [27] C. Würtele, End-On “Copper Dioxygen Adduct Complexes” PhD thesis. <http://geb.uni-giessen.de/geb/volltexte/2008/6469/pdf/WuerteleChristian-2008-09-26.pdf>, 2008.
- [28] M. Schatz, M. Becker, F. Thaler, F. Hampel, S. Schindler, R.R. Jacobson, Z. Tyeklar, N.N. Murthy, P. Ghosh, Q. Chen, J. Zubieta, K.D. Karlin, Copper(I) complexes, copper(I)/O<sub>2</sub> reactivity, and copper(II) complex adducts, with a series of tetradentate tripyridylalkylamine tripodal ligands, *Inorg. Chem.* 40 (2001) 2312–2322, <https://doi.org/10.1021/ic000924n>.
- [29] M. Becker, F.W. Heinemann, S. Schindler, Reversible binding of dioxygen by a copper (I) complex with Tris(2-dimethylaminoethyl)amine (Me<sub>6</sub>Tren) as a ligand, *Chem. Eur. J.* 5 (1999) 3124–3129, <https://doi.org/10.1021/ic025941m>.
- [30] D. Maiti, J.S. Woertink, A.A.N. Sarjeant, E.I. Solomon, K.D. Karlin, Copper dioxygen adducts: formation of Bis( $\mu$ -oxo)dicopper(III) versus ( $\mu$ -1,2) Peroxodicopper(II) complexes with small changes in one Pyridyl-ligand substituent, *Inorg. Chem.* 47 (2008) 3787–3800, <https://doi.org/10.1021/ic702437c>.
- [31] J.V. Folgado, E. Coronado, D. Beltrán-Porter, R. Burriel, A. Fuentes, C. Miravittles, Crystal structures and magnetic properties of the mono- $\mu$ -halogeno-bridged copper (I) chains Cu(pcp)X [pcp = N-(2'-pyridylcarbonyl)pyridine-2- carboximidate, X = Cl or Br], *J. Chem. Soc. Dalton Trans.* (1988) 3041–3045, <https://doi.org/10.1039/DT9880003041>.
- [32] K. Abdi, H. Hadadzadeh, M. Weil, H.A. Rudbari, Mono- and polynuclear copper(II) complexes based on 2,4,6-tris(2-pyridyl)-1,3,5-triazine and its hydrolyzed form, *Inorg. Chim. Acta* 416 (2014) 109–121, <https://doi.org/10.1016/j.ica.2014.03.021>.
- [33] M. Schatz, M. Becker, O. Walter, G. Liehr, S. Schindler, Reactivity towards dioxygen of a copper(I) complex of tris(2-benzylaminoethyl)amine, *Inorg. Chim. Acta* 324 (2001) 173–179, [https://doi.org/10.1016/S0020-1693\(01\)00588-6](https://doi.org/10.1016/S0020-1693(01)00588-6).
- [34] T.D.J. Stumpf, M. Steinbach, C. Würtele, J. Becker, S. Becker, R. Fröhlich, R. Göttlich, S. Schindler, Reactivity of copper complexes with Bis(piperidyl) methane and Bis(quinolinyl)methane ligands, *Eur. J. Inorg. Chem.* (2017) 4246–4258, <https://doi.org/10.1002/ejic.201700755>.
- [35] A.A.O. Sarhan, M.S. Ibrahim, M.M. Kamal, K. Mitobe, T. Izumi, Synthesis, cyclic voltammetry, and UV-Vis studies of ferrocene- diethylenetriamine as anticipated electron-donor materials, *Monatsh. Chem.* 140 (2009) 315–323, <https://doi.org/10.1007/s00706-008-0025-2>.
- [36] S. Schindler, Reactivity of copper(I) complexes towards Dioxygen, *Eur. J. Inorg. Chem.* (2000) 2311–2326, [https://doi.org/10.1002/1099-0682\(200011\)2000:11<2311::aid-ejic2311>3.0.co;2-7](https://doi.org/10.1002/1099-0682(200011)2000:11<2311::aid-ejic2311>3.0.co;2-7).
- [37] C.E. Elwell, N.L. Gagnon, B.D. Neisen, D. Dhar, A.D. Spaeth, G.M. Yee, W. B. Tolman, Copper-oxygen complexes revisited: structure, spectroscopy, and

- reactivity, Chem. Rev. 117 (2017) 2059–2107, <https://doi.org/10.1021/acs.chemrev.6b00636>.
- [38] L.M. Mirica, X. Ottenwaelder, T.D.P. Stack, Structure and spectroscopy of copper-dioxygen complexes, Chem. Rev. 104 (2004) 1013–1045, <https://doi.org/10.1021/cr020632z>.
- [39] D. Maiti, D.-H. Lee, K. Gaoutchenova, C. Würtele, M.C. Holthausen, A.A. Narducci Sarjeant, J. Sundermeyer, S. Schindler, K.D. Karlin, Reactions of a copper(II) superoxo complex Lead to C-H and O-H substrate oxygenation: modeling copper-monoxygenase C-H hydroxylation, Angew. Chem. 120 (2008) 88–91, <https://doi.org/10.1002/ange.200704389>.
- [40] S. Itoh, Developing mononuclear copper-active-oxygen complexes relevant to reactive intermediates of biological oxidation reactions, Acc. Chem. Res. 48 (2015) 2066–2074, <https://doi.org/10.1021/acs.accounts.5b00140>.
- [41] G. Socrates, Infrared and Raman Characteristic Group Frequencies. Tables and Charts Vol.3, J. Wiley and Sons, Chichester, 2001.
- [42] A.Y. Kovalevsky, P. Coppens, CSD Communications, CSD Commun, 1999, <https://doi.org/10.5517/cc424x>.
- [43] L.A. Dakin, P.C. Ong, J.S. Panek, R.J. Staples, P. Stavropoulos, Speciation and mechanistic studies of chiral copper(I) Schiff Base precursors mediating asymmetric Carbenoid insertion reactions of Diazoacetates into the Si-H bond of Silanes, Organometallics. 19 (2000) 2896–2908, <https://doi.org/10.1021/om0003786>.
- [44] S. Fujinami, A. Hashimoto, K. Komiyama, S. Nagatomo, T. Kitagawa, M. Suzuki, H. Hayashi, H. Furutachi, Dioxygen reactivity of copper(I) complexes with Tetradentate Tripodal ligands having aliphatic nitrogen donors: synthesis, structures, and properties of Peroxo and Superoxo complexes, Bull. Chem. Soc. Jpn. 77 (2004) 59–72, <https://doi.org/10.1246/bcsj.77.59>.
- [45] T. Hoppe, S. Schaub, J. Becker, C. Würtele, S. Schindler, Charakterisierung eines makrocyclischen "end-on"-Peroxidokupferkomplexes, Angew. Chem. 125 (2013) 904–907, <https://doi.org/10.1002/ange.201205663>.



### 5. References

- [1] J. N. Armor, *Catal. Today* **2011**, *163*, 3–9.
- [2] F. G. Meussdoerffer, in *Handbook of Brewing* (Ed.: H.M. Eßlinger), Wiley-VCH Verlag GmbH & Co. KGaA, Weinheim, Germany, **2009**, pp. 1–42.
- [3] J. Wisniak, *Educ. Química* **2010**, *21*, 60–69.
- [4] S. C. Weiner, in *J. Chem. Inf. Model.*, **1998**, pp. 915–921.
- [5] C. N. Cornell, M. S. Sigman, in *Activation of Small Molecules* (Ed.: W.B. Tolman), Wiley-VCH Verlag GmbH & Co. KGaA, Weinheim, Germany, **2006**, pp. 159–186.
- [6] L. R. Kump, *Nature* **2008**, *451*, 277–278.
- [7] R. A. Sheldon, *Green Chem.* **2016**, *18*, 3180–3183.
- [8] A. S. Borovik, P. J. Zinn, M. K. Zart, in *Activation of Small Molecules* (Ed.: W.B. Tolman), Wiley-VCH, Weinheim, **2006**, pp. 187–234.
- [9] X. Liu, Y. Ryabenkova, M. Conte, *Phys. Chem. Chem. Phys.* **2015**, *17*, 715–731.
- [10] J. C. Védrine, *ChemSusChem* **2019**, *12*, 577–588.
- [11] E. Riedel, C. Janiak, in *Anorganische Chemie*, De Gruyter, Berlin, Boston, **2015**, pp. 472–480.
- [12] W. Kaim, B. Schwederski, in *Bioanorganische Chemie*, Vieweg+Teubner Verlag, Wiesbaden, **2005**, pp. 6–39.
- [13] J. I. Mujika, E. Rezabal, J. M. Mercero, F. Ruipérez, D. Costa, J. M. Ugalde, X. Lopez, *Comput. Struct. Biotechnol. J.* **2014**, *9*, e201403002.
- [14] W. Kaim, B. Schwederski, in *Bioanorganische Chemie*, Vieweg+Teubner Verlag, Wiesbaden, **2005**, pp. 87–108.
- [15] M.-C. Kafentzi, M. Orío, M. Réglie, S. Yao, U. Kuhlmann, P. Hildebrandt, M. Driess, A. J. Simaan, K. Ray, *Dalton Trans.* **2016**, *45*, 15994–16000.
- [16] A. A. Yaroshevsky, *Geochem. Int.* **2006**, *44*, 48–55.
- [17] X. Huang, J. T. Groves, *Chem. Rev.* **2018**, *118*, 2491–2553.
- [18] N. Bistolas, U. Wollenberger, C. Jung, F. W. Scheller, *Biosens. Bioelectron.* **2005**, *20*, 2408–2423.
- [19] W. Kaim, B. Schwederski, in *Bioanorganische Chemie*, Vieweg+Teubner Verlag, Wiesbaden, **2005**, pp. 114–132.
- [20] D. Svedružić, S. Jónsson, C. G. Toyota, L. A. Reinhardt, S. Ricagno, Y. Lindqvist, N. G. J. Richards, *Arch. Biochem. Biophys.* **2005**, *433*, 176–192.

- 
- [21] K. von der Saal, in *Biochemie*, Springer Berlin Heidelberg, Berlin, Heidelberg, **2020**, pp. 159–167.
- [22] D. Nianios, S. Thierbach, L. Steimer, P. Lulchev, D. Klostermeier, S. Fetzner, *BMC Biochem.* **2015**, *16*, 1–11.
- [23] A. T. Fiedler, A. A. Fischer, *J. Biol. Inorg. Chem.* **2017**, *22*, 407–424.
- [24] H. Tapiero, D. M. Townsend, K. D. Tew, *Biomed. Pharmacother.* **2003**, *57*, 386–398.
- [25] A. C. Rosenzweig, M. H. Sazinsky, *Curr. Opin. Struct. Biol.* **2006**, *16*, 729–735.
- [26] E. I. Solomon, D. E. Heppner, E. M. Johnston, J. W. Ginsbach, J. Cirera, M. Qayyum, M. T. Kieber-Emmons, C. H. Kjaergaard, R. G. Hadt, L. Tian, *Chem. Rev.* **2014**, *114*, 3659–3853.
- [27] M. Pascaly, I. Jolk, B. Krebs, *Chemie in unserer Zeit* **1999**, *33*, 334–341.
- [28] I. S. MacPherson, M. E. P. Murphy, *Cell. Mol. Life Sci.* **2007**, *64*, 2887–2899.
- [29] H. Decker, T. Schweikardt, F. Tuczek, *Angew. Chem. Int. Ed.* **2006**, *45*, 4546–4550.
- [30] H. S. Mason, W. L. Fowlks, E. Peterson, *J. Am. Chem. Soc.* **1955**, *77*, 2914–2915.
- [31] I. A. Koval, P. Gamez, C. Belle, K. Selmeczi, J. Reedijk, *Chem. Soc. Rev.* **2006**, *35*, 814–840.
- [32] D. A. Quist, D. E. Diaz, J. J. Liu, K. D. Karlin, *J. Biol. Inorg. Chem.* **2017**, *22*, 253–288.
- [33] L. M. Mirica, X. Ottenwaelder, T. D. P. Stack, *Chem. Rev.* **2004**, *104*, 1013–1046.
- [34] R. L. Osborne, J. P. Klinman, in *Copper-Oxygen Chemistry* (Eds.: K.D. Karlin, S. Itoh), John Wiley & Sons, Inc., Hoboken, NJ, USA, **2011**, pp. 1–22.
- [35] W. T. Beeson, V. V. Vu, E. A. Span, C. M. Phillips, M. A. Marletta, *Annu. Rev. Biochem.* **2015**, *84*, 923–946.
- [36] L. Ciano, G. J. Davies, W. B. Tolman, P. H. Walton, *Nat. Catal.* **2018**, *1*, 571–577.
- [37] J. S. Woertink, L. Tian, D. Maiti, H. R. Lucas, R. A. Himes, K. D. Karlin, F. Neese, C. Würtele, M. C. Holthausen, E. Bill, *et al.*, *Inorg. Chem.* **2010**, *49*, 9450–9459.
- [38] R. E. Cowley, L. Tian, E. I. Solomon, *Proc. Natl. Acad. Sci. USA* **2016**, *113*, 12035–12040.
- [39] E. I. Solomon, *Inorg. Chem.* **2016**, *55*, 6364–6375.
- [40] J. W. Ginsbach, R. L. Peterson, R. E. Cowley, K. D. Karlin, E. I. Solomon,
-

## 5. References

---

- Inorg. Chem.* **2013**, *52*, 12872–12874.
- [41] M. Bhadra, W. J. Transue, H. Lim, R. E. Cowley, J. Y. C. Lee, M. A. Siegler, P. Josephs, G. Henkel, M. Lerch, S. Schindler, *et al.*, *J. Am. Chem. Soc.* **2021**, *143*, 3707–3713.
- [42] P. Wu, F. Fan, J. Song, W. Peng, J. Liu, C. Li, Z. Cao, B. Wang, *J. Am. Chem. Soc.* **2019**, *141*, 19776–19789.
- [43] J. P. Klinman, *J. Biol. Chem.* **2006**, *281*, 3013–3016.
- [44] S. T. Prigge, *Science* **2004**, *304*, 864–867.
- [45] M. F. Qayyum, R. Sarangi, K. Fujisawa, T. D. P. Stack, K. D. Karlin, K. O. Hodgson, B. Hedman, E. I. Solomon, *J. Am. Chem. Soc.* **2013**, *135*, 17417–17431.
- [46] Y. Matoba, T. Kumagai, A. Yamamoto, H. Yoshitsu, M. Sugiyama, *J. Biol. Chem.* **2006**, *281*, 8981–8990.
- [47] D. Sehnal, S. Bittrich, M. Deshpande, R. Svobodová, K. Berka, V. Bazgier, S. Velankar, S. K. Burley, J. Koča, A. S. Rose, *Nucleic Acids Res.* **2021**, *49*, W431–W437.
- [48] M. Rolff, J. Schottenheim, H. Decker, F. Tuczec, *Chem. Soc. Rev.* **2011**, *40*, 4077–4098.
- [49] H. Decker, N. Hellmann, E. Jaenicke, B. Lieb, U. Meissner, J. Markl, *Integr. Comp. Biol.* **2007**, *47*, 631–644.
- [50] R. Trammell, K. Rajabimoghadam, I. Garcia-Bosch, *Chem. Rev.* **2019**, *119*, 2954–3031.
- [51] M. Yamada, K. D. Karlin, S. Fukuzumi, K. Sato, M. Aoki, R. Noyori, *Chem. Sci.* **2016**, *7*, 2856–2863.
- [52] K. Sato, *Science* **1998**, *281*, 1646–1647.
- [53] C. Gawlig, S. Schindler, S. Becker, *Eur. J. Inorg. Chem.* **2020**, *2020*, 248–252.
- [54] B. N. Sánchez-Eguía, M. Flores-Alamo, M. Orió, I. Castillo, *Chem. Commun.* **2015**, *51*, 11134–11137.
- [55] K. Fujisawa, M. Tanaka, Y. Moro-oka, N. Kitajima, *J. Am. Chem. Soc.* **1994**, *116*, 12079–12080.
- [56] B. N. Sánchez-Eguía, M. Flores-Alamo, M. Orió, I. Castillo, D. A. Iovan, A. T. Wrobel, A. A. McClelland, A. B. Scharf, G. A. Edouard, T. A. Betley, *Chem. Commun.* **2017**, *51*, 10306–10309.
- [57] R. Sarangi, N. Aboeella, K. Fujisawa, W. B. Tolman, B. Hedman, K. O. Hodgson, E. I. Solomon, *J. Am. Chem. Soc.* **2006**, *128*, 8286–8296.
- [58] J. J. Liu, D. E. Diaz, D. A. Quist, K. D. Karlin, *Isr. J. Chem.* **2016**, *56*, 738–755.
-

- 
- [59] R. L. Peterson, R. A. Himes, H. Kotani, T. Suenobu, L. Tian, M. A. Siegler, E. I. Solomon, S. Fukuzumi, K. D. Karlin, *J. Am. Chem. Soc.* **2011**, *133*, 1702–1705.
- [60] D. E. Diaz, D. A. Quist, A. E. Herzog, A. W. Schaefer, I. Kipouros, M. Bhadra, E. I. Solomon, K. D. Karlin, *Angew. Chem. Int. Ed.* **2019**, *58*, 17572–17576.
- [61] S. Kim, J. Y. Lee, R. E. Cowley, J. W. Ginsbach, M. A. Siegler, E. I. Solomon, K. D. Karlin, *J. Am. Chem. Soc.* **2015**, *137*, 2796–2799.
- [62] A. Kunishita, M. Kubo, H. Sugimoto, T. Ogura, K. Sato, T. Takui, S. Itoh, *J. Am. Chem. Soc.* **2009**, *131*, 2788–2789.
- [63] A. Kunishita, M. Z. Ertem, Y. Okubo, T. Tano, H. Sugimoto, K. Ohkubo, N. Fujieda, S. Fukuzumi, C. J. Cramer, S. Itoh, *Inorg. Chem.* **2012**, *51*, 9465–9480.
- [64] S. Itoh, *Acc. Chem. Res.* **2015**, *48*, 2066–2074.
- [65] M. Schatz, V. Raab, S. P. Foxon, G. Brehm, S. Schneider, M. Reiher, M. C. Holthausen, J. Sundermeyer, S. Schindler, *Angew. Chem. Int. Ed.* **2004**, *43*, 4360–4363.
- [66] C. Würtele, E. Gaoutchenova, K. Harms, M. C. Holthausen, J. Sundermeyer, S. Schindler, *Angew. Chem. Int. Ed.* **2006**, *45*, 3867–3869.
- [67] D. Maiti, D.-H. Lee, K. Gaoutchenova, C. Würtele, M. C. Holthausen, A. A. Narducci Sarjeant, J. Sundermeyer, S. Schindler, K. D. Karlin, *Angew. Chem. Int. Ed.* **2008**, *47*, 82–85.
- [68] N. Wei, N. N. Murthy, Q. Chen, J. Zubieta, K. D. Karlin, *Inorg. Chem.* **1994**, *33*, 1953–1965.
- [69] S. Muthuramalingam, K. Anandababu, M. Velusamy, R. Mayilmurugan, *Inorg. Chem.* **2020**, *59*, 5918–5928.
- [70] N. Kitajima, K. Fujisawa, Y. Morooka, K. Toriumi, *J. Am. Chem. Soc.* **1989**, *111*, 8975–8976.
- [71] L. Casella, E. Monzani, M. Gullotti, D. Cavagnino, G. Cerina, L. Santagostini, R. Ugo, *Inorg. Chem.* **1996**, *35*, 7516–7525.
- [72] C. E. Elwell, N. L. Gagnon, B. D. Neisen, D. Dhar, A. D. Spaeth, G. M. Yee, W. B. Tolman, *Chem. Rev.* **2017**, *117*, 2059–2107.
- [73] J. A. Halfen, S. Mahapatra, E. C. Wilkinson, S. Kaderli, V. G. Young, L. Que, A. D. Zuberbühler, W. B. Tolman, *Science* **1996**, *271*, 1397–1400.
- [74] M. H. Mahyuddin, Y. Shiota, A. Staykov, K. Yoshizawa, *Acc. Chem. Res.* **2018**, *51*, 2382–2390.
- [75] P. L. Holland, K. R. Rodgers, W. B. Tolman, *Angew. Chem. Int. Ed.* **1999**, *38*, 1139–1142.
- [76] B. Schönecker, T. Zheldakova, Y. Liu, M. Kötteritzsch, W. Günther, H. Görls,
-

## 5. References

---

- Angew. Chem. Int. Ed.* **2003**, *42*, 3240–3244.
- [77] J. Becker, Y. Y. Zhyhadlo, E. D. Butova, A. A. Fokin, P. R. Schreiner, M. Förster, M. C. Holthausen, P. Specht, S. Schindler, *Chem. Eur. J.* **2018**, *24*, 15543–15549.
- [78] J. Becker, P. Gupta, F. Angersbach, F. Tuczek, C. Näther, M. C. Holthausen, S. Schindler, *Chem. Eur. J.* **2015**, *21*, 11735–11744.
- [79] P. Specht, A. Petrillo, J. Becker, S. Schindler, *Eur. J. Inorg. Chem.* **2021**, *2021*, 1961–1970.
- [80] Y. Y. See, A. T. Herrmann, Y. Aihara, P. S. Baran, *J. Am. Chem. Soc.* **2015**, *137*, 13776–13779.
- [81] R. Trammell, Y. Y. See, A. T. Herrmann, N. Xie, D. E. Díaz, M. A. Siegler, P. S. Baran, I. Garcia-Bosch, *J. Org. Chem.* **2017**, *82*, 7887–7904.
- [82] R. Trammell, L. D'Amore, A. Cordova, P. Polunin, N. Xie, M. A. Siegler, P. Belanzoni, M. Swart, I. Garcia-Bosch, *Inorg. Chem.* **2019**, *58*, 7584–7592.
- [83] R. R. Jacobson, Z. Tyeklar, A. Farooq, K. D. Karlin, S. Liu, J. Zubieta, *J. Am. Chem. Soc.* **1988**, *110*, 3690–3692.
- [84] H. R. Lucas, L. Li, A. A. N. Sarjeant, M. A. Vance, E. I. Solomon, K. D. Karlin, *J. Am. Chem. Soc.* **2009**, *131*, 3230–3245.
- [85] K. Komiyama, H. Furutachi, S. Nagatomo, A. Hashimoto, H. Hayashi, S. Fujinami, M. Suzuki, T. Kitagawa, *Bull. Chem. Soc. Jpn.* **2004**, *77*, 59–72.
- [86] C. Würtele, O. Sander, V. Lutz, T. Waitz, F. Tuczek, S. Schindler, *J. Am. Chem. Soc.* **2009**, *131*, 7544–7545.
- [87] D. Maiti, J. S. Woertink, A. A. Narducci Sarjeant, E. I. Solomon, K. D. Karlin, *Inorg. Chem.* **2008**, *47*, 3787–3800.
- [88] I. Garcia-Bosch, A. Company, J. R. Frisch, M. Torrent-Sucarrat, M. Cardellach, I. Gamba, M. Güell, L. Casella, L. Que, X. Ribas, *et al.*, *Angew. Chem. Int. Ed.* **2010**, *49*, 2406–2409.
- [89] A. Andersen, *Int. J. Toxicol.* **2006**, *25*, 11–27.
- [90] J. A. B. Satrio, L. . Doraiswamy, *Chem. Eng. J.* **2001**, *82*, 43–56.
- [91] B. Rosche, V. Sandford, M. Breuer, B. Hauer, P. Rogers, *Appl. Microbiol. Biotechnol.* **2001**, *57*, 309–315.
- [92] S. Pugh, R. McKenna, I. Halloum, D. R. Nielsen, *Metab. Eng. Commun.* **2015**, *2*, 39–45.
- [93] T. B. Adams, S. M. Cohen, J. Doull, V. J. Feron, J. I. Goodman, L. J. Marnett, I. C. Munro, P. S. Portoghese, R. L. Smith, W. J. Waddell, *et al.*, *Food Chem. Toxicol.* **2005**, *43*, 1207–1240.
- [94] F. Wöhler, J. Liebig, *Ann. Pharm.* **1832**, *3*, 249–282.
-

- 
- [95] H. Li, Y. Meng, C. Shu, X. Li, A. A. Kiss, X. Gao, *ACS Sustainable Chem. Eng.* **2018**, *6*, 14114–14124.
- [96] E. Breitmaier, G. Jung, in *Organische Chemie*, Thieme Verlag, Stuttgart, **2009**, pp. 312–318.
- [97] J. Buddrus, in *Grundlagen Der Organischen Chemie*, De Gruyter, Berlin; New York, **2011**, pp. 473–515.
- [98] L. Gattermann, J. A. Koch, *Chem. Ber.* **1897**, *30*, 1622–1624.
- [99] F. Wang, J. Xu, X. Li, J. Gao, L. Zhou, R. Ohnishi, *Adv. Synth. Catal.* **2005**, *347*, 1987–1992.
- [100] S. Gast, J. H. Matthies, U. S. Tuttlies, U. Nieken, *Chem. Eng. Technol.* **2017**, *40*, 1445–1452.
- [101] F. Valentini, G. Ferracci, P. Galloni, G. Pomarico, V. Conte, F. Sabuzi, *Catalysts* **2021**, *11*, 262.
- [102] W. Wu, G. Zhang, J. Zhang, G. Wang, C. H. Tung, Y. Wang, *Chem. Eng. J.* **2021**, *404*, 126433.
- [103] S. Fukuzumi, Y. Lee, W. Nam, *ChemCatChem* **2018**, *10*, 1686–1702.
- [104] L. Kesavan, R. Tiruvalam, M. H. A. Rahim, M. I. bin Saiman, D. I. Enache, R. L. Jenkins, N. Dimitratos, J. A. Lopez-Sanchez, S. H. Taylor, D. W. Knight, *et al.*, *Science* **2011**, *331*, 195–199.
- [105] M. Romero-Fernández, F. Paradisi, *Curr. Opin. Chem. Biol.* **2020**, *55*, 1–8.
- [106] A. Mattern, F. Machka, M. S. Wickleder, O. S. Ilyaskina, M. Bünemann, M. Diener, E. Pouokam, *Org. Biomol. Chem.* **2018**, *16*, 6680–6687.
- [107] J. Creus, R. Matheu, I. Peñafiel, D. Moonshiram, P. Blondeau, J. Benet-Buchholz, J. García-Antón, X. Sala, C. Godard, A. Llobet, *Angew. Chem. Int. Ed.* **2016**, *55*, 15382–15386.
- [108] K. Szymańska, K. Odrozek, A. Zniszczoł, G. Torrelo, V. Resch, U. Hanefeld, A. B. Jarzębski, *Catal. Sci. Technol.* **2016**, *6*, 4882–4888.
- [109] I. Hatay, R. Gup, M. Ersöz, *J. Hazard. Mater.* **2008**, *150*, 546–553.
- [110] R. J. Perry, M. J. O'Brien, *Energy Fuels* **2011**, *25*, 1906–1918.
- [111] A. Basso, S. Serban, *Mol. Catal.* **2019**, *479*, 110607.
- [112] Y. Aratani, Y. Yamada, S. Fukuzumi, *Chem. Commun.* **2015**, *51*, 4662–4665.
- [113] C.-C. Liu, T.-S. Lin, S. I. Chan, C.-Y. Mou, *J. Catal.* **2015**, *322*, 139–151.
- [114] F. Hoffmann, M. Cornelius, J. Morell, M. Fröba, *Angew. Chem. Int. Ed.* **2006**, *45*, 3216–3251.
- [115] K. Machado, P. B. Tavares, C. Freire, G. S. Mishra, *Polyhedron* **2014**, *69*, 119–
-

## 5. References

---

- 126.
- [116] M. H. Lim, C. F. Blanford, A. Stein, *J. Am. Chem. Soc.* **1997**, *119*, 4090–4091.
- [117] C. Suspène, S. Brandès, R. Guillard, *Chem. Eur. J.* **2010**, *16*, 6352–6364.
- [118] S. Sun, Y. Cao, J. Feng, P. Wu, *J. Mater. Chem.* **2010**, *20*, 5605.
- [119] M. Nemati, T. Tamoradi, H. Veisi, *Polyhedron* **2019**, *167*, 75–84.
- [120] A. M. Lazarin, Y. Gushikem, S. C. de Castro, *J. Mater. Chem.* **2000**, *10*, 2526–2531.
- [121] P. K. Jal, *Talanta* **2004**, *62*, 1005–1028.
- [122] T. Hara, S. Mascotto, C. Weidmann, B. M. Smarsly, *J. Chromatogr. A* **2011**, *1218*, 3624–3635.
- [123] R. Meinus, R. Ellinghaus, K. Hormann, U. Tallarek, B. M. Smarsly, *Phys. Chem. Chem. Phys.* **2017**, *19*, 14821–14834.
- [124] D. Huebner, V. Koch, B. Ebeling, J. Mechau, J. E. Steinhoff, P. Vana, *J. Polym. Sci. Part A* **2015**, *53*, 103–113.
- [125] J. B. Mandel, C. Maricondi, B. E. Douglas, *Inorg. Chem.* **1988**, *27*, 2990–2996.